# Robust Network Calibration and Therapy Design in Systems Biology

by

Bo S. Kim

S.B., Massachusetts Institute of Technology (2004)

M.Eng., Massachusetts Institute of Technology (2005)



Submitted to the
Department of Electrical Engineering and Computer Science
in partial fulfillment of the requirements for the degree of

Doctor of Philosophy in Electrical Engineering and Computer Science

at the

MASSACHUSETTS INSTITUTE OF TECHNOLOGY

September 2010



Author .....
Department of Electrical Engineering and Computer Science
September 3, 2010

Certified by .....
Jacob K. White
Professor of Electrical Engineering and Computer Science
Thesis Supervisor

Certified by .....
Bruce Tidor
Professor of Biological Engineering and Computer Science
Thesis Supervisor

Accepted by .....
Terry P. Orlando
Chair, Department Committee on Graduate Students

**Robust Network Calibration and Therapy Design in Systems Biology**

by

Bo S. Kim

Submitted to the Department of Electrical Engineering and Computer Science
on September 3, 2010, in partial fulfillment of the
requirements for the degree of
Doctor of Philosophy in Electrical Engineering and Computer Science

## Abstract

Mathematical modeling of biological networks is under active research, receiving attention for its ability to quantitatively represent the modeler's systems-level understanding of network functionalities. Computational methods that enhance the usefulness of mathematical models are thus being increasingly sought after, as they face a variety of difficulties that originate from limitations in model accuracy and experimental precision. This thesis explores robust optimization as a tool to counter the effects of these uncertainty-based difficulties in calibrating biological network models and in designing protocols for cancer immunotherapy.

The robust approach to network calibration and therapy design aims to account for the worst-case uncertainty scenario that could threaten successful determination of network parameters or therapeutic protocols, by explicitly identifying and sampling the region of potential uncertainties corresponding to worst-case. Through designating individual numerical ranges that uncertain model parameters are each expected to lie within, the region of uncertainties is defined as a hypercube that encompasses a particular uncertainty range along each of its dimensions. For investigating its applicability to parameter estimation, the performance of the optimization method that embodies this robust approach is examined in the context of a model of a unit belonging to the mitogen-activated protein kinase pathway. For its significance in therapeutic design, the method is applied to both a canonical mathematical model of the tumor-immune system and a model specific to treating superficial bladder cancer with *Bacillus Calmette-Guérin*, which have both been selected to examine the plausibility of applying the method to either discrete-dose or continuous-dose administrations of immunotherapeutic agents.

The robust optimization method is evaluated against a standard optimization method by comparing the relative robustness of their respective estimated parameters or designed therapies. Further analysis of the results obtained using the robust method points to properties and limitations, and in turn directions for improvement, of existing models and design frameworks for applying the robust method to network calibration and protocol design. An alternative mathematical formulation to solving the worst-case optimization problem is also studied, one that replaces the sampling process of the previous method with a linearization of the objective function's parameter space over the region of uncertainties. This formulation's relative computational

efficiency additionally gives rise to a novel approach to experimental guidance directed at improving modeling efforts under uncertainties, which may potentially further fuel the advancement of quantitative systems biological research.

Thesis Supervisor: Jacob K. White
Title: Professor of Electrical Engineering and Computer Science

Thesis Supervisor: Bruce Tidor
Title: Professor of Biological Engineering and Computer Science

# Acknowledgments

I begin by expressing my gratitude for the tremendous amount of guidance and support from Prof. Jacob White and Prof. Bruce Tidor. Their passion both for our research and in being my mentors is but one of countless reasons why I feel most honored to be able to call myself their student.

Being a member of their research groups, it follows as no surprise how grateful I am for my amazing labmates Lei Zhang, Amit Hochman, Bradley Bond, Tarek Moselhy, Homer Reid, Yu-Chung Hsiao, Zohaib Mahmood, Yan Zhao, Omar Mysore, Kai Pan, Bracken King, David Hagen, David Witmer, Filipe Gracio, Gil Kwak, Ishan Patel, Jason Biddle, Matthew Fay, Nathaniel Silver, Nirmala Paudel, Timothy Curran, Yang Shen, Yuanyuan Cui, Jaydeep Bardhan, Carlos Coelho, Xin Hu, Shih-Hsien Kuo, Junghoon Lee, Stephen Leibman, Laura Proctor, Kin Sou, Dmitry Vasilyev, David Willis, Joshua Apgar, Kathryn Armstrong, Caitlin Bever, David Huggins, Brian Joughin, Shaun Lippow, Mala Radhakrishnan, Kelly Thayer, Jared Toettcher, Katharina Wilkins, and Aurore Zyto. I particularly thank Lei for filling our office with endless laughter while letting me be me, Jay for advising me on everything from surviving in Singapore to considering career paths, and Josh for showing me that battling with matrices can be just as cool as rocking out to live rap. I also thank Prof. Luca Daniel and Dr. Yehuda Avniel for their generous encouragement, and Chadwick Collins and Nira Manokharan for assuring that necessary matters are taken care of without any difficulties.

I treasure my interactions with Prof. Ernest Fraenkel on my thesis committee for filling my studies with new ideas and considerations for future directions beyond my research thus far, which has been funded by both the Integrative Cancer Biology Program of the NIH and the Singapore-MIT Alliance. Participating in these initiatives, I continue to learn so much from Dr. Lisa Tucker-Kellogg and the Computational and Systems Biology community at MIT as a whole. Beyond the campus, working with

Dr. Jeff Sachs, Dr. Robert Nachbar, Francisco Cruz, and fellow colleagues at Merck's Applied Computer Science and Mathematics department is an experience that I find truly valuable to my endeavors from here onwards.

Starting with Hansen Bow, Salil Desai, Jianping Fu, James Geraci, Cody Gilleland, Christopher Rohde, Brian Taff, and the rest of my wonderful 36-7th/8th floormates, there are simply too many who deserve to be acknowledged; here is only an abbreviated list comprising mainly of those who I drew a large part of my strength from in recent years. I thank Anna, for being everything that I could hope for in a friend and more; Bryce, for challenging me to aim for heights that may initially seem too high; Jay, for decorating my memories since ABCs and for many more years to come; Jun, for encouraging by example rather than words to guide the path I follow; Lily, for hugging me with warm wishes from no matter how many miles away; Namiko, for keeping me on track with smiles through every step of this journey; Ram, for making sure that I do not lose touch with the real world; Ross, for remaining the same Ross that I can laugh with over almost anything; Ryu, for writing out the very definitions of patience and sincerity in my dictionary; Brent and John, for opportunities to have my voice heard; Danielle, Dave, Danny, Lisa, Toshika, and Dina, for weekdays as fun as weekends; Errol, Dennis, Jim, and Tito, for greetings that turn even the longest days short; Kageyama-sensei, Fujikura-sensei, Yamanaka-sensei, Prof. Cranston, and Prof. Smentek, for broadening my perspective; Mrs. Lavina, for believing in me.

Uncle and Aunt, I strive to be there for those who are dear to you.

TJ, I could not have done this without you.

Mom and Dad, I thank you, I respect you, and I love you.

# Contents

# List of Figures

# List of Tables

# Chapter 1

# Introduction

Computational methods are being actively applied to advancing the field of systems biology. This direction of advancement holds the goal of putting to use the advantages of quantitatively characterizing the systems biological knowledge available. One of the main advantages arises from the exactness with which such characterization can take place. In particular, a mathematical representation, or model, of how a system works contains no less and no more than the components that the modeler has decided use to replicate the workings of the system. By checking whether the model can accurately trace the system behavior under conditions of interest, the modeler can decide whether the components that have been included are of the right size or are connected with one another in the correct manner. This work deals with the former of the two, where effort is put into searching for the right size of components to use in making system models behave as desired.

Model calibration as discussed in this work points to the task of determining the component sizes that would make the model outputs match analogous outputs measured from experiments performed on the actual system. In other words, the desirable model behavior in this case is one that makes the outputs as close to the measurements as possible. The best component sizes for performing this task can be sought for by using optimization, once what is desired is formulated as a mathematical problem minimizing the difference between the model and actual outputs.

Therapeutic protocol design as covered by this work is approached through opti-

mization as well. In this instance, the desirable model behavior is one that minimizes the adverse effects of being subject to both the disease itself (e.g., tumor cell count in cancer patients) and the treatments administered (e.g., side effects of drugs). The amount and timing of therapeutic intervention are in turn the components whose sizes are to be determined to make these effects as small as possible, a problem that can once again be posed mathematically as a minimization.

Optimization in both cases is thus a tool that helps identify the choices that lead to optimal model behavior. There is, however, a need for caution in using this mathematical tool. On the flip side of the much desired exactness offered by quantitative representation of these tasks lies the pitfall as well, which is that the decisions made do not have in them any consideration for matters that have not explicitly been included into defining what indeed is optimal. For example, the schematic plot in Fig. 1-1(i) shows the range of choices that can be made on the horizontal axis (e.g., the amount of therapeutic agent to administer to a cancer patient) and the corresponding range of costs associated with the choices on the vertical axis (e.g., the amount of toxic side effects due to therapeutic agent administered). If the optimal choice is defined as the one associated with the lowest cost, the optimizer should pick choice $c_1$. However, notice that if there were to be slight fluctuations in the value of $c_1$ along the horizontal axis (e.g., the amount of therapeutic agent administered is not $c_1$ but slightly higher or lower than $c_1$), the corresponding costs will actually be considerably high. On the other hand, although the exact choice $c_2$ is associated with a higher cost than the exact choice $c_1$, slight fluctuations in $c_2$ do not largely affect the resulting cost.

Considering that it is realistic to assume the existence of such fluctuations and other uncertainties in modeling real-world phenomena in systems biology, this work focuses on analyzing the effects of defining the optimal choice while taking the fluctuations and uncertainties into account. It works with the concept of robust optimization, a type of optimization that can be specified to favor more robust solutions to optimization problems (i.e., the robust optimizer can be designed to pick choice $c_2$ in Fig. 1-1(i) over choice $c_1$). An interesting additional variation to the robust

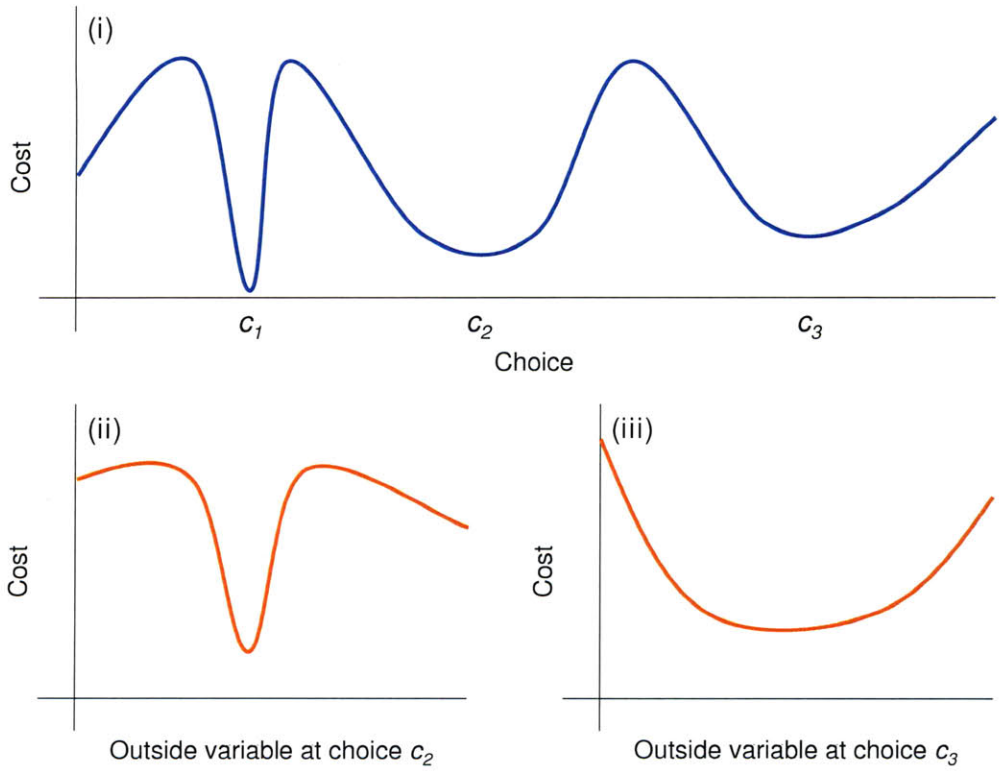


Figure 1-1: **Characterizing robust choices schematically.** (i) Choice $c_1$ is associated with the lowest cost, but is less robust than choice $c_2$ or choice $c_3$ to slight fluctuations in the value of the respective choice along the horizontal axis. Although they are similarly robust to the value of their respective choices, $c_3$ (iii) is more robust than $c_2$ (ii) to fluctuations in an outside variable that also affects the cost.

optimizer's task that is also covered in this work can be schematically seen through comparing (ii) and (iii) of Fig. 1-1, which represent how the cost is affected by an outside variable (e.g., the patient's ability to counter side effects) at choice $c_2$ and at choice $c_3$, respectively. Although there is not a noticeable difference in how robust $c_2$ and $c_3$ each are to the choice itself (i.e., the decision variable of the optimization problem) being implemented with slight fluctuations, $c_3$ is more robust to outside uncertainties that affect the cost (i.e., parameters, other than the decision variable, of the objective function that is minimized by the optimizer). Fig. 1-2 clarifies this idea by schematically showing the cost being a function of both the choice and the

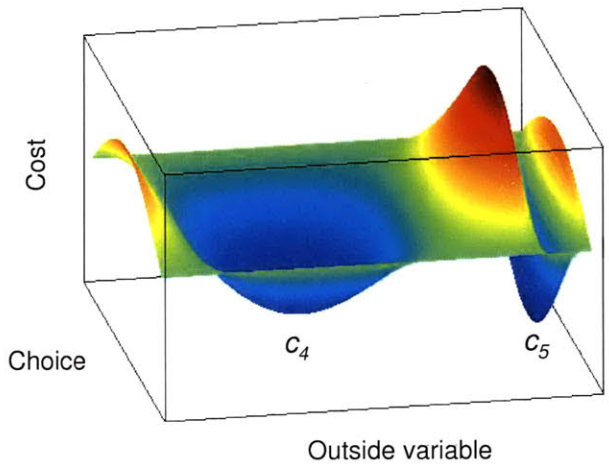


Figure 1-2: **Schematically visualizing cost being affected by both choice and outside variable.** Choice $c_5$ is associated with the lower cost, and is about as robust as choice $c_4$ to slight fluctuations in the value of the respective choice, but $c_5$ is less robust than $c_4$ to fluctuations in an outside variable that also affects the cost.

outside variable simultaneously; although choices $c_4$ and $c_5$ are comparably robust to slight fluctuations in the value of the respective choice, $c_4$ is more robust than $c_5$ to fluctuations in the outside variable.

Following this introduction, Ch. 2 surveys the published literature relevant to this work. Each of its sections are arranged to relate in particular to one of the following main three chapters of this dissertation, although many of the ideas pertaining to model-based research methodologies expand beyond the boundaries of their respective sections into others. Ch. 3 explores the use of robust optimization for estimating parameters of quantitative models in systems biology. The study applies the concept to a typical model of the mitogen-activated protein kinase (MAPK) pathway,

which has been found to exist as a part of a number of cellular networks whose behaviors are affected by cancer. After familiarizing the reader to this work's general approach to robust optimization through the MAPK study, Ch. 4 investigates the effectiveness of using robust optimization for determining treatment protocols for cancer immunotherapy. Protocols are computationally designed for one type of therapy using the bacterium *Bacillus Calmette-Guérin* (BCG) and another using a combination of cytotoxic T lymphocytes (CTL) and interleukin-2 (IL-2), by utilizing models that attempt to capture the tumor-immune interaction initiated by these therapeutic agents. Ch. 5 offers an alternative mathematical formulation to the robust optimization procedure, which is computationally less expensive than the one originally used for robust approaches in Chs. 3 and 4. Besides analyzing its application to designing protocols for BCG immunotherapy, this chapter also introduces a novel approach to experimental guidance that is made possible by this computationally more efficient formulation. And finally, Ch. 6 summarizes this dissertation as a whole and shares ideas regarding future research directions that have materialized from the valuable lessons learned while carrying out this work.

# Chapter 2

# Background

## 2.1 Biological network calibration

### Building mathematical models

A mathematical model of a biochemical network represents the modeler's understanding of the network's mechanistic details. The model is specified by which components it contains, in what ways the components are interconnected, and how strong the connections are. Which components are included depends on the adequate level of abstraction of the actual network by the model, and is dictated by the purpose behind which the model is built. The nature and the strengths of the connections between the components initially arise from prior knowledge that the modeler has about the network, based on previously conducted studies and available experimental data.

The validity of the model is evaluated on its ability to exhibit the actual network's properties of interest. Systematic methods for model validation are thus in high demand, as it allows the model, and in turn the modeler's understanding of the network, to evolve together to remain consistent with new findings. One such method is proposed in ref. [1], where Apgar et al. design dynamic stimuli in stimulus-response experiments of systems for which there exist multiple parameterized models, differing from one another in the reaction mechanisms that are included. By designing stimuli that maximize the difference between the candidate models' simulations of measurable

outputs, models that do not succeed in matching the outputs of experiments run under those stimuli can be eliminated.

The process of calibrating such models to match experimental outputs uses the data-based modeling approach widely practiced in systems biology. Maiwald and Timmer present a framework for modeling signal transduction pathways and metabolic networks based on available data from multiple experiments [2]. Focused on dealing with the often noisy and partially observed nature of the data coming from these types of systems, both deterministic and stochastic optimization routines are implemented within the framework. These routines are used to analyze the identifiability of model parameters from available data, generate predictions that can be experimentally tested using different parameters, and run statistical tests to enable qualitative comparison of alternative models that may exist for a system.

Hirmajer et al. also present an optimization framework for modeling networks in systems biology, taking into consideration the dynamic characterization of these networks that are commonly expressed through ordinary differential equations (ODEs) [3]. This consideration is embodied by the framework's ability to handle time-dependent decision variables, and performance analyses are carried out on sample problems that range in applications from bioreactor designs to drug-based patient therapy. In addition to the deterministic local optimization strategy, multiple alternative strategies are made available, including successive re-optimization and hybrid optimization, where the latter combines global stochastic and local deterministic solvers. This variety is meant to handle the nonconvexity associated with many optimization problems that arise in the context of networks studied in systems biology.

These types of software tools also exist for mathematically modeling more specific types of biological networks. Dilão and Muraro, for instance, propose a methodology for building genetic regulatory networks [4], which are responsible for dictating the expression level of genes within the cell to determine its phenotype and function. The operon model of Jacob and Monod is the particular protein-gene interaction implemented for this tool, which characterizes the activation or repression of a gene's transcription to be controlled by the proteins that bind to its regulatory sequences [5].

The tool is applied to modeling gene regulations that are involved in early development of *Drosophila*, which is a genus of small flies that are commonly referred to as fruit flies.

## Identifying model parameters

Characterizing a mathematical model requires quantitatively specifying the components included. This task is what parameter estimation is concerned with, as it aims to determine concentrations of involved species and rates of their chemical reactions that would allow the model to exhibit properties observed in the actual biochemical network. The optimization problem that solves for the model parameters that would minimize the difference between the observed data and the model outputs is often made difficult due to nonlinear relationships between the parameters and the outputs. Moreover, both the small amount of available experimental data and their varied sources add to the challenge.

The difficulty arising from the nonlinearity and the data limitations commonly takes the form of there existing multiple sets of parameters that allow the model outputs to closely match the observed data. Besides the nonlinearity possibly leading to isolated sets in parameter space that can successfully calibrate the model, Gutenkunst et al. examine the parameter spaces of biochemical network models to show large ranges of parameters within which selecting any parameter set does not notably alter the associated model's behavior [6].

Besides studies such as these that demonstrate through considering local sensitivities that system behavior is largely affected by only a few parameters, there are others that focus on identifying regions of parameter space and their shapes as they relate to behavioral changes. Coelho et al. offer a generic approach to identifying boundaries between regions in parameter space that relate to distinct behaviors [7]. Analogous to the magnitudes of sensitivity ranges as they pertain to local analyses, the concept of global tolerance is explored, together with the relationship that it shows against local performance. The concept is illustrated in modeling moiety-transfer cycles, which require values of the parameters to strictly remain within their boundaries to guarantee

certain phenotypical expressions.

Vilela et al. extend this concept of insensitivity, which has come to commonly be referred to as sloppiness, beyond values of model parameters to structures of models [8]. By allowing parameters that quantify the connections within a network to range across negative through positive values in the fitting process, ensembles of models are found that all match the experimental data reasonably well. This methodology of model identification is applied to generate models of the glycolytic pathway in *Lactococcus lactis*, a bacterium recently explored for its usage in treating Crohn's disease [9]. By suggesting plausible competing model structures, the methodology helps form a basis for designing experiments to be performed on the system to discriminate among the structures.

The idea that many mathematical models in systems biology inherently embody sloppiness is supported by a number of works such as ref. [10], in which Ashyraliyev et al. argue the difficulty of extracting dependable quantitative information from models that can be calibrated with many different sets of parameters to all match the experimental data equally well. Illustrating this concept by applying it to gene circuit models of early *Drosophila* embryos, they devote a part of their work to showing that using less noisy data does not lead to higher determinability of model parameters, and in turn conclude sloppiness to be a property of the model. Studies such as these leave open the question of how the types of experimental data gathered (i.e., the types of experiments performed) contribute to parameter identifiability, as explored by Apgar et al. in ref. [11].

## Experimental design for identifiability

Whether model parameters can be uniquely identified is dependent on what data is used in the calibration process. The ranges of parameters found in ref. [6], for example, are only as large as published when the observations of model behavior are made under a single set of experimental conditions [12]. Designing experiments for gathering the data most useful for parameter estimation is thus a field of active research. The optimization for this design process determines the experiments that would maximize

the information that the resulting data can provide about the parameters, while keeping in mind the constraints of costs and measurement feasibilities.

Bandara et al. apply this concept of optimal experimental design (OED) to a cell signaling model, constraining the types of experiments to ones that can be realistically performed [12]. They find that data gathered from optimally designed experiments are able to define much narrower ranges for the model's pharmacological and kinetic parameters than data gathered from intuitively designed, and therefore commonly performed, experiments. The positive results presented are heavily dependent on the types of allowed experiments being sufficient for extensively exploring the space of parameters of interest; this dependency may suggest the potential of OED to provide valuable information on experimental limits of parameter identification, and in turn meaningful levels of model abstraction.

The types of experiments that can be considered as being realistic certainly undergo change with the continued advancement of new experimental technologies. In addition to designing inputs that can be administered to a system, Mélykúti et al. investigate OED for experiments that involve altering the initial conditions of the species tracked in the system and the reaction rates with which they undergo dynamic changes, under the assumption that developing procedures such as RNAi technology could make possible such experiments [13]. They apply their design methodologies to discriminating between two different models of signal processing that is carried out by *Dictyostelium* amoebae, which are widely used to study fundamental cellular processes in cell and developmental biology.

Donckels et al. emphasize the significance of the times at which experimental measurements are taken in whether or not candidate models can be successfully discriminated [14]. They focus on offering a methodology for determining optimal sampling times that is useful even when discrimination needs to be performed on models that have loosely estimated parameters. They approach the task in two stages; the first stage designs an experiment to improve parameter accuracy for all the competing models simultaneously, then the second stage designs an experiment to optimally discriminate among them. The methodology is applied to determine the most likely

set of reactions that is involved in the functioning of glucokinase, an enzyme that regulates carbohydrate metabolism in vertebrae by sensing the level of glucose present.

The importance of parameter identifiability in model-based studies is made apparent by how investigative reports of such studies rarely fail to include the dependence of their results on the choice of parameters used in their mathematical models. One way in which studies aim to enhance the validity of their findings is through performing their analyses on ensembles of models. Tasseff et al., for example, tackle the issue of parameter uncertainty in their prostate cancer model by using an ensemble of 107 models to conduct their studies [15]. They draw on the quantified amount of certainty they have about individual parameters to explain qualitative physical mechanisms of the system that can be expected to have small or large effects on system behavior as a whole, which is also a common practice of model-based studies that are meant to extract as much knowledge as possible from available quantitative information.

## Efforts to enhance identifiability

Although richness in the data used to estimate the parameters, potentially from collecting data under numerous experimental conditions, is essential for increasing parameter identifiability, notable efforts are under way to enhance the identifiability even under the types of data that are already currently available [16]. These efforts use additional information arising from biological insights to further constrain their optimization problems in estimating parameters. The main challenge faced by these approaches lie in the confidence with which their respective insights can be viewed as reasonable biological assumptions.

An approach that involves augmenting the data used in the optimization problem is proposed in ref. [17]. Using available measurements of the network under consideration, Gadkar et al. generate estimates of all protein concentrations and reaction rates, which are functions of the parameters of interest, through a state regulator approach. Successfully identifying the parameters from the data augmented with these estimates is found to depend on optimally selecting the measurements initially used to generate the estimates.

Locke et al. augment the cost function to be minimized in the optimization problem with terms that represent the model's ability to match notable qualitative features of the actual system that are observed in the experimental process [18]. In order to balance the effects of the various terms included in the cost function, each term is weighted to contribute equally under tolerable deviation from its respective observation. Minimizing this augmented cost function leads to a parameterization of the model that can reproduce several of the notable features considered.

Reducing the dimensionality of the optimization problem is the approach taken in ref. [19]. Bentele et al. divide the model into subunits, with each subunit consisting of components of the model that share the same level of data quality and abundance. Investigating the model's response to changes in individual parameters helps in both performing the process of subdivision iteratively and revealing network characteristics of modularity and robustness, where most species' concentrations seem to be sensitive only to a subset of parameters.

## Robustness in biochemical networks

The property of robustness, proposed by this work as the biological constraint to add when optimizing for the model parameters, is viewed as one of the fundamental characteristics of biological systems [20]. Its commonly accepted definition, that "robustness is a property that allows a system to maintain its functions against internal and external perturbations [21]," reflects its systems-based conceptualization. And as biochemical networks are increasingly studied as interrelated components at the systems level, many reports probe the mechanistic sources of observed biological robustness.

Based on the argument that proper functioning of biochemical networks requires their key features to be robust, Barkai and Leibler propose a quantitative model for bacterial chemotaxis, a widely-studied signal transduction network, which consistently exhibits a key feature of chemotaxis over a wide range of model parameter values [22]. By demonstrating this robust model's ability to match experimental observations, they emphasize the potential for robustness investigations to allow ad-

vances in systems-level understanding of complex biochemical networks.

Morohashi et al. also argue that robustness is an essential property of biochemical networks, particularly in those that are involved in carrying out cellular processes conserved across multiple species [23]. They take two models of one such process, the cell cycle, and compare their robustness to parameter variations. By designating the more robust model as the more plausible one, they suggest that mechanisms giving rise to network structures that cause such robustness to parameter variations are more likely to have protected conserved cellular processes against evolutionary mutations.

## 2.2 Cancer immunotherapy design

### Nonlinear dynamics of immunogenic tumors

Tumors evoke immune responses, and such immunogenicity has long been shown through historical data of the immune system's effect on cancer progression. Genetic defects that cause cancer lead to the production of abnormal proteins, to which the immune system responds to. This response is exhibited through a change in the concentration of effector cells, which are the white blood cells mainly responsible for the body's cell-mediated immunity against foreign materials. The dynamics of the interaction between effector cells and tumor cells point to how immune responses are generated.

Kuznetsov et al. explore these dynamics through studying how an immunogenic tumor's growth affects the response of CTL, which recruit other white blood cells to surround and destroy the cancerous cells that they recognize to be antigenic [24]. The study is conducted through formulating a mathematical model of the CTL response, calibrated to observations from experiments performed on mice. The model attempts to capture tumor cells' evasion of the immune response, their exhibition of a dormant state, and their growth's reaction to the immune response being present.

A property of the immune response that is also of interest is how effector cells are distributed through normal and tumor tissues across different organs in the body.

Zhu et al. develop a mathematical model that simulates this effector cell distribution for various animal species [25]. By fitting their model to experimental biodistribution data of mice, rats, and humans, they find that effector cells being highly retained in normal tissue serves as an explanation for their limited interaction with tumor tissue. Based on this model-driven hypothesis, they suggest research in immunotherapy to pursue the direction of decreasing the adhesion rate of effector cells to normal tissue, possibly through mechanisms that can limit effector cell interaction with normal tissue and can in turn retain their concentrations in the systemic circulation.

The use of bifunctional antibodies that bind to both effector and tumor cells is explored for this purpose of leading effector cells more effectively to tumor cells. Friedrich et al. include these antibody dynamics into a mathematical model of the tumor-immune system to enable a systematic analysis of how these antibodies affect effector cell distribution [26]. Using the model enables them to quantitatively solve for optimal conditions under which tumor therapy using these antibodies should be performed. By showing that the model predicts successful therapy to be highly dependent on these physiological conditions being met, they offer a possible reason for limited success thus far in using these bifunctional antibodies for directed effector cell therapy.

A recent application of such antibody usage is reported by Bühler et al. in ref. [27] for treating prostate cancer. Drawing on the prostate-specific membrane antigen's potential of being a tumor target, they use a bifunctional antibody that expresses specificity to this membrane antigen and the effector cell antigen CD3 to promote directed killing of prostate cancer cells. More generally, Reusch et al. explore the potency of a different bifunctional antibody that expresses specificity to epidermal growth factor receptor (EGFR) as well as to CD3, based on EGFR being commonly overexpressed in a number of cancer types [28]. They propose the additional cytolytic activity against the tumor cells, provided by the effector cells that are transported to them by the antibody, as a reason for greater effectiveness of the antibody compared to other monoclonal antibodies that only bind to EGFR with the purpose of inhibiting tumor cell proliferation.

## Immunotherapy of tumor-immune interaction

Triggering the immune system to respond to tumor is the underlying premise of immunotherapy. However, as abnormal proteins produced by cancerous cells are often tolerated by the system, such direct stimulation of immunity is difficult to achieve. Immunotherapy today thus focuses on supplying the very substance of the response itself (i.e., effector cells) into the system. Additionally suppliable are cytokines such as interleukin, which are proteins both produced by and that enhance the activity of effector cells.

Kirschner and Panetta integrate effector cells and cytokine IL-2 into a mathematical model of immunotherapy [29]. The model is used to study the dynamics between these therapeutic agents and tumor cells, attempting to find explanations for experimentally observed tumor oscillations and relapse. Such adoptive cellular therapy has been reported to potentially counter the tolerance of cancerous cells by the immune system, and the model helps define the circumstances under which successful immunotherapy can in turn be accomplished.

One type of cancer for which immunotherapeutic interventions are being actively explored is malignant melanoma. A large portion of these explorations has been devoted to therapies involving IL-2, particularly for advanced stages of the disease. However, better patient survival has not widely been reported for IL-2 usage alone, leading to Halama et al.'s investigation into possible new immunotherapeutic agents for alternative or combined therapy [30]. They point out the move of cancer therapy towards combination therapy, which is particularly fueled by reports of therapeutic success for effective combinations for specific situations. This specificity is in line with the growing demand of personalized therapeutics for disease treatment as a whole.

Immunotherapeutic strategies, particularly those using methodologies that target specific antigens using antibodies, lend well to personalized medicine. Schilsky discusses the potential of such immunotherapy and targeted therapy to be the future of cancer treatment, especially as it has long been accepted that tumor progression and patterns often vary noticeably from patient to patient [31]. He notes the shortage

of clinically meaningful biomarkers, which can serve as a prediction for whether or not a patient will respond positively to a certain type of targeted therapy, to be a hindrance to developments in personalized immunotherapy. He attributes the difficulty of biomarker identification to both the mutation-prone biology of cancer and the challenges faced by research conducted in the realm of regulatory affairs.

Well-observed mutations caused by cancer can become the very targets of immunotherapy, such as mutations in Ras proteins studied by Lu et al. in ref. [32]. The study builds on their earlier development of a method that uses whole yeast for immunotherapy, which is based on yeast's molecular patterns being close to those that are commonly regarded as pathogens by the body's immune system. They show lung cancer cells being effectively controlled through this whole-yeast immunotherapy in mice, and mention that the relevance of their work to human lung cancer is dependent on whether analogies to human tumor progression can be drawn from mouse tumor studies. This relevance is further investigated by Wansley et al., testing in mice how plausible such yeast-based therapy is for inducing immune responses against carcinoembryonic antigen, which has been observed on many occasions for human carcinomas [33].

## BCG immunotherapy in superficial bladder cancer

Bladder cancer, typically found in older adults, is often diagnosed at an early stage. Treatment for early-stage, or superficial, bladder cancer is likely to involve a combination of surgical and immunotherapeutic procedures. Used prior to surgery for shrinking tumor size or following surgery for preventing tumor recurrence, immunotherapeutic agents are generally administered to the bladder intravesically through the urethra. A common treatment is one that uses BCG, a bacterium most well-known as a vaccine against tuberculosis.

In an effort to clarify the dynamics of BCG therapy for superficial bladder cancer, Bunimovich-Mendrazitsky et al. provide a mathematical model for the tumor-immune interaction involved [34]. The model is calibrated to observations from in vitro, mouse, and human experiments, bringing to light the difficult task of determining the ideal

strength of BCG administration for eradicating the tumor without causing severe side effects. The studies performed also help identify externally controllable factors that may potentially improve therapeutic results.

Frequency of relapses and patients developing resistance have been reported as major shortcomings of BCG immunotherapy for bladder cancer. Mangsbo et al. find CpG DNA, derived from bacterial DNA, to be more effective than BCG against more aggressive forms of bladder cancer [35]. Their study also suggests the usefulness of binding directly to toll-like receptors, which are proteins that activate immune cell responses by recognizing molecules that are commonly found on pathogens. Kresowik and Griffith, even as they review the application of BCG immunotherapy for bladder cancer, support this claim by mentioning the lower effectiveness of immunotherapy measures that do not perform this direct binding [36].

The relationship between BCG immunotherapy and tumor necrosis factor-related apoptosis-inducing ligand (TRAIL), a protein that has been found to induce apoptosis in tumor cells but not in normal cells, is highlighted by Kresowik and Griffith in ref. [36] and further reviewed in ref. [37]. Therapies that target the TRAIL receptor are under active research for various cancers including the non-small cell lung cancer, where combination therapies using this target along with other therapeutics are being explored to maximize the recognition of these therapies by the receptor; some of these combinations under investigation include the use of EGFR inhibitors or agents that target other apoptosis regulator proteins such as B-cell lymphoma 2 [38].

The promising performance of BCG immunotherapy in treating superficial bladder cancer has triggered the study of recombinant BCG strains as well. Chade et al. evaluate one such strain, rBCG-S1PT, and find that it induces a stronger cellular immune response than wild-type BCG [39]. Arnold et al. examine bladder cancer immunotherapy using another strain that expresses interferon-gamma [40], which is a cytokine that is produced by effector cells as a part of the body's innate immune response and is known to promote effector cell activity. Through murine experiments, they identify a principal cause for the stronger immune response to lie in the recombinant strain's ability to recruit more effector cells into the bladder than the

strain without interferon-gamma, in turn prolonging survival significantly under even a low-dose treatment regimen.

## Optimal therapeutic protocols in cancer immunotherapy

Fighting cancerous cells that evade the immune system inevitably calls for a stronger immunotherapeutic intervention. An increase in the amount of therapeutic agent administered, however, may lead to an increase also in toxic side effects of therapy. Furthermore, if multiple agents are used simultaneously, their combined effect on the system will most likely not be simply additive of their individual effects. Determining treatment protocols that can maximize the benefits of therapy while limiting its costs is in turn a problem of optimization.

Cappuccio et al. formulate such an optimization problem for determining immunotherapy protocols [41]. The formulation is applied to the tumor-immune system model of Kirschner and Panetta [29], aiming to identify the administration timing and dosage of CTL and IL-2 for successful therapy. Decreasing the tumor size by the end of the treatment time period is but one of several factors that are balanced, which include ensuring that the tumor does not grow too large over the entire treatment period and refraining from clustering administration timings to be too close to one another.

Following the recent discovery of interleukin-21 (IL-21), Cappuccio et al. also study optimal protocol determination specific to IL-21 immunotherapy in ref. [42]. Approved for Phase 1 clinical trials for patients with metastatic melanoma and renal cell carcinoma, IL-21 is a cytokine that plays a key role in the immune response to tumor by enhancing the cytotoxicity of effector cells. The optimization is set up to balance IL-21's benefits for tumor killing against noteworthy costs that include possible inhibition of effector cells and toxicity. The mathematical model used is that of murine melanoma, as IL-21 has been explored for its potential use and toxicity in mice. As a direction for future research, they point to the possibility of using real-time feedback information on the most recent tumor state for improved treatment design.

Another immunotherapeutic strategy involves the adoptive transfer of dendritic cells, which have been found to efficiently induce CTL. Ludewig et al. attempt to better understand the dynamics between these dendritic cells and CTL to enhance their potential for usage in treating human cancer [43]. Their work uses a mathematical model representing the dynamics, fit to mice data, and identifies parameters of the model that seem to have the largest effects on the level of CTL response caused by dendritic cells. Relating these significant parameters to physical phenomena that they represent, the study reveals that the recipient having high avidity effector cells, coupled with the optimal delivery regimen being applied, is essential for successful immunotherapy using dendritic cell transfer.

Optimal scheduling for interventions is also found to significantly affect the performance of combined immunotherapy using both dentritic cells and CTL [44]. Park et al. find such scheduling to be necessary to ensure successful immunotherapy in the context of the subtle interplay between gradual immune response induction by dendritic cells and rapid decrease of the transferred CTL population. This type of combined therapy is often also referred to as vaccine therapy, as the function of the dendritic cells can be viewed as priming, or preparing, the CTL to become of high avidity to effectively kill tumor cells. Dendritic cell vaccination is also being actively explored in further combination with radiotherapy, following initial reports of radiotherapy enhancing the efficacy of vaccine therapy in murine studies [45].

## Mixed immunotherapy and chemotherapy of tumors

As another form of nonsurgical therapy, chemotherapy has been found to treat many types of tumors effectively. Its potency is nevertheless clouded by abundant reports of both mild and severe side effects that can possibly lead to serious complications for the cancer patient. Growing interest in immunotherapy is to a great extent due to its potential complementary use with chemotherapy. Such mixed therapy holds the hope of consequently limiting the amount of often highly toxic chemotherapeutic drugs from being administered.

By developing a mathematical model of tumor response to such combination ther-

apy, de Pillis et al. analyze the effectiveness of implementing both chemotherapeutic and immunotherapeutic protocols in fighting cancer [46]. Analysis is mainly performed through numerical simulations of the model, which is calibrated to observations from both human and mouse experiments. Building on previous findings regarding the benefits of combining vaccine therapy with chemotherapy [47], the model also captures the effects of vaccine therapy on the tumor system.

Chareyron and Alamir implement the concept of feedback control into de Pillis et al.'s mathematical model of mixed therapy to enable the design of reactive treatments [48]. They perform their studies on the model that has been fit to human data, and also show the difficulty of guaranteeing successful therapy under only one of immunotherapy or chemotherapy. Their results indicating the benefit of using feedback-based treatments as a way to handle modeling uncertainties is also noteworthy, as is the applicability of their feedback scheme to models other than the one of combined immunotherapy and chemotherapy that they use in their work. Such applicability cannot be ignored in assessing newly developed methodologies for computational studies of tumor treatment models, as these models are subject to continuous development and change themselves.

As one example of this change, Karev et al. include the characteristic of tumor heterogeneity into their mathematical modeling of therapy [49]. Variability in tumor progression and treatment efficacy have long been attributed to such heterogeneity, which consists of tumor cells within a single population showing noticeably different survival and development patterns. The type of heterogeneity that they explore is parametric heterogeneity, where they allow parameter values of their model to vary within continuous distributions around mean values. As the model itself is of tumor therapy using oncolytic viruses, they particularly subject the parameters that relate to cell reproduction, cell death, and cell infection by the virus to this parametric heterogeneity in performing their studies.

The relevance of such viral therapy to immunotherapy is highlighted in ref. [50], where the possibility of their combined usage for cancer treatment is explored. The ability of oncolytic viruses to preferentially select and destroy tumor cells has un-

doubtedly brought much attention to their possible role in therapy, despite their limitations that include their rejection by the innate immune system. Bridle et al. look to overcome this major hurdle by utilizing the difference in the strength of primary and secondary immune responses of a patient; they propose preimmunizing, or vaccinating, the tumor patient against a tumor antigen, then designing oncolytic viruses with that very antigen to subsequently administer to that patient. Testing their hypothesis on mice, they found the interval between the vaccination and the viral administration to play a major role in determining therapeutic success, which is a realm that potentially can be extensively investigated using mathematical modeling and optimization.

## 2.3 Robust optimization

### Methodology of robust optimization

An optimal choice is defined as a decision that is as effective or functional as possible in fulfilling an objective at hand. Mathematical optimization in turn refers to the mathematical procedures taken to arrive at this choice. Robust optimization is a methodology that characterizes the manner in which these procedures are taken; it is applied when there is uncertainty in the data being used in the procedures [51].

Consider $f(\mathbf{x}, \mathbf{p})$, a mathematical function whose output is a scalar value that is dependent on $\mathbf{x}$, a vector of inputs, and $\mathbf{p}$, a vector of parameters. The optimization problem of finding the $\mathbf{x}$ that minimizes $f(\mathbf{x}, \mathbf{p})$ is

$$\min_{\mathbf{x}} f(\mathbf{x}, \mathbf{p}) \ . \tag{2.1}$$

Robust optimization aims to solve Eqn. (2.1) under circumstances in which there exist uncertainties in $\mathbf{x}$ and $\mathbf{p}$; i.e. the input vector can be any $\hat{\mathbf{x}} = \mathbf{x} + \triangle\mathbf{x}$ instead of $\mathbf{x}$, and the parameter vector can be any $\hat{\mathbf{p}} = \mathbf{p} + \triangle\mathbf{p}$ instead of $\mathbf{p}$. The optimization problem of finding the $\mathbf{x}$ that minimizes $f(\hat{\mathbf{x}}, \hat{\mathbf{p}})$ can be expressed as

$$\min_{\mathbf{x}} f(\mathbf{x} + \triangle\mathbf{x}, \mathbf{p} + \triangle\mathbf{p}) \ . \tag{2.2}$$

## Worst-case robust optimization

For $\triangle\mathbf{x}$ and $\triangle\mathbf{p}$ arising from uncertainty sets $U^{\triangle\mathbf{x}}$ and $U^{\triangle\mathbf{p}}$, respectively, worst-case robust optimization is concerned with finding the $\mathbf{x}$ that minimizes the largest value that $f(\hat{\mathbf{x}}, \hat{\mathbf{p}})$ takes on, given that $\triangle\mathbf{x}$ and $\triangle\mathbf{p}$ can be any member of $U^{\triangle\mathbf{x}}$ and $U^{\triangle\mathbf{p}}$, respectively. This optimization problem can be expressed as

$$\min_{\mathbf{x}} \max_{\triangle\mathbf{x}\in U^{\triangle\mathbf{x}}, \triangle\mathbf{p}\in U^{\triangle\mathbf{p}}} f(\mathbf{x} + \triangle\mathbf{x}, \mathbf{p} + \triangle\mathbf{p}) \ . \tag{2.3}$$

For linear, quadratic, and semidefinite optimization problems with uncertainty sets taking on particular geometric shapes in data space (e.g., ellipsoidal or box), Ben-Tal and Nemirovski illustrate the possibility of reformulating Eqn. (2.3), or its close approximation, into computationally tractable convex optimization problems [51]. Such reformulation has been applied to solving problems in a wide range of fields in engineering; for instance, Luo surveys its impact, combined with advances made in interior point methods, on signal processing and digital communication [52], while Atamtürk and Zhang specialize it for network flow and design problems in operations research [53].

## Nonconvex worst-case robust optimization

Many, if not most, problems of interest that hold real-world applications have difficulty fitting into the realm of convex, or even approximately convex, problems. For these nonconvex problems, developments in worst-case robust optimization can generally be divided into two categories.

The first of these categories applies the reformulation techniques mentioned above to convexified approximations of nonconvex problems. Such approximations most often take the form of linearization, in which a nonlinear function is approximated around a point using a substitute linear function. An example of this approach is

an optimization method presented by Zhang, where the worst-case of the linearized problem is optimized [54]. This method is thus appropriate for nonlinear problems that can be closely approximated by their linearizations.

The second category of approaches to nonconvex worst-case robust optimization searches for the worst-case by sampling multiple instances of the uncertainties within $U^{\triangle \mathbf{x}}$ and $U^{\triangle \mathbf{p}}$. The sampling is integrated into iterative methods for nonconvex optimization, using information from the approximate worst-case found for the solution $\mathbf{x}$ at one iteration to decide on the update to be made to $\mathbf{x}$ for the subsequent iteration. An example of this approach, outside of this work, is an optimization method presented by Bertsimas et al., where the updates are made to find an $\mathbf{x}$ for which the largest $f(\hat{\mathbf{x}}, \mathbf{p})$ among all of the sampled instances of $U^{\triangle \mathbf{x}}$ is made as small as possible [55].

## Robust optimization in network calibration

The robustness of a biochemical network's behavior to parameter variations is a common topic of exploration, where methods for quantifying the degree of this robustness is an active field of research (e.g., ref. [56]). Such exploration, however, is often performed for sets of parameters that have already been found through optimization to plausibly calibrate the network to match available data. Consequently, it is difficult to find works that explicitly incorporate the robustness to parameter variations into either the optimization problem formulation or the solution process.

Parameter estimation methods are most likely to be characterized as being robust, not due to their application of the robust optimization methodology, but rather due to their ability, analyzed post-optimization, to consistently reach similar estimates for various uncertainties that may exist in the available data. In other words, robustness in this context is used as a measure of how successfully a given parameter estimation method can select one parameter set among many candidates, and can therefore be regarded as being synonymous to the method's effectiveness in carrying out the calibration. For instance, Rodriguez-Fernandez et al. evaluate their parameter estimation method, a hybrid of deterministic optimization and stochastic

search methods, by considering how well it can estimate model parameters when the available data are subject to various amounts of noise [57].

## Robust optimization in therapy design

The field of radiation oncology actively applies robust optimization to planning proton radiation treatments. The nature of these treatments involves many stages of planning and execution, and sources of uncertainty are likely to exist at almost every stage. For example, imaging procedures and scanning beams that deposit the radiation are subject to errors in placement and strength. The notable effects of such setup uncertainties on therapeutic success have been reported for numerous types of cancer, including focal liver tumors [58] and prostate cancer [59]. Unkelbach et al. account for uncertainties in the patient's body position and the proton range of each beam used by setting up the objective function in their optimization to be dependent on random variables that parameterize the amount of treatment dose delivered [60]. They also present a worst-case formulation for considering range uncertainties in an earlier work [61], which is applied by Pflugfelder et al. to a clinical case beyond simple tumor geometry [62].

As is the case for parameter estimation, methods used for designing medical treatments are also often referred to as being robust for their ability to consistently reach what is suspected to be the global minimum in their respective objective functions. For instance, Mahfouz et al. present a method for registering three-dimensional knee implant models onto two-dimensional images, which they regard to be a robust method based on their application of simulated annealing successfully yielding the global minimum without being halted at various local minima [63].

# Chapter 3

# Robust Calibration of Biological Network Model

## 3.1 Motivation

As biological systems are being increasingly investigated from the network point of view, there is an escalated demand for computational models that quantitatively characterize those systems. For instance, as dysregulation of apoptosis is found to contribute to various autoimmune diseases and cancer [64], developing comprehensive and predictive models of the signaling pathways for apoptosis may help quantify the effectiveness of candidate treatment targets.

Using data to define the parameters that characterize the model is an essential yet time-consuming task in building models. When signaling pathways are modeled using differential equations derived from chemical kinetics, the parameters subject to estimation are chemical reaction rates and initial concentrations of species. The task then is to determine the set of parameter values that would enable the model to generate outputs that match experimental measurements.

A major barrier to successful model calibration is the limited amount of available experimental data. Therefore, it is often the case that multiple sets of parameters produce outputs that match the measured data, and it is difficult to determine which of these many parameter sets correspond to a model that will be predictive. Because

many parameters must be estimated from only a small amount of data, additional biologically reasonable constraints that keep the estimation problem tractable may be especially useful in order to select the correct parameter set among many.

Based on the intuition that a critical behavior of a system is not likely to have been designed to react dramatically to ubiquitous noise and varying surrounding conditions that cause small parameter changes, a robust optimization method for biological network calibration is provided here. The performance of the method is examined by applying it to a model typical of an individual layer of MAPK pathways [65].

The MAPK pathway has been identified as being a part of numerous signal transduction pathways, many of which have long been under heavy investigation for their relevance to cancer research. In particular, components of the EGFR pathway have been targeted for cancer therapy, with malignant cells of multiple myeloma patients being found to over-express a number of EGFRs and their ligands [66].

## 3.2 Model calibration procedures

### 3.2.1 Methods

Suppose a biological system is described by the interaction of three species, $X_1$, $X_2$, and $X_3$, represented through the chemical reaction equation

$$X_1 + X_2 \underset{k_2}{\overset{k_1}{\rightleftharpoons}} X_3 \ . \tag{3.1}$$

Letting $[X_i]$ denote the concentration of $X_i$, the concentration change of $X_1$, $X_2$, and $X_3$ over time can be modeled using the system of ODEs derived from Eqn. (3.1)

$$\frac{d}{dt}\begin{bmatrix} [X_1] \\ [X_2] \\ [X_3] \end{bmatrix} = \begin{bmatrix} k_2[X_3] - k_1[X_1][X_2] \\ k_2[X_3] - k_1[X_1][X_2] \\ -k_2[X_3] + k_1[X_1][X_2] \end{bmatrix} \ . \tag{3.2}$$

The simulated output $\mathbf{y}$ of the model is the concentration of one or more species at designated points in time. For instance, if measured data for $X_2$ is available at times

$t_1, t_2, ..., t_5$, then

$$\mathbf{y} = \begin{bmatrix} [X_2](t_1) \\ [X_2](t_2) \\ . \\ . \\ . \\ [X_2](t_5) \end{bmatrix} . \tag{3.3}$$

Calibrating the model refers to finding a set of model parameters that would cause the model to output a $\mathbf{y}$ that is close to the corresponding measured data

$$\mathbf{y_m} = \begin{bmatrix} [X_2]_\mathbf{m}(t_1) \\ [X_2]_\mathbf{m}(t_2) \\ . \\ . \\ . \\ [X_2]_\mathbf{m}(t_5) \end{bmatrix} , \tag{3.4}$$

where $[X_2]_\mathbf{m}$ is the measured counterpart of the simulated $[X_2]$.

In this work, the parameter set $\mathbf{p}$ that is subject to calibration is taken to be either the set of reaction rate constants associated with the chemical reaction given by Eqn. (3.1)

$$\mathbf{p} = \begin{bmatrix} k_1 \\ k_2 \end{bmatrix} , \tag{3.5}$$

or the set of initial concentrations of the species

$$\mathbf{p} = \begin{bmatrix} [X_1]_0 \\ [X_2]_0 \\ [X_3]_0 \end{bmatrix} . \tag{3.6}$$

The algorithm for a standard approach to model calibration is given below, followed

by the algorithm for the proposed robust approach.

### Standard approach

The standard approach to calibrating the model is as follows:

**Step 1.** Guess at a solution, $\mathbf{p}^0$. If $\|\mathbf{y}(\mathbf{p}^0) - \mathbf{y_m}\|^2 < tolerance$, then return $\mathbf{p}^0$ as the solution and terminate. Else, set $s = 1$.

**Step 2.** Select the $\check{\mathbf{d}}^s$ that is expected to minimize $\|\mathbf{y}(\mathbf{p}^{s-1} + \check{\mathbf{d}}^s) - \mathbf{y_m}\|^2$ using the Gauss-Newton method for nonlinear least-squares.

**Step 3.** Search for the $a$ that minimizes $\|\mathbf{y}(\mathbf{p}^{s-1} + a\check{\mathbf{d}}^s) - \mathbf{y_m}\|^2$; set $\mathbf{d}^s = a\check{\mathbf{d}}^s$ and $\mathbf{p}^s = \mathbf{p}^{s-1} + \mathbf{d}^s$.

**Step 4.** If $\|\mathbf{y}(\mathbf{p}^s) - \mathbf{y_m}\|^2 < tolerance$, then return $\mathbf{p}^s$ as the solution and terminate. Else, set $s = s + 1$ and go back to Step 2.

### Robust approach

For calibrating the model using the robust approach, define the neighborhood of $\mathbf{p} = (p_1, p_2, ..., p_n)$, $N(\mathbf{p})$, to consist of all vectors $\mathbf{q} = (q_1, q_2, ..., q_n)$, such that each $q_i$ is within the interval $[(1-\delta)p_i, (1+\delta)p_i]$, $0 \leq \delta \leq 1$. Let $Q(\mathbf{p})$ be a subset of $N(\mathbf{p})$, made up of $\mathbf{p}$ and 100 vectors randomly sampled from $N(\mathbf{p})$, based on a uniform distribution across $[(1-\delta)p_i, (1+\delta)p_i]$, $\forall i$. Then the robust approach is as follows:

**Step 1.** Guess at a solution, $\mathbf{p}^0$. Assemble $Q(\mathbf{p}^0)$ from $N(\mathbf{p}^0)$, and choose $\mathbf{q}^0 \in Q(\mathbf{p}^0)$ under which $\|\mathbf{y}(\mathbf{q}^0) - \mathbf{y_m}\|^2$ is maximized. If $\|\mathbf{y}(\mathbf{q}^0) - \mathbf{y_m}\|^2 < tolerance$, then return $\mathbf{p}^0$ as the solution and terminate. Else, set $s = 1$.

**Step 2.** Select the $\check{\mathbf{d}}^s$ that is expected to minimize $\|\mathbf{y}(\mathbf{q}^{s-1} + \check{\mathbf{d}}^s) - \mathbf{y_m}\|^2$ using the Gauss-Newton method for nonlinear least-squares.

**Step 3.** Search for the $a$ that minimizes the maximum of $\|\mathbf{y}(\mathbf{p}^{s-1}+a\check{\mathbf{d}}^s)-\mathbf{y_m}\|^2$ among all $Q(\mathbf{p}^{s-1} + a\check{\mathbf{d}}^s)$ assembled from $N(\mathbf{p}^{s-1} + a\check{\mathbf{d}}^s)$; set $\mathbf{d}^s = a\check{\mathbf{d}}^s$ and $\mathbf{p}^s = \mathbf{p}^{s-1} + \mathbf{d}^s$.

**Step 4.** Assemble $Q(\mathbf{p}^s)$ from $N(\mathbf{p}^s)$, and choose $\mathbf{q}^s \in Q(\mathbf{p}^s)$ under which $\|\mathbf{y}(\mathbf{q}^s) - \mathbf{y_m}\|^2$ is maximized. If $\|\mathbf{y}(\mathbf{q}^s) - \mathbf{y_m}\|^2 < tolerance$, then return $\mathbf{p}^s$ as the solution and terminate. Else, set $s = s + 1$ and go back to Step 2.

### 3.2.2 Model

To illustrate the effectiveness of the proposed robust approach, its performance is compared to that of the standard approach for calibrating a model typical of an individual layer of MAPK pathways [65]. The model, based on [67] and as communicated by [65], is represented through the chemical reaction equations

$$\begin{aligned} F + A &\underset{d_1}{\overset{a_1}{\rightleftharpoons}} F : A \xrightarrow{k_1} F + A' \\ F + A' &\underset{d_2}{\overset{a_2}{\rightleftharpoons}} F : A' \xrightarrow{k_2} F + A'' \\ R + A'' &\underset{d_3}{\overset{a_3}{\rightleftharpoons}} R : A'' \xrightarrow{k_3} R + A' \\ R + A' &\underset{d_4}{\overset{a_4}{\rightleftharpoons}} R : A' \xrightarrow{k_4} R + A \ . \end{aligned} \tag{3.7}$$

$A$ is representative of a protein that can be modified by enzyme $F$ to become $A'$, which can in turn be modified by $F$ again to become $A''$; enzyme $R$ can unmodify $A''$ into $A'$, which it can further unmodify into $A$ [65].

Letting $[X]$ denote the concentration of species $X$, Eqns. (3.7) gives rise to the ODEs

$$
\begin{aligned}
\frac{d}{dt}[F] &= -a_1[F][A] + (d_1 + k_1)[F:A] - a_2[F][A'] + (d_2 + k_2)[F:A'] \qquad (3.8)\\
\frac{d}{dt}[A] &= -a_1[F][A] + d_1[F:A] + k_4[R:A']\\
\frac{d}{dt}[F:A] &= a_1[F][A] - (d_1 + k_1)[F:A]\\
\frac{d}{dt}[A'] &= k_1[F:A] - a_2[F][A'] + d_2[F:A'] + k_3[R:A''] - a_4[R][A'] + d_4[R:A']\\
\frac{d}{dt}[F:A'] &= a_2[F][A'] - (d_2 + k_2)[F:A']\\
\frac{d}{dt}[A''] &= k_2[F:A'] - a_3[R][A''] + d_3[R:A'']\\
\frac{d}{dt}[R] &= -a_3[R][A''] + (d_3 + k_3)[R:A''] - a_4[R][A'] + (d_4 + k_4)[R:A']\\
\frac{d}{dt}[R:A''] &= a_3[R][A''] - (d_3 + k_3)[R:A'']\\
\frac{d}{dt}[R:A'] &= a_4[R][A'] - (d_4 + k_4)[R:A'] \ .
\end{aligned}
$$

The `ode15s` function in MATLAB [68] is used to numerically integrate Eqns. (3.8) to simulate the concentration changes of the species over time. The measured data

$$
\mathbf{y_m} = \begin{bmatrix} [A'']_{\mathbf{m}}(t_1) \\ [A'']_{\mathbf{m}}(t_2) \\ \cdot \\ \cdot \\ \cdot \\ [A'']_{\mathbf{m}}(t_T) \end{bmatrix} \qquad (3.9)
$$

is imitated by running the model with a set of nominal reaction rates and initial concentrations (Table 3.1), adopted from [65], then taking the concentration of $A''$ at specified points in time. $T$ is number of time points at which the data is considered available, and $t_1$ through $t_T$ are evenly spaced between 0 and 200 seconds.

Table 3.1: **Nominal parameter values used in Eqns. (3.8).**

| Parameter | Value | Units |
|---|---|---|
| $a_1,\ a_2$ | 0.1 | $\mu M^{-1}s^{-1}$ |
| $d_1,\ d_2$ | 0.033 | $s^{-1}$ |
| $k_1,\ k_2$ | 16 | $s^{-1}$ |
| $a_3,\ a_4$ | 5 | $\mu M^{-1}s^{-1}$ |
| $d_3,\ d_4$ | 0.5 | $s^{-1}$ |
| $k_3,\ k_4$ | 0.3 | $s^{-1}$ |
| $[F]_0$ | 20 | $\mu M$ |
| $[A]_0$ | 34 | $\mu M$ |
| $[F:A]_0$ | 0 | $\mu M$ |
| $[A']_0$ | 0 | $\mu M$ |
| $[F:A']_0$ | 0 | $\mu M$ |
| $[A'']_0$ | 0 | $\mu M$ |
| $[R]_0$ | 16 | $\mu M$ |
| $[R:A'']_0$ | 0 | $\mu M$ |
| $[R:A']_0$ | 0 | $\mu M$ |

## 3.3 Application to estimating reaction rates

The set of reaction rate constants associated with Eqns. (3.7) was first designated to be the parameter set subject to calibration

$$\begin{aligned} \mathbf{p} &= (a_1, d_1, k_1, a_2, d_2, k_2, a_3, d_3, k_3, a_4, d_4, k_4) \\ &= (p_1, p_2, ..., p_{12}) \ , \end{aligned} \tag{3.10}$$

with the goal of estimating the values in the nominal parameter set

$$\begin{aligned} \mathbf{p_m} &= (0.1, 0.033, 16, 0.1, 0.033, 16, 5, 0.5, 0.3, 5, 0.5, 0.3) \\ &= (p_{\mathbf{m}1}, p_{\mathbf{m}2}, ..., p_{\mathbf{m}12}) \end{aligned} \tag{3.11}$$

as closely as possible from the measured data $\mathbf{y_m}$.

For $T = 5$, 100 initial guesses for $\mathbf{p}^0 = (p_1^0, p_2^0, ..., p_{12}^0)$ were randomly sampled from a uniform distribution across the interval $[(0.2)p_{\mathbf{m}i}, (1.8)p_{\mathbf{m}i}]$, $\forall i$. Each $\mathbf{p}^0$ was used to initialize the standard approach and the robust approach. The robust approach was

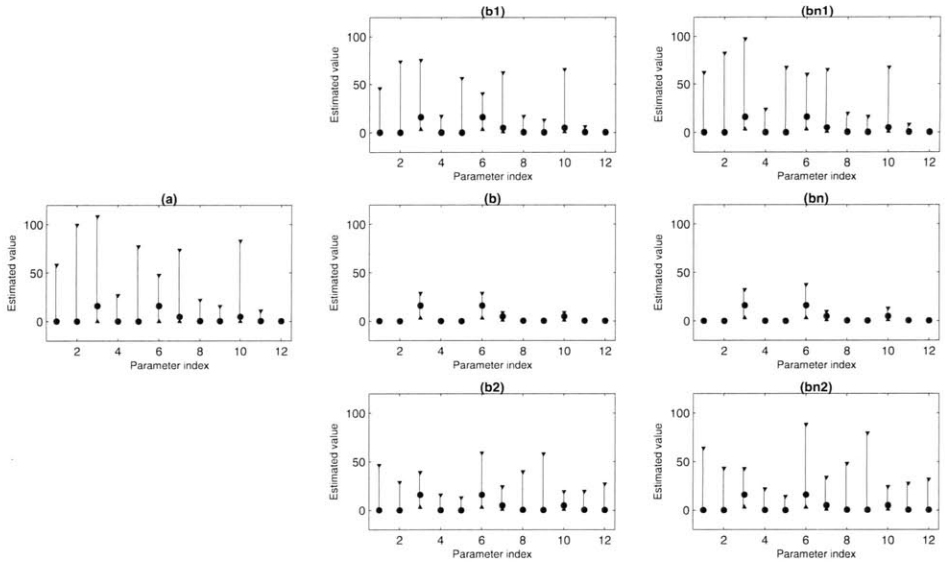


Figure 3-1: **Ranges of estimated reaction rates when $\mathbf{T = 5}$** for (a) standard approach, (b) robust approach with $\delta = 0.1$, (b1) robust approach with $\delta = 0.025$, and (b2) robust approach with $\delta = 0.4$. Analogous ranges from using noisy $\mathbf{y_m}$ for (bn) robust approach with $\delta = 0.1$, (bn1) robust approach with $\delta = 0.025$, and (bn2) robust approach with $\delta = 0.4$. The black dots represent nominal parameter values.

further varied by trying $\delta$ values of 0.025, 0.1, and 0.4. (a), (b), (b1), and (b2) of Fig. 3-1 show the ranges of terminating values given by the approaches when provided with these 100 initial guesses for $\mathbf{p}^0$.

Then for $\delta = 0.1$, the performances of the two approaches for different numbers of data points $T$ were compared. (a), (b), (aa), and (bb) of Fig. 3-2 show the results for $T$ values of 5 and 25, using the same 100 initial guesses for $\mathbf{p}^0$.

As measurements are often subject to noise, $\mathbf{y_m}$ was then imitated more realistically by introducing random perturbations to the $\mathbf{y}(\mathbf{p_m})$ generated by the model. From a normal distribution across $[(0.8)\mathbf{y}(\mathbf{p_m})_i, (1.2)\mathbf{y}(\mathbf{p_m})_i]$, $\forall i$, 100 different vectors to be regarded as $\mathbf{y_m}$ were sampled. The combined results from repeating the experiments above for each noisy $\mathbf{y_m}$ are shown in (bn), (bn1), (bn2), and (bbn) of Figs. 3-1 and 3-2, analogous to (b), (b1), (b2), and (bb), respectively.

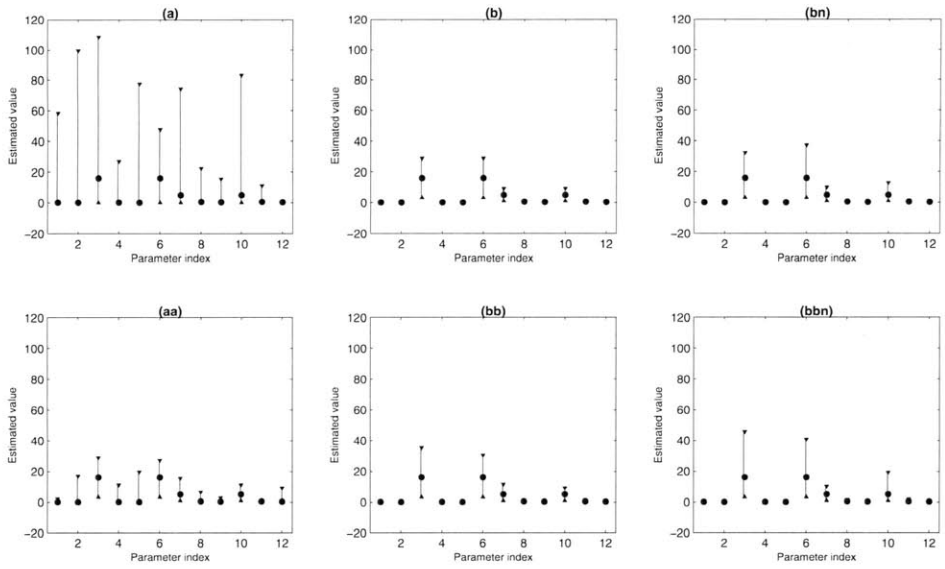


Figure 3-2: **Ranges of estimated reaction rates when $\delta = 0.1$** for (a) standard approach with $T = 5$, (b) robust approach with $T = 5$, (aa) standard approach with $T = 25$, and (bb) robust approach with $T = 25$. Analogous ranges from using noisy $\mathbf{y_m}$ for (bn) robust approach with $T = 5$ and (bbn) robust approach with $T = 25$. The black dots represent nominal parameter values.

## 3.4 Application to estimating initial concentrations

The set of initial concentrations of the species was then designated to be the parameter set subject to calibration

$$\begin{aligned} \mathbf{p} &= ([F]_0, [A]_0, [F:A]_0, [A']_0, [F:A']_0, [A'']_0, [R]_0, [R:A'']_0, [R:A']_0) \quad (3.12) \\ &= (p_1, p_2, ..., p_9) \ , \end{aligned}$$

with the nominal parameter set now being

$$\begin{aligned} \mathbf{p_m} &= (20, 34, 0, 0, 0, 0, 16, 0, 0) \quad (3.13) \\ &= (p_{\mathbf{m}1}, p_{\mathbf{m}2}, ..., p_{\mathbf{m}9}) \ . \end{aligned}$$

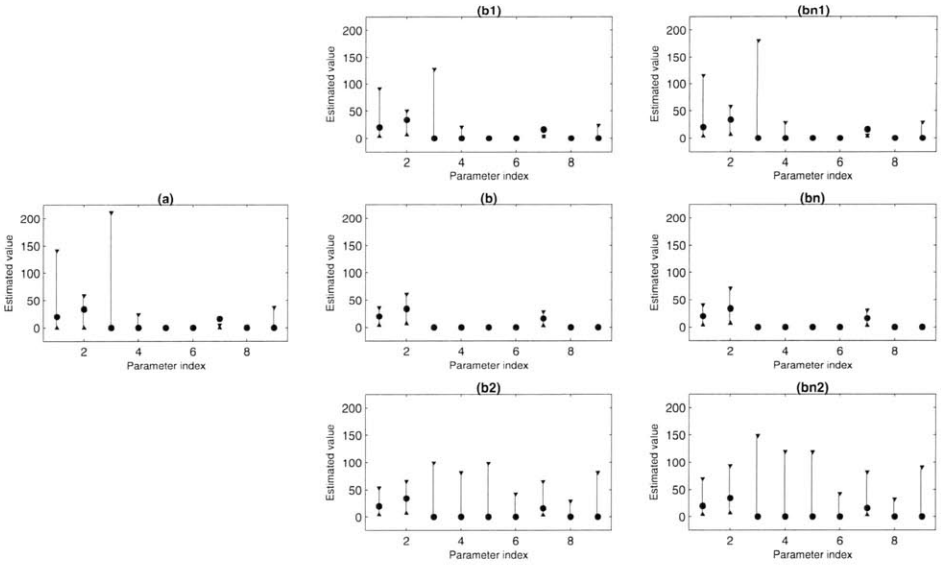


Figure 3-3: **Ranges of estimated initial concentrations when $\mathbf{T = 5}$** for (a) standard approach, (b) robust approach with $\delta = 0.1$, (b1) robust approach with $\delta = 0.025$, and (b2) robust approach with $\delta = 0.4$. Analogous ranges from using noisy $\mathbf{y_m}$ for (bn) robust approach with $\delta = 0.1$, (bn1) robust approach with $\delta = 0.025$, and (bn2) robust approach with $\delta = 0.4$. The black dots represent nominal parameter values.

As in the case of estimating reaction rates, 100 initial guesses for $\mathbf{p}^0 = (p_1^0, p_2^0, ..., p_9^0)$ were randomly sampled from a uniform distribution across the interval $[(0.2)p_{\mathbf{m}i}, (1.8)p_{\mathbf{m}i}]$, $\forall i$, for $T = 5$. Once again, each $\mathbf{p}^0$ was used to initialize the standard approach and the robust approach, with the robust approach being further varied by trying $\delta$ values of 0.025, 0.1, and 0.4. (a), (b), (b1), and (b2) of Fig. 3-3 show the ranges of terminating values given by the approaches when provided with these 100 initial guesses for $\mathbf{p}^0$.

Then similarly, the performances of the two approaches for different numbers of data points $T$, for $\delta = 0.1$, were also compared. (a), (b), (aa), and (bb) of Fig. 3-4 show the results for $T$ values of 5 and 25, using the same 100 initial guesses for $\mathbf{p}^0$.

Finally, the experiments above were repeated for each noisy $\mathbf{y_m}$ that had earlier been specified for estimating reaction rates. The combined results are shown in (bn), (bn1), (bn2), and (bbn) of Figs. 3-3 and 3-4, analogous to (b), (b1), (b2), and (bb), respectively.

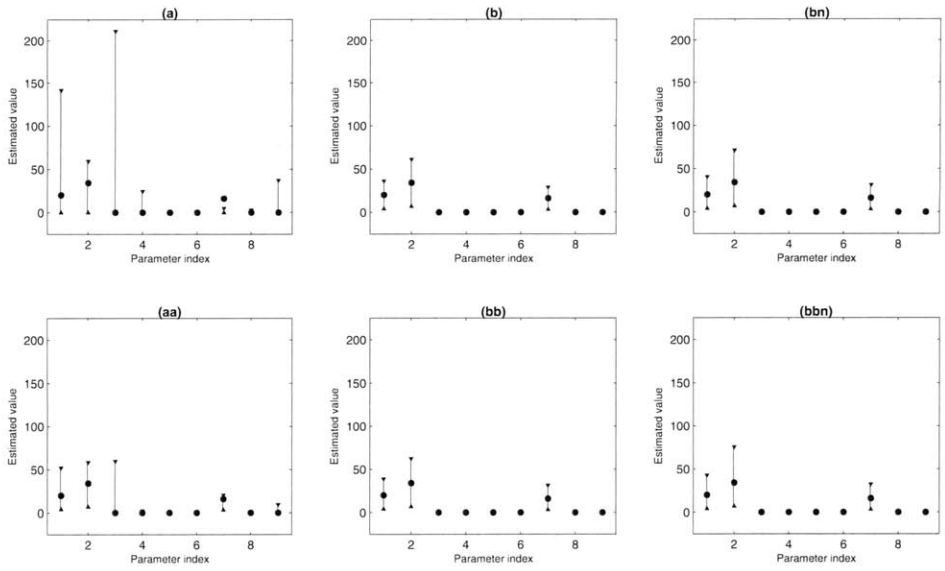


Figure 3-4: **Ranges of estimated initial concentrations when $\delta = 0.1$** for (a) standard approach with $T = 5$, (b) robust approach with $T = 5$, (aa) standard approach with $T = 25$, and (bb) robust approach with $T = 25$. Analogous ranges from using noisy $\mathbf{y_m}$ for (bn) robust approach with $T = 5$ and (bbn) robust approach with $T = 25$. The black dots represent nominal parameter values.

## 3.5 Discussion

The results obtained suggest the usefulness of including robustness as a constraint when calibrating biological networks. When using 5 data points in time for calibration ($T = 5$), (a) and (b) of Figs. 3-1 and 3-3 show that requiring the output to be robust to each parameter varying up to 10% of its nominal value ($\delta = 0.1$) improves the preciseness of fit, as 100 identical initial guesses lead to much narrower ranges of terminating values using the robust approach. Moreover, comparing (b) of Figs. 3-1 and 3-3 with their respective (bn) reveals the relative insensitivity of the robust terminating values to noise in the measured data.

(b1) and (b2) of Figs. 3-1 and 3-3 illustrate the performance of the robust approach as $\delta$ is varied. As $\delta$ decreases below 0.1, the performance nears that of the standard approach, which can be characterized as an instance of the robust approach with $\delta$ being 0. As $\delta$ increases above 0.1, the performance also deteriorates, possibly due to the output not being robust to more than approximately 20% variation in the

nominal values. (bn1) and (bn2) of Figs. 3-1 and 3-3 show that these observations also hold in cases where the data used to calibrate the model is noisy.

Figs. 3-2 and 3-4 demonstrate the change in the relative effectiveness of the robust approach over the standard approach as the number of data points $T$ is varied ($\delta$ is set to 0.1). For $T = 5$, the robust approach in (b) exhibits a higher preciseness of fit than the standard approach in (a). However, this effect diminishes as more data become available; for $T = 25$, the performance of the standard approach in (aa) is more comparable to that of the robust approach in (bb). And once again, (bn) and (bbn) of Figs. 3-2 and 3-4 report similar findings under the presence of noise in the data. This phenomenon is consistent with the notion that successful calibration is limited by the small amount of available data, and with the purpose of adding robustness as an additional constraint when many parameters must be estimated from much less data.

Nevertheless, significant challenges still lie ahead. For instance, it is difficult to fully survey the neighborhood of a parameter set only through sampling. Although there may exist neighboring sets that cause a notably different output, such a case will be overlooked by the current robust approach if the output is deemed robust to all the sampled neighbors. Another issue lies in deciding the value of $\delta$, i.e. the degree of robustness that is to be enforced as a constraint in the calibration process. The model provided here seems to suggest a $\delta$ of approximately 0.1, but that is at most specific to this model and only determinable from knowing the nominal parameter set to begin with. Furthermore, there is no guarantee that the output of a system will not also be robust to variation in incorrect parameters.

The existing challenges indicate the directions in which to move forward to make the robust approach useful for a wider variety of biological networks. For a network whose proper functioning is expected to exhibit robustness to small perturbations in its parameters, the performance of the method must be systematically categorized for successive levels of robustness required. Such classification would call for a more precise mathematical representation of the robustness constraints to better represent the neighborhood of a parameter set. Applying the analytically refined constraints

to the robust optimization process would then allow further progress to be made in calibrating biological networks.

More specifically, with regards to progress in systematic categorization of robustness levels, the focus need not be tied to looking only at uniform levels of robustness (i.e., the same $\delta$ for all model parameters) as done in this study. Gutenkunst et al.'s work in ref. [6] shows a wide variation in the ranges that fit parameters can belong to. The ranges, furthermore, do not necessarily lie along the the axes of the parameters themselves; eigenanalysis is performed to find meaningful combinations of parameters along which the ranges lie. That parameter combinations are worth considering is also supported by Coelho et al.'s work in ref. [7], which attempts to identify regions of parameter space in terms of their shapes and boundaries in relating them to distinct model behaviors. As the regions found to contain parameter sets exhibiting similar behavior do not match hypercubes that lie perfectly along the individual parameters, using the idea of carving out a neighborhood around solutions for the robust approach developed here may require a more sophisticated way of characterizing the boundaries within which the robust approach should sample.

The robust approach also has the potential to take part in experimental design for increasing identifiability. For instance, Bandara et al. report in ref. [12] that their optimally designed experiments produce data that can be used to estimate model parameters down to much narrower ranges than those estimated using data from conventional experiments. Incorporating the robust approach here would start by first asking whether the optimal experiments designed can lead to useful data even if there were to exist experimental and measurement uncertainties. This type of incorporation of the approach is also conceivable for work done by Donckels et al. in ref. [14], which determines the optimal sampling times for experiments that are performed for model discrimination. The work takes into account that parameters of models are uncertain up to considerable ranges, but does not explicitly take into account that the sampling may not occur at the exact times designed.

Requiring robustness in model calibration is a way of constraining the optimization problem at hand to favor solutions that are robust to fluctuations in model

parameters. With other efforts for selecting parameter estimates from many possible sets of values actively under way, it would interesting to see how the robustness requirement relates to those other approaches. For example, Gadkar et al. take a data augmentation approach to enhance identifiability in ref. [17], by generating estimates of additional values of concentrations and rates, which are functions of model parameters being estimated, to add to the data to be used for calibration. Would adding the robustness requirement in the context of such augmented data serve to effectively further constrain the optimization problem? Also, Bentele et al. reduce the dimensionality of the optimization problem in ref. [19] for better identifiability. Can or should robustness to uncertainty or fluctuation in pre-reduced parameters be taken into account prior to the reduction?

Through these possible future studies, the methodology of robust model calibration introduced in this work can offer a different way to view and analyze the existing knowledge regarding biological systems. In particular, networks can be systematically probed using the robust approach, possibly in combination with the other approaches mentioned above, to enable a deeper understanding about the reasons behind the robustness or lack of robustness associated with systems that have evolved to exist today. The application of the robust approach to parameter estimation may indeed only be the very beginning of how robust optimization can take part in systems biological research from here onwards.

# Chapter 4

# Robust Protocol Design for Cancer Immunotherapy

## 4.1 Motivation

Cancer immunotherapy is receiving increased attention as both an alternative and a complementary strategy for treating cancer patients. It focuses on stimulating the inherent immune system of a patient to fight against the proliferation of cancerous cells. With immunotherapy being an active field of research, proteins such as mesothelin are being closely studied not only as a biomarker for pancreatic adenocarcinomas and other histologic types of tumors, but also as a potential target for inducing the immune response in pancreatic cancer patients [69].

Cappuccio et al. formulate an optimization problem for determining the administration timing and dosage of therapeutic agents for successful therapy [41], applied to the tumor-immune system model of Kirshner and Panetta [29]. Yet how robust is the performance of the determined protocol in fighting the tumor? Will the protocol remain effective (i.e., will the minimized objective function value remain small) even if there exist errors in the timing and the dosage of the administrations? What if the parameters specified in the quantitative model, such as the initial state and the reaction rates, do not exactly match those of the actual system, due either to inherent inaccuracy of the model or variation among patients?

Although advances in immunology are leading to the proposal of novel immunotherapeutic strategies [70], the use of dynamic quantitative models of immune system response to cancer in determining the details of therapeutic protocols remains notably limited. This scarcity may be a reflection of the fear of unexpected variability in the success of model-designed protocols in combating tumor, across different patients as well as between the model and the actual system being treated. Fig. 4-1A schematically represents such a scenario; under realistic discrepancies between the model tumor system and the actual tumor system, coupled with expected administrative imprecision in delivering the immunotherapeutic protocol as designed, a protocol that is designed to optimally treat the model tumor may not necessarily perform well in treating the actual tumor.

In an effort to enhance the effectiveness of using quantitative models for treatment design despite the existence of such discrepancies, a method for model-based determination of immunotherapeutic protocols under uncertainties in model accuracy and treatment administration is introduced here. The robust optimization method is provided in the context of the immunotherapy model of Bunimovich-Mendrazitsky et al., which exhibits a continuous-dose administration of BCG into the tumor-immune system [34]. Results show that under uncertainties, the robustly determined protocol outperforms the protocol determined through a standard optimization method in decreasing the tumor size over the course of the treatment, as shown in Fig. 4-1B. The advantage of using the robust method in designing treatment protocols is then also examined for the immunotherapy model of Cappuccio et al. introduced above, which exhibits discrete-dose administrations of CTL and IL-2 [41]. CTL and IL-2 continue to be subjects of widespread investigation for their use in immunotherapy for cancers such as glioblastoma [71, 72].

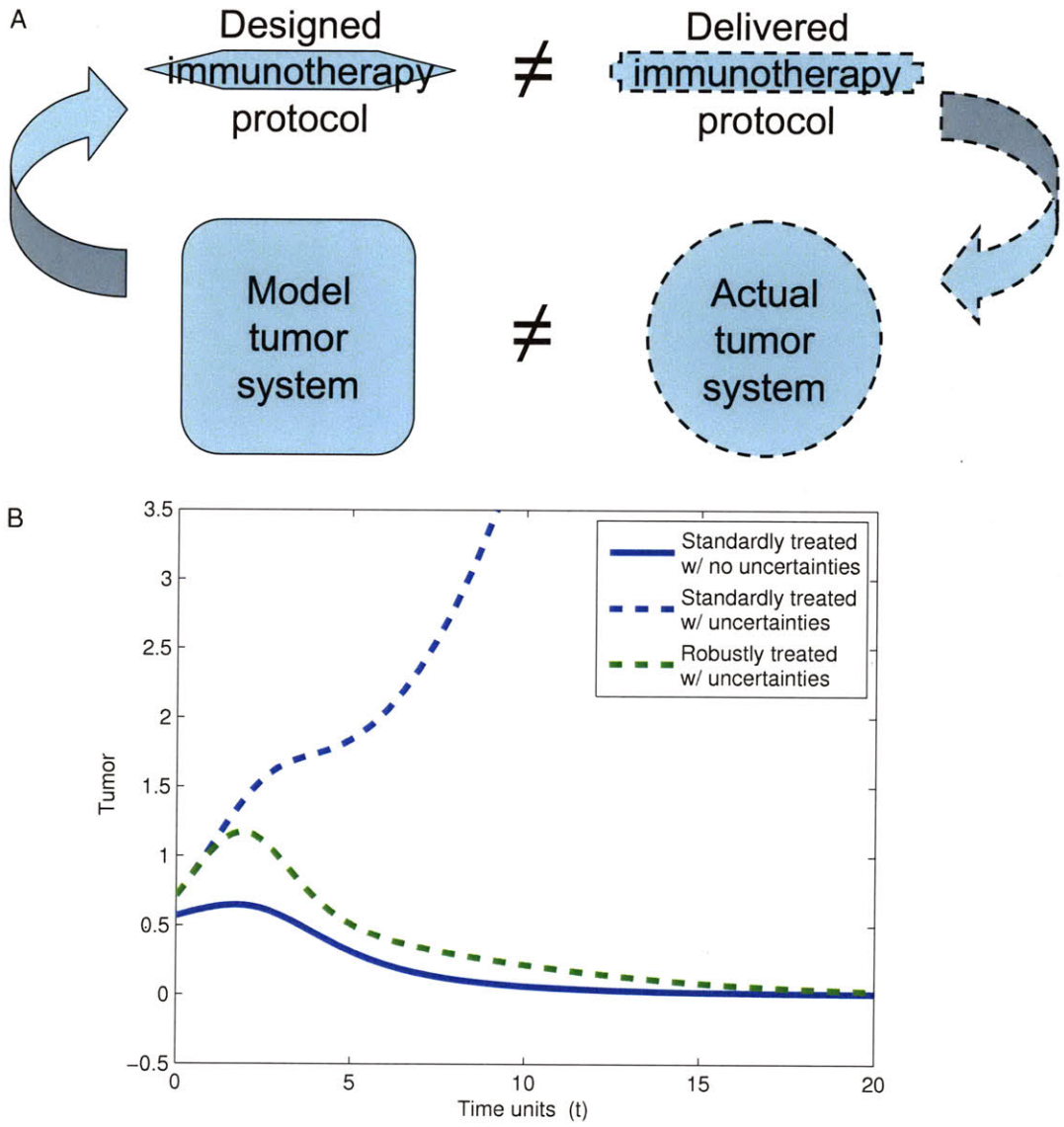


Figure 4-1: **Considering uncertainties when designing immunotherapeutic protocols.** (A) Schematic representation of uncertainties in model-based protocol design. (B) Tumor size under standardly designed protocol for BCG immunotherapy when no uncertainties are present (solid blue), under standardly designed protocol when uncertainties are present (dashed blue), and under robustly designed protocol when uncertainties are present (dashed green).

## 4.2 Therapeutic design procedures

### 4.2.1 Continuous-dose therapy using BCG

This work uses the following ODE model presented by Bunimovich-Mendrazitsky et al. in ref. [34]:

$$\begin{aligned}
\frac{dB}{dt} &= B(-1 - p_1 E - p_2 T_u) + b \\
\frac{dE}{dt} &= E(-\mu + p_4 B - p_5 T_i) + \alpha T_i \\
\frac{dT_i}{dt} &= -p_3 E T_i + p_2 B T_u \\
\frac{dT_u}{dt} &= T_u(-p_2 B + r[1 - \beta T_u]) \ .
\end{aligned} \tag{4.1}$$

$B$, $E$, $T_i$, and $T_u$ represent concentrations of BCG, effector cells, tumor cells infected with BCG, and tumor cells uninfected by BCG, respectively. The effects covered by the model include encounters between BCG, effector cells, and tumor cells, which lead to BCG infection of tumor cells, effector cell recruitment, and immune response activation. In addition to tumor cell destruction and effector cell inactivation, net mortalities of the cells, as well as logistic tumor growth, are also included in the model. The nominal values of the model parameters that represent these effects, as well as initial amounts of each cell type at the initiation of therapy, are shown in Table 4.1 [34]. The values here are in dimensionless form as used in ref. [34], based on a time scale of $[(0.1)^{-1} days]$ and a cell count scale of $[(10^6) cells]$. This work uses these adimensional values for model simulations, and the numerical results presented and discussed for this model are accompanied by these scalings for clarity.

Table 4.1: **Nominal parameter values used in Eqns. (4.1).**

| Parameter | Value | Description |
|---|---|---|
| $\mu$ | 0.41 | Mortality of effector cells / net mortality of BCG |
| $p_1$ | 1.25 | Loss of BCG by encounter with effector cells |
| $p_2$ | 0.285 | Infection of uninfected tumor cells with BCG |
| $p_3$ | 1.1 | Destruction of infected tumor cells by encounter with effector cells |
| $p_4$ | 0.12 | Encounter of effector cells with BCG (immune response activation) |
| $p_5$ | 0.003 | Effector cell inactivation by encounter with infected tumor cells |
| $\alpha$ | 0.52 | Stimulation of effector cell recruitment by infected tumor cells |
| $\beta$ | 0.0155 | Inverse of carrying capacity of tumor cells |
| $r$ | 0.12 | Growth rate of tumor cells |
| $B_0$ | 0.02 | Initial amount of BCG |
| $E_0$ | 0.04 | Initial amount of effector cells |
| $T_{i0}$ | 0.01 | Initial amount of tumor cells infected with BCG |
| $T_{u0}$ | 0.56 | Initial amount of tumor cells uninfected with BCG |

The values shown are adimensional estimates used in ref. [34], based on a time scale of $[(0.1)^{-1} days]$ and a cell count scale of $[(10^6) cells]$.

$b$ represents the constant rate at which BCG is administered, and is in turn the

decision variable of the optimization problem. The objective function to be minimized, $F(b)$, is a combination of the following $\varrho_j(b)$ for $j = 1, 2, 3$:

$\varrho_1(b)$: Final amount (at time $\tau$) of tumor cells
$\varrho_2(b)$: Tumor cells through time
$\varrho_3(b)$: Total amount of BCG administered .

Specifically, for the system in Eqns. (4.1) behaving under a protocol $b$,

$$\varrho_1(b) = T_i(\tau) + T_u(\tau) \tag{4.2}$$
$$\varrho_2(b) = \int_0^\tau [T_i(t)]^2 \, dt + \int_0^\tau [T_u(t)]^2 \, dt \tag{4.3}$$
$$\varrho_3(b) = b\tau \ . \tag{4.4}$$

Each $\varrho_j(b)$ is weighted by its associated $u_j$; i.e.,

$$F(b) = \textstyle\sum_j u_j \varrho_j(b), \quad u_j = 1/\varrho_j(b^{nom}) \ , \tag{4.5}$$

where

$$b^{nom} = 1.9 \tag{4.6}$$

is the nominal $b$ (based on Fig. 4 of ref. [34]) used to set the weights. $\tau = 20$ and the values for $\beta$, $r$, $B_0$, $E_0$, $T_{i0}$, and $T_{u0}$ in Table 4.1 are also based on Fig. 4 of ref. [34]. This problem setup is implemented in MATLAB; the `ode15s` function [68] is used to numerically integrate Eqns. (4.1).

The types of uncertainty considered are as follows:

1) BCG is administered at some rate $\hat{b} = b + z_1 b$, where $-1 \leq z_1 \leq 1$, instead of at $b$.
2) At $t = 0$, the initial concentrations of the species are $\hat{B_0} = B_0 + z_2 B_0$, $\hat{E_0} =$

$E_0 + z_3 E_0$, $\hat{T_{i0}} = T_{i0} + z_4 T_{i0}$, and $\hat{T_{u0}} = T_{u0} + z_5 T_{u0}$, where $-1 \leq z_k \leq 1$ for $k = \{2, 3, 4, 5\}$, instead of $B_0$, $E_0$, $T_{i0}$, and $T_{u0}$, respectively.
3) $\beta = z_6$ and $r = z_7$, where $0.013 \leq z_6 \leq 0.022$ and $0.1 \leq z_7 \leq 0.45$ [34], instead of $\beta = 0.0155$ and $r = 0.12$.

The aim is thus to implement a robust optimization method to design protocols that would be effective across this range of uncertainties.

### Standard optimization procedure

The standard approach to finding the $b$ that minimizes $F(b)$ is as follows:
**Step 1.** Guess at a solution, $b^0$, and set $s = 1$.
**Step 2.** Select the $\check{d}^s$ that is expected to minimize $F(b^{s-1} + \check{d}^s)$ using Newton's method.
**Step 3.** Search for the $a$ that minimizes $F(b^{s-1} + a\check{d}^s)$; set $d^s = a\check{d}^s$ and $b^s = b^{s-1} + d^s$.
**Step 4.** If $d^s < tolerance$, then return $b^s$ as the solution and terminate. Else, set $s = s + 1$ and go back to Step 2.

### Robust optimization procedure

For using the robust approach, a region of potential uncertainties is specified. This specification is carried out by first designating a numerical range that each uncertain model parameter is expected to belong to. Then, taking each of those ranges to span a particular dimension of uncertainty, a resulting hypercube of uncertainties, where each corner represents an intersection of the ends of all the ranges considered, is created to be the region of potential uncertainties to be accounted for in the optimization process.

Specifically, define $U(b)$ as the space of uncertainty that consists of all vectors $\mathbf{z} = (z_1, z_2, ..., z_7)$, such that $-M_m \leq z_m \leq M_m$ for $m = \{1, ..., 5\}$, where $0 \leq M_m \leq 1$, and $M_{lm} \leq z_m \leq M_{um}$ for $m = \{6, 7\}$, where $0 \leq M_{l6} \leq 0.0155$, $M_{u6} \geq 0.0155$, $0 \leq M_{l7} \leq 0.12$, and $M_{u7} \geq 0.12$. Let $Z(b)$ be a subset of $U(b)$, made up of $\mathbf{z} = (0, 0, 0, 0, 0, 0.0155, 0.12)$ and $n$ vectors additionally sampled from $U(b)$. Then

the robust approach is as follows:

**Step 1.** Guess at a solution, $b^0$, and set $s = 1$.

**Step 2.** Assemble $Z(b^{s-1})$ from $U(b^{s-1})$.

**Step 3.** Choose $\mathbf{z}^{s-1} \in Z(b^{s-1})$ under which $F(b^{s-1})$ is maximized.

**Step 4.** Select the $\check{d}^s$ that is expected to minimize $F(b^{s-1} + \check{d}^s)$ under $\mathbf{z}^{s-1}$ using Newton's method.

**Step 5.** Search for the $a$ that minimizes the maximum of $F(b^{s-1} + a\check{d}^s)$ among being under all $Z(b^{s-1} + a\check{d}^s)$ assembled from $U(b^{s-1} + a\check{d}^s)$; set $d^s = a\check{d}^s$ and $b^s = b^{s-1} + d^s$.

**Step 6.** If $d^s < tolerance$, then return $b^s$ as the solution and terminate. Else, set $s = s + 1$ and go back to Step 2.

Unless otherwise stated, this work specifies $U(b)$ used in the robust procedure with $M_m = 0.25$ for $m = \{1, ..., 5\}$, $M_{l6} = 0.013$, $M_{u6} = 0.022$, $M_{l7} = 0.1$, and $M_{u7} = 0.45$, and chooses the $n$ members of $Z(b)$ within the iterations of the algorithm to be $\mathbf{z}$ made up of every combination of $z_1 = \{-M_m, M_m\}$, $z_2 = \{-M_m, M_m\}$, $z_3 = \{-M_m, M_m\}$, $z_4 = \{-M_m, M_m\}$, $z_5 = \{-M_m, M_m\}$, $z_6 = \{M_{l6}, M_{u6}\}$, and $z_7 = \{M_{l7}, M_{u7}\}$. This space, or region, of uncertainty $U(b)$ is referred to as the uncertainty hypercube of size 25% in discussing the results presented.

When the performance of a protocol $b$ against uncertainty scenarios sampled from within this hypercube is evaluated, $F(b)$ is computed under every member of $Z(b)$ drawn from $U(b)$. In addition to $\mathbf{z} = (0, 0, 0, 0, 0, 0.0155, 0.12)$, members of $Z(b)$ for this evaluation are chosen to be $\mathbf{z}$ made up of every combination of $z_1 = \{-p, p\}$, $z_2 = \{-p, p\}$, $z_3 = \{-p, p\}$, $z_4 = \{-p, p\}$, $z_5 = \{-p, p\}$, $z_6 = \{M_{l6}, M_{u6}\}$, and $z_7 = \{M_{l7}, M_{u7}\}$, for every 0.05 increment of $p$ between 0 and 0.25. The worst uncertainty scenario $\mathbf{z} \in Z(b)$ that maximizes $F(b)$ is designated as $\mathbf{z}^{worst}$.

### 4.2.2 Discrete-dose therapy using CTL and IL-2

This work uses the following ODE model of Kirschner and Panetta, as presented by Cappuccio et al. in ref. [29]:

$$\begin{aligned} \frac{dE}{dt} &= cT - \mu_2 E + \frac{p_1 E I_L}{g_1 + I_L} + \psi_1 \\ \frac{dT}{dt} &= r_2 T(1 - bT) - \frac{aET}{g_2 + T} \\ \frac{dI_L}{dt} &= \frac{p_2 ET}{g_3 + T} - \mu_3 I_L + \psi_2 \ . \end{aligned} \tag{4.7}$$

$E$, $T$, and $I_L$ represent concentrations of effector cells, tumor cells, and IL-2, respectively. Cappuccio et al. point out in ref. [41] that the model captures tumor oscillations and recurrence, which have both been observed experimentally [73–76]. The model covers the interactions between the cells by specifying how effector cells are stimulated by IL-2 and how IL-2 growth is affected by effector cells encountering with tumor cells, which also leads to the immune response. Additionally, the antigenicity and growth of the tumor and mortalities of the cells are also included in the model. The nominal values of the model parameters that represent these effects, as well as initial amounts of each cell type at the initiation of therapy, are shown in Table 4.2 [41]. The values here are in dimensionless form as used in ref. [41], based on a time scale of $[(0.18)^{-1} days]$ and a cell count scale of $[(10^9) cells]$ [29]. This work uses these adimensional values for model simulations, and the numerical results presented and discussed for this model are accompanied by these scalings for clarity.

Table 4.2: **Nominal parameter values used in Eqns. (4.7).**

| Parameter | Value | Description |
|---|---|---|
| $c$ | 1.009 | Antigenicity of tumor cells |
| $\mu_2$ | 0.0378 | Mortality of effector cells |
| $p_1$ | 0.044 | Stimulation of effector cells by IL-2 |
| $g_1$ | 0.02 | Michaelis constant for effector cell stimulation by Michaelis-Menten kinetics |
| $r_2$ | 0.123 | Growth rate of tumor cells |
| $b$ | 1 | Inverse of carrying capacity of tumor cells |
| $a$ | 0.018 | Strength of immune response |
| $g_2$ | $10^{-4}$ | Michaelis constant for tumor antigenicity by Michaelis-Menten kinetics |
| $p_2$ | 0.9 | IL-2 growth by effector cell encounter with tumor cells |
| $g_3$ | $10^{-5}$ | Michaelis constant for IL-2 growth by Michaelis-Menten kinetics |
| $\mu_3$ | 1.8 | Mortality of IL-2 |
| $E_0$ | $10^{-5}$ | Initial amount of effector cells |
| $T_0$ | $10^{-5}$ | Initial amount of tumor cells |
| $I_{L0}$ | $10^{-5}$ | Initial amount of IL-2 |

The values shown are adimensional estimates used in refs. [41] and [29], based on a time scale of $[(0.18)^{-1} days]$ and a cell count scale of $[(10^9) cells]$.

$\psi_1$ and $\psi_2$ represent the administrations of CTL and IL-2 (denoted therapeutic agent 1 and agent 2, respectively), and are defined as

$$\psi_k(t) = \begin{array}{ll} u_{ki}, & t = t_i \\ 0, & otherwise \end{array} , \tag{4.8}$$

for $k = \{1, 2\}$ and $i = \{1, ..., N\}$. $k$ indicates the therapeutic agent type, $i$ the $i$th administration, and $N$ the total number of administrations. An administration of agent $k$ at time $t_i$ thus affects the ODE system as a discrete impulse of height $u_{ki}$. The decision vector $\mathbf{x}$ of the optimization problem is in turn

$$\mathbf{x} = (t_1, ..., t_N, u_{11}, ..., u_{1N}, u_{21}, ..., u_{2N}) \ . \tag{4.9}$$

The objective function to be minimized, $G(\mathbf{x})$, is a combination of the following $\phi_j(\mathbf{x})$ for $j = 1, 2, 3, 4$:

$\phi_1(\mathbf{x})$: Final amount (at time $\tau$) of tumor cells
$\phi_2(\mathbf{x})$: Tumor cells exceeding a safety threshold amount ($T^{max}$) through time
$\phi_3(\mathbf{x})$: Total amount of therapeutic agent administered
$\phi_4(\mathbf{x})$: Penalty for close successive administrations [41] .

Specifically, for the system in Eqns. (4.7) behaving under a protocol $\mathbf{x}$,

$$\phi_1(\mathbf{x}) = T(\tau) \tag{4.10}$$

$$\phi_2(\mathbf{x}) = \int_0^\tau ([T(t) - T^{max}]_+)^2 \, dt \tag{4.11}$$

$$\phi_3(\mathbf{x}) = \sum_{k=1}^{2} \sum_{i=1}^{N} u_{ki} \tag{4.12}$$

$$\phi_4(\mathbf{x}) = \sum_{h=1}^{N-1} e^{-0.05(t_{h+1} - t_h)} \ . \tag{4.13}$$

Each $\phi_j(\mathbf{x})$ is weighted by its associated $w_j$; i.e.,

$$G(\mathbf{x}) = \sum_j w_j \phi_j(\mathbf{x}), \quad \begin{aligned} w_j &= 1/\phi_j(\mathbf{x}^{nom}),\ j = 1, 2, 4 \\ w_3 &= 0.0005/\phi_3(\mathbf{x}^{nom}) \ , \end{aligned} \tag{4.14}$$

where

$$\begin{aligned} \mathbf{x}^{nom} = (&106.8, 157.8, 164.9, 354.2, 475.3, \\ &10^{-4}, 10^{-4}, 10^{-4}, 10^{-4}, 10^{-4}, \\ &10^{-3}, 10^{-3}, 10^{-3}, 10^{-3}, 10^{-3}) \end{aligned} \tag{4.15}$$

is the nominal $\mathbf{x}$ used in ref. [41] to set the weights. $N$, $\tau$, and $T^{max}$ are taken from Fig. 4(c) of ref. [41] to be 4, 500, and $10^{-5}$, respectively. This problem setup is implemented in MATLAB; the `ode15s` function [68] is used to numerically integrate Eqns. (4.7).

The types of uncertainty considered are as follows:

1) For $k = \{1, 2\}$, therapeutic agent $k$ is administered as some $\hat{\psi}_k(t) = \psi_k(t) + z_k\psi_k(t)$, $-1 \leq z_k \leq 1$, instead of as $\psi_k(t)$.
2) Instead of $c$ and $a$ (which represent the antigenicity of the tumor and the strength of the immune response, respectively [41]), $\hat{c} = c + z_3 c$, $-1 \leq z_3 \leq 1$, and $\hat{a} = a + z_4 a$, $-1 \leq z_4 \leq 1$, respectively, are what make up the actual system.
3) The actual system is $z_5$ time units out of phase with the model, which can also be thought of as initiating the treatment at $t = z_5$ instead of at $t = 0$.

For minimizing $G(\mathbf{x})$ using the robust approach, define $U(\mathbf{x})$ as the space of uncertainty that consists of all vectors $\mathbf{z} = (z_1, z_2, z_3, z_4, z_5)$, such that $-M_m \leq z_m \leq M_m$ for $m = \{1, ..., 4\}$, where $0 \leq M_m \leq 1$, and $0 \leq z_5 \leq M_5$. Let $Z(\mathbf{x})$ be a subset of $U(\mathbf{x})$, made up of $\mathbf{z} = (0, 0, 0, 0, 0)$ and $n$ vectors additionally sampled from $U(\mathbf{x})$.

Unless otherwise stated, this work specifies $U(\mathbf{x})$ used in the robust procedure with $M_m = 0.25$ for $m = \{1, ..., 4\}$ and $M_5 = 110$, and chooses the $n$ members of $Z(\mathbf{x})$ within the iterations of the algorithm to be $\mathbf{z}$ made up of every combination of $z_1 = \{-M_m, M_m\}$, $z_2 = \{-M_m, M_m\}$, $z_3 = \{-M_m, M_m\}$, $z_4 = \{-M_m, M_m\}$,

and $z_5 = \{0, (0.25)M_5, (0.5)M_5, (0.75)M_5, M_5\}$. This space, or region, of uncertainty $U(\mathbf{x})$ is referred to as the uncertainty hypercube of size 25% in discussing the results presented.

When the performance of a protocol $\mathbf{x}$ against uncertainty scenarios sampled from within this hypercube is evaluated, $G(\mathbf{x})$ is computed under every member of $Z(\mathbf{x})$ drawn from $U(\mathbf{x})$. In addition to $\mathbf{z} = (0, 0, 0, 0, 0)$, members of $Z(\mathbf{x})$ for this evaluation are chosen to be $\mathbf{z}$ made up of every combination of $z_1 = \{-p, p\}$, $z_2 = \{-p, p\}$, $z_3 = \{-p, p\}$, $z_4 = \{-p, p\}$, and $z_5 = \{0, (0.25)M_5, (0.5)M_5, (0.75)M_5, M_5\}$, for every 0.05 increment of $p$ between 0 and 0.25. The worst uncertainty scenario $\mathbf{z} \in Z(\mathbf{x})$ that maximizes $G(\mathbf{x})$ is designated as $\mathbf{z}^{worst}$.

## 4.3 Application to treatment using BCG

The standard and robust approaches described in Sec. 4.2 were implemented to determine the continuous rate at which the bacterium BCG should be administered to treat superficial bladder cancer, using the ODE model of BCG immunotherapy from ref. [34]. In seeking the optimal rate of administration, the standard approach aims to minimize the value of the objective function in Eqn. (4.5), which accounts for both the negative effects of increased BCG levels and the successful elimination of tumor cells (see Sec. 4.2). The robust approach, instead of focusing solely on minimizing the objective function value, aims to do so even if BCG ends up being administered at a slightly different rate than intended, and possibly also with limited knowledge regarding the exact values of the model parameters used in the protocol design process.

The protocol designed using the standard approach, denoted $b^{stn}$, was $b^{stn} = 2.8375$ reduced units (equal to 283750 $cells\ days^{-1}$), associated with an objective function value of $F(b^{stn}) = 2.4659$. A trajectory of the total number of tumor cells as a function of time $[T(t) = T_i(t) + T_u(t)]$ under this protocol $b^{stn}$ is shown in Fig. 4-2A. The trajectory (solid blue line) shows that the therapy controls the number of tumor cells and leads to a rapid decrease in tumor size. Once under control, the

tumor shrinks monotonically with no net growth.

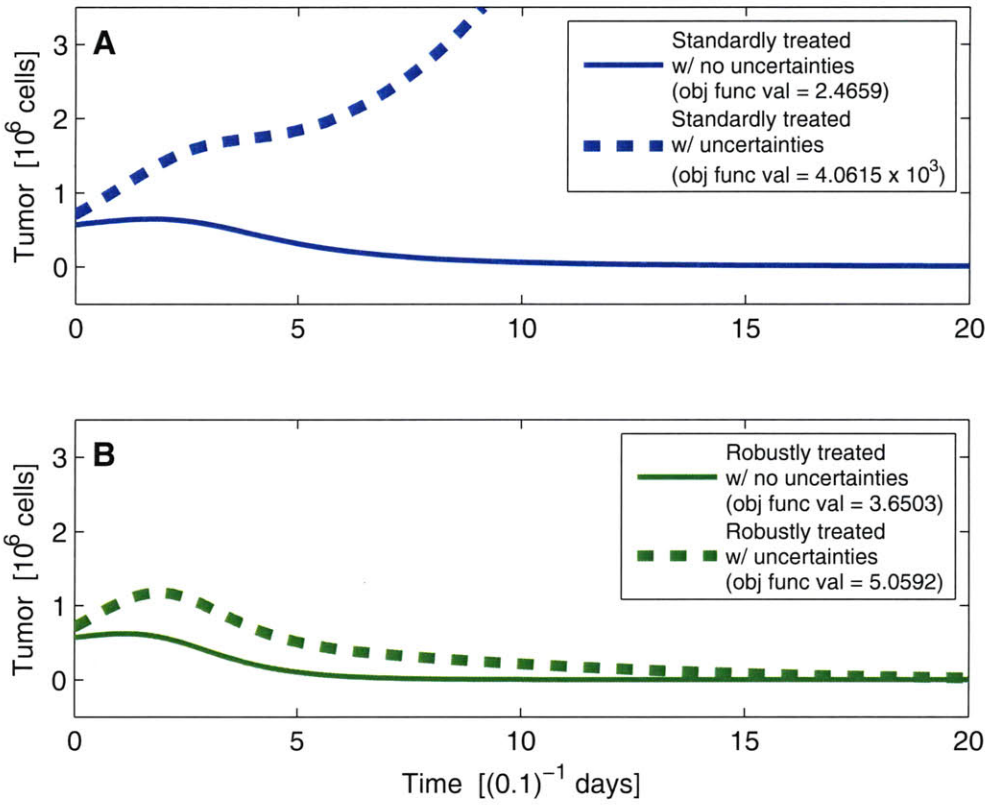


Figure 4-2: **Tumor response under designed continuous-dose therapy.** (A) Total number of tumor cells $[T(t) = T_i(t) + T_u(t)]$ under standardly designed protocol $b^{stn}$ (solid blue) and with its worst-case uncertainty $\mathbf{z}^{stn,worst}$ (dashed blue). (B) $T(t)$ under robustly designed protocol $b^{rob}$ (solid green) and with its worst-case uncertainty $\mathbf{z}^{rob,worst}$ (dashed green).

Essentially this result means that, in principle, a perfectly modeled tumor will be well controlled by a perfectly implemented therapy. In this case the therapy is a constant level of administration of the bacterium BCG. To assess the effect of inaccuracies in the model or the delivery of therapy on the control of tumor growth, we enumerated a range of inaccuracies for the model and the therapy delivery, and we examined the effect of the intended standard optimized therapy ($b^{stn}$) on each. Specifically, we enumerated up to 25% variation in the initial conditions of the model and the applied therapeutic dose (as compared to the intended dose) as well as vari-

ation in the parameters $\beta \in [0.013, 0.022]$ and $r \in [0.10, 0.45]$ (see Sec. 4.2). The least favorable objective function value was observed for one corner of this parameter hypercube, although approximately eleven values were enumerated along each hyperaxis. The worst point is $\mathbf{z}^{stn,worst} = (-0.25, -0.25, 0.25, 0.25, 0.25, 0.013, 0.45)$ with objective function value $F(b^{stn}) = 4061.5$, and the resulting trajectory is shown (dashed blue line) alongside the perfect trajectory (solid blue line) in Fig. 4-2A. The model and therapeutic uncertainty causes a therapy designed as optimal without accounting for uncertainty to perform quite poorly. In fact, the tumor grows without control.

A new treatment was designed using the robust approach developed here. A detailed description is given in Sec. 4.2. Briefly stated, the objective function is evaluated across a family of models and protocols with altered parameter values representing uncertainty in the model and the delivery of the intended therapy. The actual objective function value used in the optimization is the maximum value over the various uncertainties and so represents a "best treatment in the worst case." Using a range of uncertainty (25%) corresponding to that used to test the standard optimized therapy above, the resulting optimized treatment was computed to be $b^{rob} = 5.9304$ reduced units (equal to 593040 $cells\ days^{-1}$), with objective function value $F(b^{rob}) = 3.6503$. A trajectory of tumor cell number versus time under this protocol is shown in Fig. 4-2B (solid green line). This robust treatment protocol controls tumor growth very well and in a manner similar to the standard protocol, which is reasonable because the robust protocol corresponds to more than twice the dose level compared to the standard one.

The strength of the robust protocol can be seen from its behavior across the same uncertainties in model and treatment tested for the standard treatment optimum. The same point in the uncertainty space produced the worst performance for the robust protocol as the standard protocol $\mathbf{z}^{rob,worst} = \mathbf{z}^{stn,worst}$, and the resulting trajectory is shown in Fig. 4-2B (green dashed line) with associated objective value $F(b^{rob}) = 5.0592$. The trajectory shows that the robust protocol is able to control the worst uncertain model/treatment combination, in contrast to the standard optimization,

yet it takes a little longer for the treatment to reduce the tumor to negligible size in the uncertain case compared to its performance in the perfect case.

The performance of the robustly determined protocol $b^{rob}$ compared to that of the standardly determined protocol $b^{stn}$ was then examined in unfavorable uncertainty scenarios besides the single worst case and the exact realm of 25% uncertainty hypercube accounted for in its design process. The comparison was carried out between the objective function values $F(b^{stn})$ and $F(b^{rob})$ over the worst 10% of uncertainties considered, at every 5% increment of uncertainty hypercube sizes. The midpoint along the x-axis of the plot shown in Fig. 4-3 marks the 25% uncertainty hypercube that was accounted for in designing the robust protocol. The average objective function value over the worst 10% of uncertainties for that hypercube size is much higher for the standard protocol (blue) than for the robust one (green). Furthermore, even for smaller uncertainty hypercubes (i.e., to the left of the 25% midpoint of the x-axis), the robust protocol performs much better on average across the respective worst 10% of uncertainty scenarios considered than the standard one. Essentially, unless there is no uncertainty present, $b^{rob}$ is able to better maintain a low objective function value than $b^{stn}$ in the presence of unfavorable uncertainties. And only as the scenarios considered move beyond the 25% uncertainty hypercube that was originally accounted for in its design, $b^{rob}$ shows a gradual decrease in performance (i.e., a rise in the objective function value), as shown to the right of the 25% midpoint of the x-axis in Fig. 4-3.

### 4.3.1 Effect of therapeutic cost

Each optimization approach balances competing contributions to the objective function in order to achieve an optimal solution to the therapeutic problem posed. The objective employed here includes penalties for the final and integrated number of tumor cells as well as a third penalty for the integrated therapeutic dose, which includes risk due to side effects and possibly the financial cost of treatment. The standard and robust solutions differ in that the robust solution is more effective over a significant uncertainty range, which was included in the optimization, and the robust solution

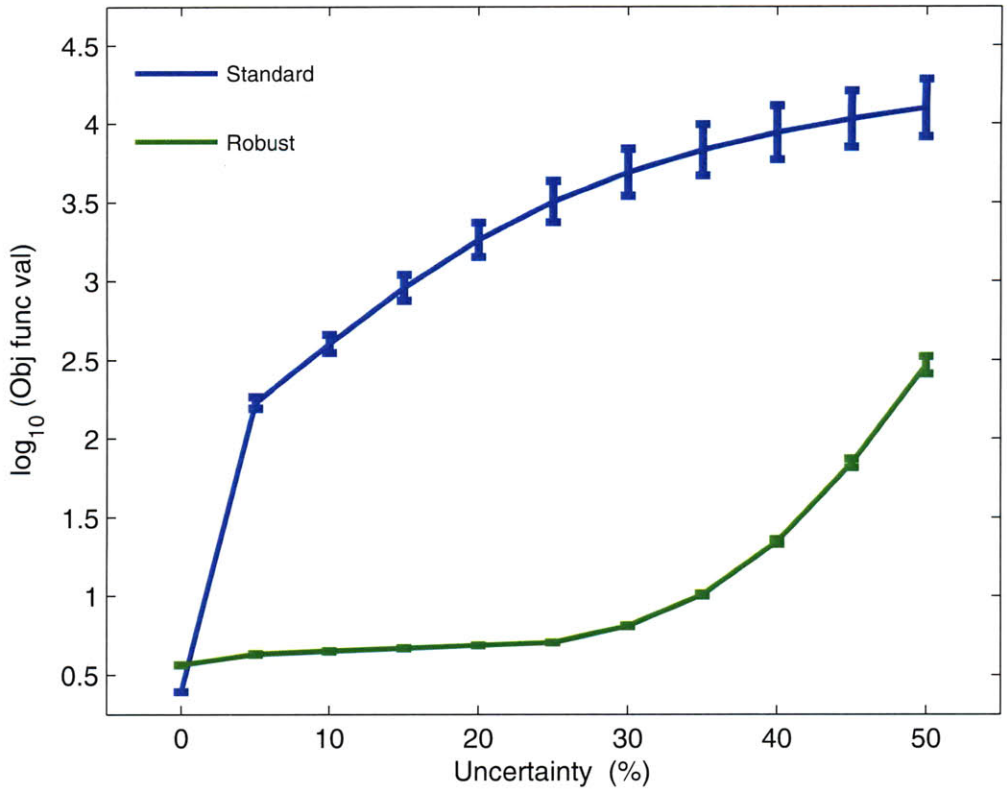


Figure 4-3: **Average costs of designed continuous-dose therapy over worst 10% of uncertainty scenarios considered.** Unless there is essentially no uncertainty present, the robustly designed protocol $b^{rob}$ (green) is better able to maintain a low objective function value than the standardly designed protocol $b^{stn}$ (blue) in the worst 10% of uncertainty scenarios examined.

uses a larger therapeutic dose.

To examine this effect in more detail, we repeated the standard and robust optimizations for a variety of values of $u_3$, the weight of the integrated therapeutic dose in the objective function. Fig. 4-4A plots $b$, the optimized rate of BCG administration, for these protocols as a function of the order of magnitude change applied to the $u_3$ in Eqn. (4.5). The plots show a trend of increasing optimized therapeutic dose with decreasing weight $u_3$ for the dose penalty, consistent with the notion that lower therapeutic cost drives increased doses to allow more efficient tumor killing. However, as the weight $u_3$ increases, the standard procedure leads to greater reductions in dose

whereas the robust protocol gives a nearly constant dose to retain effective tumor killing in the face of uncertainty.

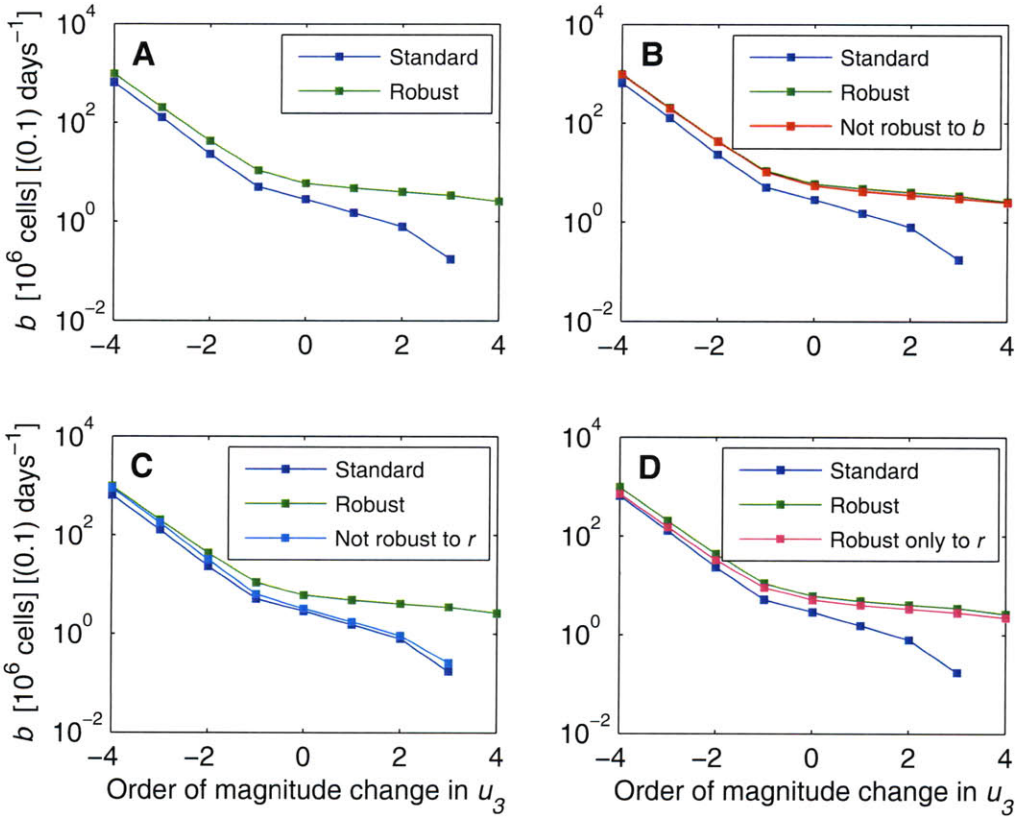


Figure 4-4: **Effect of therapeutic cost on continuous-dose therapy designed.** (A) Rate of BCG administration $b$ determined using the standard (blue) and the robust (green) optimization procedures for various orders of magnitude change applied to $u_3$, the weight of the integrated therapeutic dose, in the objective function (Eqn. (4.5)). (B) $b^{rob_{not\_b}}$ (red), robust as the fully robust protocol $b^{rob}$, except not to uncertainty in BCG administration rate $b$. (C) $b^{rob_{not\_r}}$ (light blue), robust as $b^{rob}$, except not to uncertainty in tumor growth rate $r$. (D) $b^{rob_r}$ (pink), robust only to uncertainty in tumor growth rate $r$. Determined $b$ approaches 0 in all cases as $u_3$ is increased.

As $u_3$ is decreased (i.e., as BCG usage becomes less costly), higher administration rate $b$ are determined for both protocols. Fig. 4-5, analogous to Fig. 4-2 for decreasing the $u_3$ in Eqn. (4.5) by two orders of magnitude, shows that for such high $b$, the total number of tumor cells $[T(t) = T_i(t) + T_u(t)]$ decreases over the course of the treatment in the worst uncertainty scenario even under the standard protocol (dashed blue line).

Fig. 4-6, analogous to Fig. 4-2 for increasing the $u_3$ in Eqn. (4.5) by two orders of magnitude, shows that using the standard approach may lead to designing a protocol that suggests a lower rate of BCG administration sufficing for effective treatment of the tumor, when in fact, such would not necessarily be the case with uncertainties being present.

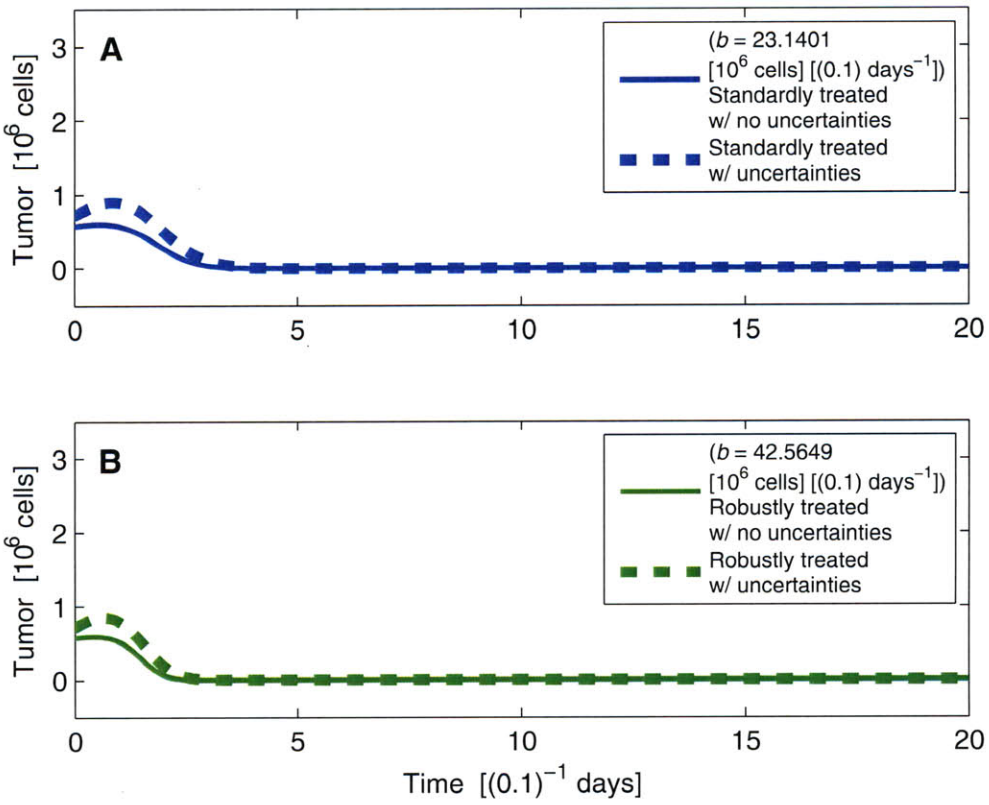


Figure 4-5: **Tumor response under continuous-dose therapy designed for lower therapeutic cost.** For the $u_3$ in Eqn. (4.5) decreased by two orders of magnitude: (A) Total number of tumor cells $[T(t) = T_i(t) + T_u(t)]$ under the standard protocol (solid blue) and with its worst-case uncertainty (dashed blue); (B) $T(t)$ under the robust protocol (solid green) and with its worst-case uncertainty (dashed green).

### 4.3.2 Comparison of uncertainty sources

Out of the multiple types of uncertainty accounted for in designing the robust treatment protocol $b^{rob}$, whether there is a single type that has the most dominant effect

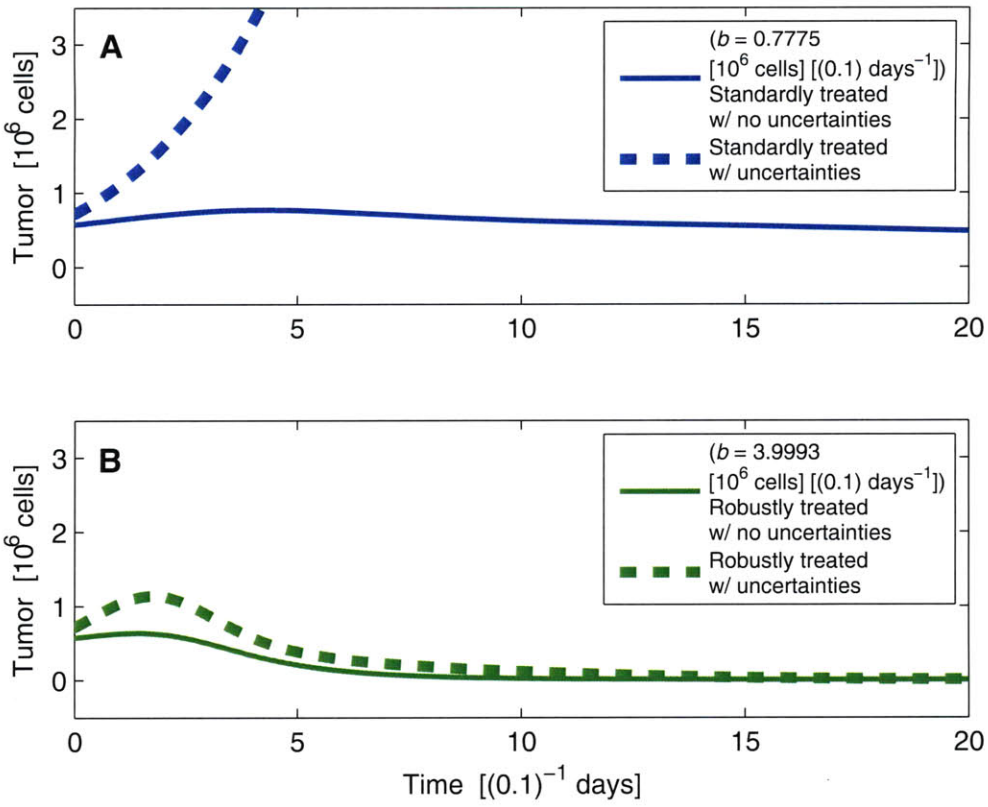


Figure 4-6: **Tumor response under continuous-dose therapy designed for higher therapeutic cost.** For the $u_3$ in Eqn. (4.5) increased by two orders of magnitude: (A) Total number of tumor cells $[T(t) = T_i(t) + T_u(t)]$ under the standard protocol (solid blue) and with its worst-case uncertainty (dashed blue); (B) $T(t)$ under the robust protocol (solid green) and with its worst-case uncertainty (dashed green).

in driving the robust approach to reach its design was then called into question. This assessment was carried out by implementing the robust approach repeatedly, accounting for a different subset of uncertainty types (i.e., a different subset of dimensions of the uncertainty hypercube) each time. These additional implementations gave rise to two interesting model observations; first, that even a very precise administration of the determined protocol will not by itself make possible an effective treatment with a lower rate of BCG administration, and second, that having limited knowledge about the exact growth rate of tumor cells ($r$ in Eqns. (4.1)) seems to be the most notable hindrance to designing an effective treatment.

Fig. 4-4B speaks to the first of these observations. The changes in the optimal BCG administration rate determined by the standard (blue) and the robust (green) approaches for varied therapeutic cost are plotted here, exactly as described earlier for Fig. 4-4A. The newly added values shown in red correspond to the robust approach being implemented for varied therapeutic cost as for the green values, but without accounting for any uncertainty in the rate of BCG administration $b$ (the resulting protocols are denoted $b^{rob_{not\_b}}$). These red values being very close to the green ones clearly indicate that even if high precision in therapeutic interventive measures could in fact be achieved, it is not enough to overcome the effects of other uncertainties that the robust protocol should be ready to encounter.

Fig. 4-4C shows a different set of these values overlaid on top of those resulting from the standand (blue) and the fully robust (green) approaches run on varied therapeutic cost. The newly added light blue values correspond to the robust approach being implemented, this time without accounting for any uncertainty in the tumor growth rate $r$. Denoted $b^{rob_{not\_r}}$, these values being very close to the blue ones indicate that knowing $r$ accurately can eliminate a large portion of unfavorable uncertainties that threaten successful therapy, making it possible for lower rates of BCG administration to be sufficient in effectively treating the tumor.

Fig. 4-4D also illustrates this observation made regarding $r$, yet in a reciprocal manner to that of Fig. 4-4C; the pink values overlaid here correspond to the robust approach being implemented, this time only accounting for the uncertainty in the tumor growth rate $r$. Denoted $b^{rob_r}$ (to clarify its reciprocity to $b^{rob_{not\_r}}$ discussed above), these values being very close to the green ones once again makes clear that out of the multiple uncertainty types considered for this model, uncertainty in $r$ makes the behavior of the tumor system most difficult to predict, in turn requiring higher rates of BCG to be administered into the system for it to be accounted for.

## 4.4 Application to treatment using CTL and IL-2

The standard and robust approaches described in Sec. 4.2 were implemented to design immunotherapeutic protocols involving discrete-dose administrations of CTL and IL-2 to treat tumor, using a canonical ODE model of the tumor-immune system in Eqns. (4.7) based on refs. [41] and [29]. The standard approach aims to design a treatment protocol that minimizes the value of the objective function in Eqn. (4.14), attempting to simultaneously limit the negative effects of increased amount and frequency of therapeutic intervention and enhance the effectiveness of tumor killing (see Sec. 4.2). The robust approach, instead of focusing solely on minimizing the objective function value, aims to do so even if the protocol that it designs is administered in the context of both inaccuracies in model parameters and imprecision in therapeutic interventive measures.

Shown in Fig. 4-7A (solid blue line) is the number of tumor cells in the system with no model or therapeutic uncertainties, being treated with the protocol designed using the standard approach, denoted $\mathbf{x}^{stn}$. The protocol administers the therapeutic agents at the times indicated by the grey vertical lines, which correspond to $t = \{1.4599, 171.7512, 331.6943, 498.8447\}$ reduced units (equal to $\{8.1106, 954.1733, 1842.7461, 2771.3594\}$ *days*). The associated amounts of CTL and IL-2 administered at those times are $\psi_1 = \{0.0091, 0.0036, 0.0048, 0.0011\}$ reduced units (equal to $\{9100000, 3600000, 4800000, 1100000\}$ *cells*) and $\psi_2 = \{0.0001, 0.0004, 0.0009, 0.0006\}$ reduced units (equal to $\{100000, 400000, 900000, 600000\}$ *cells*), respectively. As can be seen by the number of tumor cells remaining low throughout the treatment, this standard therapy is associated with a low objective function value of $G(\mathbf{x}^{stn}) = 0.0029$ in the absence of any model or therapeutic uncertainties.

The standardly designed protocol, however, is not as effective in maintaining the number of tumor cells at a low level when the system is subject to model and therapeutic uncertainties. Shown in Fig. 4-7A (dashed blue line), the number of tumor cells rises well above the safe level of $T^{max} = 10^{-5}$ reduced units (equal to $10^4$ *cells*) in the worst possible combination of such uncertainties exam-

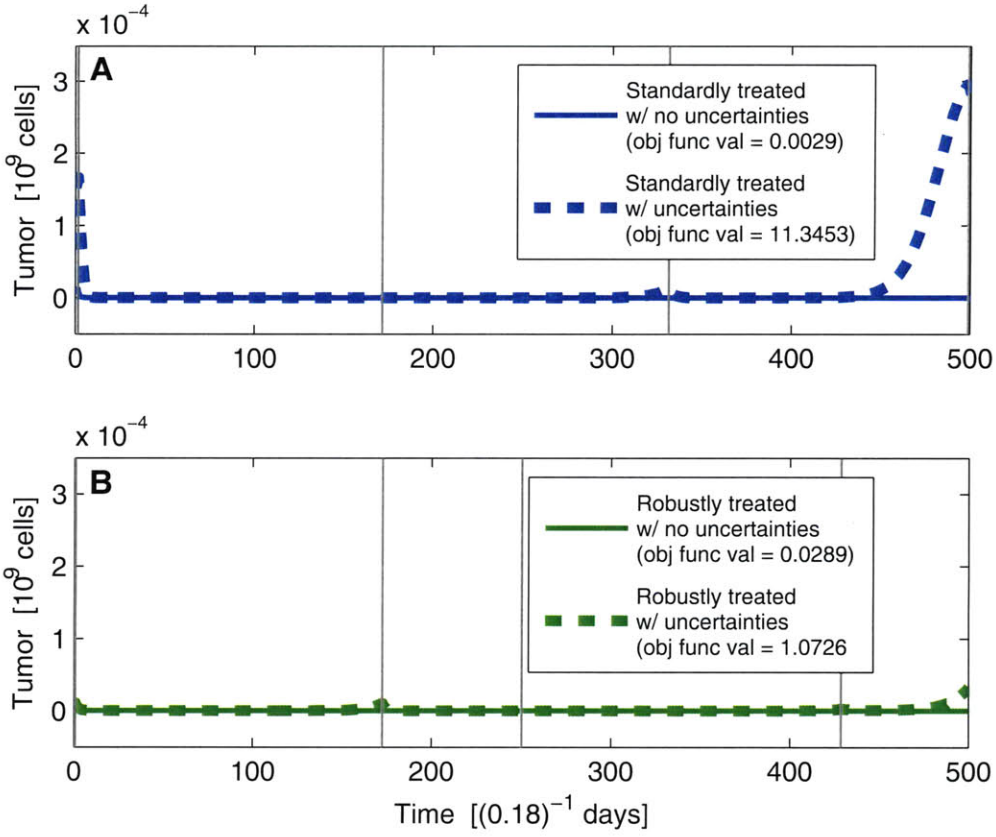


Figure 4-7: **Tumor response under designed discrete-dose therapy.** (A) Number of tumor cells $[T(t)]$ under the standardly designed protocol $\mathbf{x}^{stn}$ (solid blue) and with its worst-case uncertainty $\mathbf{z}^{stn,worst}$ (dashed blue). (B) $T(t)$ under the robustly designed protocol $\mathbf{x}^{rob}$ (solid green) and with its worst-case uncertainty $\mathbf{z}^{rob,worst}$ (dashed green). Grey vertical lines indicate times at which therapeutic administrations take place.

ined $[\mathbf{z}^{stn,worst} = (-0.20, -0.20, -0.20, -0.20, 27.5)]$ (see Sec. 4.2). The associated objective function value is $G(\mathbf{x}^{stn}) = 11.3453$, significantly higher than that for the case of no uncertainties. The space of uncertainties tested included up to 25% variations in each of the amounts of CTL and IL-2 administered, the antigenicity of the tumor ($c$ in Eqns. (4.7)), and the strength of the tumor response ($a$ in Eqns. (4.7)). Also, it included up to 110 reduced units (equal to 611.11 *days*) variation in the time of treatment initiation. (See Sec. 4.2 for details on specific combinations of these uncertainties examined, from within a 25%-sized hypercube of uncertainties.)

A protocol was then designed using the robust approach, denoted $\mathbf{x}^{rob}$, accounting

for the space of potential model and therapeutic uncertainties (see Sec. 4.2). Shown in Fig. 4-7B (solid green line) is the number of tumor cells in the system with no model or therapeutic uncertainties, being treated with this robustly determined protocol. The protocol administers the therapeutic agents at the times indicated by the grey vertical lines, which correspond to $t = \{0.5450, 172.5882, 250.2969, 428.6621\}$ reduced units (equal to $\{3.0278, 958.8233, 1390.5383, 2381.4561\}$ $days$).
The associated amounts of CTL and IL-2 administered at those times are $\psi_1 = \{0.0079, 0.0075, 0.0047, 0.0024\}$ reduced units (equal to $\{7900000, 7500000, 4700000, 2400000\}$ $cells$) and $\psi_2 = \{0.0002, 0.0006, 0.0004, 0.0003\}$ reduced units (equal to $\{200000, 600000, 400000, 300000\}$ $cells$), respectively. Although this robust therapy is associated with a higher objective function value [$G(\mathbf{x}^{rob}) = 0.0289$] than that of the standard therapy in the absence of any model or therapeutic uncertainties, it is just as effective in keeping the number of tumor cells below $T^{max}$ throughout the treatment.

The advantage of using the robustly designed protocol for tumor treatment over the standard one surfaces in the case of model and therapeutic uncertainties being present in the tumor system. $\mathbf{x}^{rob}$ was examined across the same hypercube of uncertainties as was done for $\mathbf{x}^{stn}$, and Fig. 4-7B (dashed green line) shows that even in the worst possible combination of uncertainties [$\mathbf{z}^{rob,worst} = (-0.25, -0.25, -0.25, -0.25, 0)$], unlike the standard protocol in $\mathbf{z}^{stn,worst}$, the robust protocol is able to retain the number of tumor cells at a very low level [$G(\mathbf{x}^{rob}) = 1.0726$].

### 4.4.1 Tradeoff between optimality and robustness

In addition to analyzing the performance of the robustly designed protocol $\mathbf{x}^{rob}$ against the worst uncertainty scenario found within the very hypercube of 25% uncertainty that was accounted for in its design process (see Sec. 4.2), the next step was to compare its performance to that of the standardly designed protocol $\mathbf{x}^{stn}$, against smaller and larger ranges of uncertainties (i.e., within uncertainty hypercubes of sizes other than 25%). The x-axis in Fig. 4-8A indicates this hypercube size, where the midpoint along that axis marks the size of 25%. The worst-case objective function value

for $\mathbf{x}^{stn}$ within this uncertainty hypercube ($G(\mathbf{x}^{stn}) = 11.3453$ in $\mathbf{z}^{stn}$, as discussed above) is plotted (blue) at this midpoint in Fig. 4-8A, along with the considerably lower-valued (green) worst-case for $\mathbf{x}^{rob}$ ($G(\mathbf{x}^{rob}) = 1.0726$ in $\mathbf{z}^{rob}$, also as discussed above).

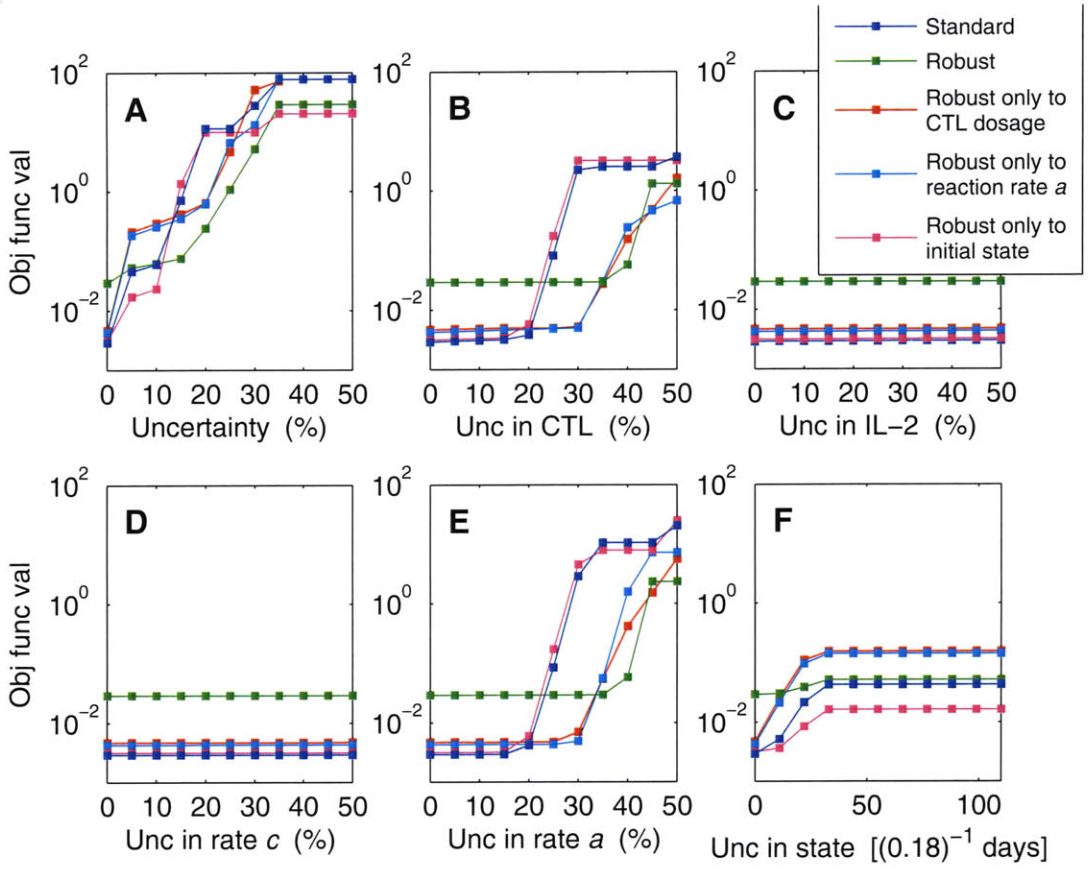


Figure 4-8: **Effect of uncertainty types and amounts on cost of designed discrete-dose therapy.** Objective function values for protocols $\mathbf{x}^{stn}$ (blue), $\mathbf{x}^{rob}$ (green), $\mathbf{x}^{rob_{CTL}}$ (red), $\mathbf{x}^{rob_a}$ (light blue), and $\mathbf{x}^{rob_{init}}$ (pink) under their respective worst uncertainty scenarios for (A) uncertainties existing in CTL dosage, IL-2 dosage, reaction rate $c$, reaction rate $a$, and initial state of tumor system, (B) uncertainty existing only in CTL dosage, (C) uncertainty existing only in IL-2 dosage, (D) uncertainty existing only in reaction rate $c$, (E) uncertainty existing only in reaction rate $a$, and (F) uncertainty existing only in the initial state of the tumor system.

Having additionally analyzed such worst-case values for every 5% increment of uncertainty hypercube size, shown along the x-axis here, and focusing only on the blue and the green values for the time being, it can be seen that $\mathbf{x}^{rob}$ performs better than

$\mathbf{x}^{stn}$ in the worst case even for amounts of uncertainty larger than the 25% accounted for in the robust design process. Notice, however, that the standard protocol $\mathbf{x}^{stn}$ (blue) outperforms the robust protocol $\mathbf{x}^{rob}$ (green) when the amount of uncertainty is limited to below 10%. By compensating for the possibility of a higher uncertainty amount during the design, there is in turn a resulting tradeoff of optimality when the actual amount of uncertainty that needs to be handled is much less than accounted for.

Seeing these effects, of treating in the presence of uncertainties besides the exact amount of uncertainty considered, called for further investigation into how protocols that have been designed to be robust to a certain type of uncertainty handle other types not accounted for. One robust protocol was designed to be robust only to 25% uncertainty in CTL dosage, denoted $\mathbf{x}^{rob_{CTL}}$. A protocol robust only to 25% uncertainty in the strength of the immune response ($a$ in Eqns. (4.7)) and another robust only to up to 110 reduced units (equal to 611.11 *days*) variability in the time at which treatment is initiated, denoted $\mathbf{x}^{rob_a}$ and $\mathbf{x}^{rob_{init}}$, respectively, were also designed.

Returning to Fig. 4-8A, the worst-case objective function values for the newly designed $\mathbf{x}^{rob_{CTL}}$ (red), $\mathbf{x}^{rob_a}$ (light blue), and $\mathbf{x}^{rob_{init}}$ (pink), against uncertainties drawn from varying sizes of uncertainty hypercubes along the x-axis, are shown. None of these protocols outperform the fully robust $\mathbf{x}^{rob}$ (green) at 25% here, which $\mathbf{x}^{rob}$ is specialized for handling. Against uncertainties only in CTL dosage, however, shown in Fig. 4-8B, $\mathbf{x}^{rob_{CTL}}$ (red), the protocol specialized to handle this uncertainty, has the lowest objective function value at the 25% midpoint along the x-axis, before gradually rising beyond that amount, worsening in performance along with the other protocols examined. Similarly, and not to great surprise, $\mathbf{x}^{rob_a}$ (light blue) and $\mathbf{x}^{rob_{init}}$ (pink) perform the best against their particular specialties, uncertainty only in immune response strength $a$ (Fig. 4-8E) and only in variability in treatment initiation time (Fig. 4-8F), respectively.

And once again, the assessment carried out here emphasizes the existence of the tradeoff that needs to be made to account for more uncertainty. If, in fact, uncer-

tainties do exist only in one of the many uncertainty dimensions accounted for by $\mathbf{x}^{rob}$, treating with this fully robust protocol will not perform as optimally in the worst-case as would have been possible to design with better knowledge regarding how much smaller the actual space of uncertainties that need to be dealt with is.

### 4.4.2 Properties of ODE model used

The worst-case performance comparisons shown in Fig. 4-8, between the standard, robust, and partially robust protocols, revealed interesting properties of the robustness analyses carried out over varying uncertainty amounts. There is striking similarity between B and E of Fig. 4-8, despite them being worst-case evaluations for distinct types of uncertainty, in CTL dosage and in immune response strength $a$, respectively; this relationship is further highlighted by protocol $\mathbf{x}^{rob_{CTL}}$ (red) performing well against 25% uncertainty in reaction rate $a$ (Fig. 4-8E), which is not what it was designed for, and also by $\mathbf{x}^{rob_a}$ (light blue) doing the same against 25% uncertainty in CTL dosage (Fig. 4-8B). Also noticeable are C and D of Fig. 4-8, which exhibit essentially no sensitivity of any protocol's performance to uncertainty either in IL-2 dosage or in tumor antigenicity ($c$ in Eqns. (4.7)). The next step in the studies was thus to figure out why the model in Eqns. (4.7) is giving rise to these properties observed.

If, instead of $a$, $\hat{a} = (1+\epsilon)a$, $-1 \leq \epsilon \leq 1$, is the strength of the immune system, the second equation in Eqns. (4.7) would be

$$\frac{dT}{dt} = r_2 T(1 - bT) - \frac{(1+\epsilon)aET}{g_2 + T} \quad . \tag{4.16}$$

Now suppose $a$ is as is, and consider $\frac{dE(t)}{dt}$ through the course of treatment (i.e., the right hand side of the first equation in Eqns. (4.7)) under protocol $\mathbf{x}^{stn}$, shown in Fig. 4-9B. C, D, and E of Fig. 4-9 show the contribution of each of the first three terms of this $\frac{dE(t)}{dt}$ as the protocol is carried out. Since the second term dominates $\frac{dE(t)}{dt}$,

$$\frac{dE(t)}{dt} \approx -\mu_2 E(t) + \psi_1(t) \quad , \tag{4.17}$$

which, with $\psi_1(t)$ defined as in Eqn. (4.8) and denoting the elements of $\mathbf{x}^{stn}$ as in Eqn. (4.9), leads to

$$\begin{aligned} E(t) \approx \quad & E(0)e^{-\mu_2 t}, \;\; 0 \le t < t_1 \\ & E(t_1)e^{-\mu_2(t-t_1)}, \;\; t_1 \le t < t_2 \\ & E(t_2)e^{-\mu_2(t-t_2)}, \;\; t_2 \le t < t_3 \\ & E(t_3)e^{-\mu_2(t-t_3)}, \;\; t_3 \le t < t_4 \\ & E(t_4)e^{-\mu_2(t-t_4)}, \;\; t_4 \le t \le 500 \;\; , \end{aligned} \tag{4.18}$$

where

$$\begin{aligned} E(t_1) \approx \quad & E(0)e^{-\mu_2 t_1} + u_{11} \\ E(t_2) \approx \quad & E(t_1)e^{-\mu_2(t_2-t_1)} + u_{12} \\ E(t_3) \approx \quad & E(t_2)e^{-\mu_2(t_3-t_2)} + u_{13} \\ E(t_4) \approx \quad & E(t_3)e^{-\mu_2(t_4-t_3)} + u_{14} \;\; . \end{aligned} \tag{4.19}$$

Since it can be seen in Fig. 4-9A that $E(t)$ leading up to each $t_i$ is much smaller than the $u_{1i}$ that gets added to it at $t_i$, Eqns. (4.19) can be further approximated as

$$\begin{aligned} E(t_1) \approx \quad & u_{11} \\ E(t_2) \approx \quad & u_{12} \\ E(t_3) \approx \quad & u_{13} \\ E(t_4) \approx \quad & u_{14} \;\; , \end{aligned} \tag{4.20}$$

which in turn allows Eqn. (4.18) to also be further approximated as

$$\begin{aligned} E(t) \approx \quad & E(0)e^{-\mu_2 t}, \;\; 0 \le t < t_1 \\ & u_{11}e^{-\mu_2(t-t_1)}, \;\; t_1 \le t < t_2 \\ & u_{12}e^{-\mu_2(t-t_2)}, \;\; t_2 \le t < t_3 \\ & u_{13}e^{-\mu_2(t-t_3)}, \;\; t_3 \le t < t_4 \\ & u_{14}e^{-\mu_2(t-t_4)}, \;\; t_4 \le t \le 500 \;\; . \end{aligned} \tag{4.21}$$

If, instead of $\psi_1(t)$, some $\hat{\psi}_1(t) = (1+\epsilon)\psi_1(t)$, $-1 \le \epsilon \le 1$, is administered as a part of protocol $\mathbf{x}^{stn}$, its effect on Eqn. (4.21) would be

$$
\begin{aligned}
(1+\epsilon)E(t) \approx \quad & E(0)e^{-\mu_2 t}, \;\; 0 \le t < t_1 \\
& (1+\epsilon)u_{11}e^{-\mu_2(t-t_1)}, \;\; t_1 \le t < t_2 \\
& (1+\epsilon)u_{12}e^{-\mu_2(t-t_2)}, \;\; t_2 \le t < t_3 \\
& (1+\epsilon)u_{13}e^{-\mu_2(t-t_3)}, \;\; t_3 \le t < t_4 \\
& (1+\epsilon)u_{14}e^{-\mu_2(t-t_4)}, \;\; t_4 \le t \le 500 \;\; ,
\end{aligned}
\tag{4.22}
$$

which leads to the second equation in Eqns. (4.7) being

$$
\frac{dT}{dt} \approx r_2 T(1-bT) - \frac{(1+\epsilon)aET}{g_2+T} \;\; , \tag{4.23}
$$

approximately equivalent to the effect of $a$ being replaced by $(1+\epsilon)a$ as in Eqn. (4.16).

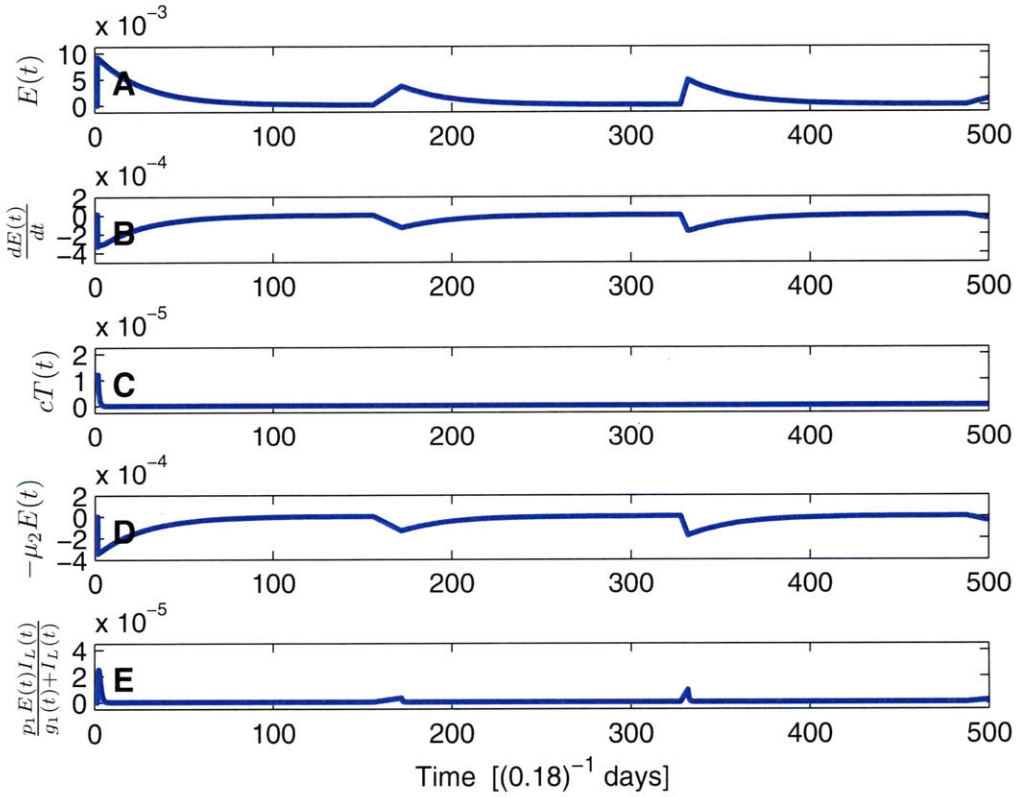


Figure 4-9: $-\mu_2\mathbf{E(t)}$ **dominates** $\frac{\mathbf{dE(t)}}{\mathbf{dt}}$ **in Eqns. (4.7).** (A) $E(t)$, (B) $\frac{dE(t)}{dt}$, (C) $cT(t)$, (D) $-\mu_2 E(t)$, and (E) $\frac{p_1 E(t) I_L(t)}{g_1+I_L(t)}$ under protocol $\mathbf{x}^{stn}$.

This approximate equivalence, and consequently the similarity between B and E of Fig. 4-8, suggests the possibility of countering the uncertainty in reaction rate $a$ by improving the precision with which CTL is delivered, and vice versa. It must be noted, however, that such is the case only under the assumption that the particular model parameters that have generated this phenomenon are close to those of an actual tumor-immune system to be treated.

In contrast to being sensitive to changes in CTL dosage or reaction rate $a$, the insensitivity of the objective function value to changes in IL-2 dosage or reaction rate $c$, as shown in C and D of Fig. 4-8, respectively, is also noteworthy. Since the performance of a protocol does not worsen under uncertainty in either IL-2 dosage or reaction rate $c$, there are no separate protocols $\mathbf{x}^{rob_{IL-2}}$ or $\mathbf{x}^{rob_c}$ found to perform better than protocol $\mathbf{x}^{stn}$ against those uncertainties.

With the nominal value of $c$ being close to 1 (as shown in Table 4.2), its effect on the tumor system is solely dependent on the the magnitude of $T(t)$. It is therefore no surprise that the performance of protocols such as $\mathbf{x}^{stn}$, which keep $T(t)$ very low through treatment, is not greatly affected by changes in $c$. And considering that $c$ represents the antigenicity of the tumor, it makes sense that its effect on the system should in fact be directly related to $T(t)$.

## 4.5 Discussion

The performance of immunotherapeutic protocols for treating tumor are found to be highly dependent on the extent of uncertainties that exist in model-based protocol design, which are likely to arise from one or more of the discrepancy between model and actual systems and the imprecision in administering the treatments. By taking these uncertainties into account in the design process, the robust optimization method introduced in this work aims to enhance the plausibility of quantitatively designing protocols for cancer immunotherapy.

In analyzing the results presented above, particular emphasis was put on tracking down, in the mathematical model itself, the sources of interesting properties observed

(e.g., the relationship between CTL dosage and immune response strength in the tumor-immune system model given in Eqns. (4.7)). These types of investigations fully put to use the advantage of model-based studies; as the mathematical model is a representation of what is known about the workings of actual tumor-immune systems, figuring out the exact aspects of the model that cause the observations made can either hypothesize causes for a model behavior that matches experimental findings or, for a behavior that is contrary to experiments, point to missing links in understanding the workings of the system. For instance, the observed insensitivity to IL-2 dosage observed for the model in Eqns. (4.7) is in line with the findings reported in ref. [41], which explains the relative effectiveness of CTL over IL-2 as being caused by the specific choice of their rates of decay. Alongside that, however, in light of continued reports of experimentally observed efficacy of IL-2 [77–79], the insensitivity observation made here also strongly indicates the need for a correction to be made to what is currently understood to be their relative decay rates.

Another potential improvement to immunotherapy design is suggested by observing what happens to the tumor size post-treatment. Fig. 4-10A shows the number of tumor cells for an additional 1000 reduced units (equal to 5555.6 *days*) after being under the standardly designed protocol $\mathbf{x}^{stn}$ between 0 and 500 reduced units (equal to 2777.8 *days*). It is clear that the tumor eventually returns to its pre-treatment levels. Treating with the robustly designed protocol $\mathbf{x}^{rob}$ instead does not provide a solution to this particular issue, as is made apparent by Fig. 4-10B. As a temporary solution, if the protocols designed here were to be repeatedly administered for every interval of 500 reduced units following the first treatment lasting between 0 and 500 reduced units, the resulting tumor behavior would be as shown in Fig. 4-11; note that, in this case as well, the robustly determined protocol (Fig. 4-11B, dashed green line) is more effective than the standardly determined protocol (Fig. 4-11A, dashed blue line) when uncertainties are present. Reports of tumor recurrence being one of the most major difficulties associated with immunotherapy practice [80,81] only add to the importance of improving the existing framework of protocol design to take post-treatment tumor levels into consideration.

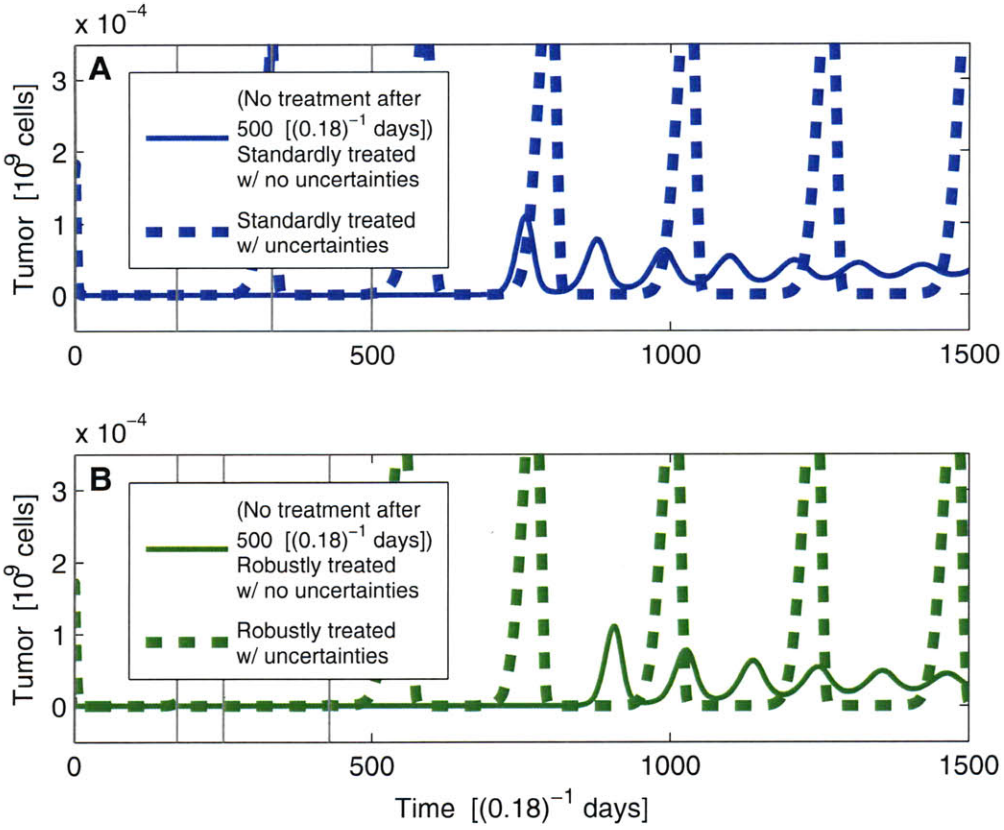


Figure 4-10: **Tumor response following designed discrete-dose therapy.** (A) Number of tumor cells $[T(t)]$ during and after being under the standardly designed protocol $\mathbf{x}^{stn}$ (solid blue) and in its worst uncertainty scenario (dashed blue). (B) $T(t)$ during and after being under the robustly designed protocol $\mathbf{x}^{rob}$ (solid green) and in its worst uncertainty scenario (dashed green). Grey vertical lines indicate times at which therapeutic administrations take place.

Regarding the investigation of the relative effects of different uncertainty sources using the BCG immunotherapy model in Eqns. (4.1), uncertainty in $r$ seemed to be the most significant consideration to be made in designing robust treatment protocols. As the growth rate of tumor cells, $r$ can be expected to vary depending on many different factors, including the fraction of tumor cells growing and the stage of clinical treatment [82]. This variability in $r$ further emphasizes the need for robust determination of treatment protocols for achieving successful immunotherapy. With reports of significant correlation between the net growth rate and response to radiation therapy in glioblastoma patients [83], allocating significant consideration to $r$ in planning can-

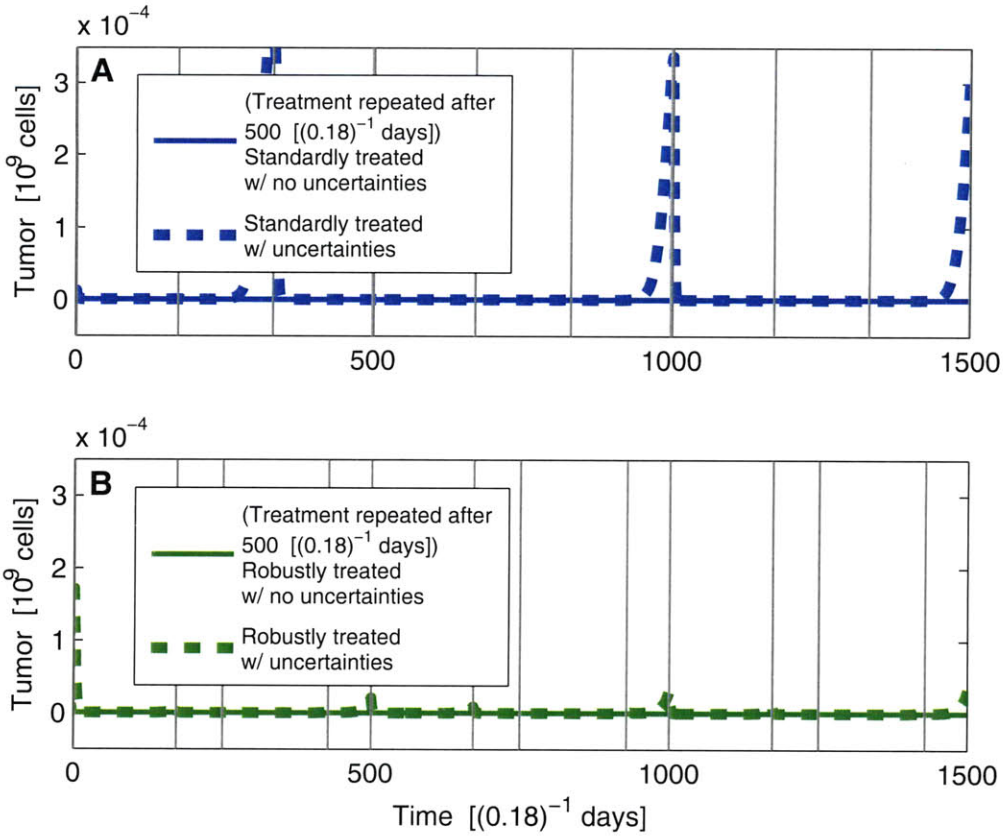


Figure 4-11: **Exploring longer-term effectiveness of designed discrete-dose therapy.** (A) Number of tumor cells $[T(t)]$ repeatedly being under the standardly designed protocol $\mathbf{x}^{stn}$ (solid blue) and in its worst uncertainty scenario (dashed blue). (B) $T(t)$ repeatedly being under the robustly designed protocol $\mathbf{x}^{rob}$ (solid green) and in its worst uncertainty scenario (dashed green). Grey vertical lines indicate times at which therapeutic administrations take place.

cer treatments seems necessary even beyond the realms of immunotherapy explored here.

One alternative form of nonsurgical cancer therapy is chemotherapy, which has been found to treat many types of tumors effectively. Its potency is nevertheless clouded by abundant reports of both mild and severe side effects that can possibly lead to serious complications for the cancer patient [84–86]. Growing interest in immunotherapy is to a great extent due to its potential complementary use with chemotherapy. Such mixed therapy holds the hope of consequently limiting the amount of often highly toxic chemotherapeutic drugs from being administered.

The enhanced effect of CTL immunotherapy when combined with chemotherapy, for instance, have been experimentally observed in mice [87], which follows a number of reports of findings regarding the benefits of combining vaccine therapy with chemotherapy [47,88,89]. With mathematical modeling efforts for cancer treatments including such combination therapy being on the rise [46, 90], and with added potential dimensions of uncertainty that are likely to accompany the combination of multiple therapeutic interventions, robust protocol design, using methods such as the one presented in this work, is expected to grow in importance.

Exciting avenues for further exploration lie ahead, particularly with regards to incorporating additional sources of uncertainty that must be accounted for in designing robust treatments. A notable source is patient-to-patient variability in responses to cancer therapy, which have been extensively observed [91–93]; this variability continues to fuel research efforts in making individualized therapy planning more plausible [94, 95]. Reaching a step further leads to considering varied effects of therapy other than reduction in tumor size; unfavorable side effects of cancer therapy range widely from metabolic and cardiovascular disruption [96, 97] to decreased bone density [98], and have long been giving rise to studies involving their effective management [99, 100]. The methodology of robust protocol design introduced in this work offers a framework for planning therapies that can treat tumors under various uncertainties, and can readily be applied to incorporate these variabilities into its mathematical optimization-based approach. Analyzing the benefits and tradeoffs of requiring robustness, both comparatively and complementarily to such individualized therapy and consideration of therapeutic effects, is a major target for future investigation that is made possible by the introduction of this robust approach to cancer treatment design. And by fully utilizing the strengths of model-based studies as was done here, such investigations can be expected to help build upon the current understanding of tumor systems as a whole.

# Chapter 5

# Robust Optimization by Linearized Worst-case Approximation

## 5.1 Motivation

The robust optimization method explored in Ch. 3 for biological network calibration and in Ch. 4 for cancer immunotherapy design approximates the worst uncertainty scenario by sampling the region of potential uncertainties for that worst-case. An alternative mathematical formulation to solving the worst-case optimization problem is offered here, one that replaces the sampling process of the previous method with a linearization of the objective function's parameter space over the region of uncertainties. Studied in the context of Bunimovich-Mendrazitsky et al.'s mathematical model of BCG immunotherapy for superficial bladder cancer shown in Eqns. (4.1) [34], this linearized worst-case approximation method is first evaluated on its ability to design comparable robust protocols as the previous method, after which it is additionally given the task of designing robust protocols against a notable increase in the number of uncertainty dimensions to be considered. Its relative computational efficiency allows it to succeed not only in carrying out this additional task, but also in giving rise to the potential for a novel approach to experimental guidance directed at improving model-based design of robust immunotherapeutic protocols.

## 5.2 Iterative minimization procedures

**Standard iterative minimization** Shown schematically in Fig. 5-1, the iterative procedure for finding the $\mathbf{x}$ that minimizes $f(\mathbf{x}, \mathbf{p})$, solving Eqn. (2.1), is as follows:

**Step 1.** Guess at a solution, $\mathbf{x}^0$, and set $s = 1$.

**Step 2.** Select the $\check{\mathbf{d}}^s$ that is expected to minimize $f(\mathbf{x}^{s-1} + \check{\mathbf{d}}^s, \mathbf{p})$ using Newton's method.

**Step 3.** Search for the $a$ that minimizes $f(\mathbf{x}^{s-1} + a\check{\mathbf{d}}^s, \mathbf{p})$; set $\mathbf{d}^s = a\check{\mathbf{d}}^s$ and $\mathbf{x}^s = \mathbf{x}^{s-1} + \mathbf{d}^s$.

**Step 4.** If $\mathbf{d}^s < tolerance$, then return $\mathbf{x}^s$ as the solution and terminate. Else, set $s = s + 1$ and go back to Step 2.

**Robust iterative minimization** The iterative procedure for finding the $\mathbf{x}$ that minimizes $f(\hat{\mathbf{x}}, \hat{\mathbf{p}})$ in the worst-case, solving Eqn. (2.3), is as follows:

**Step 1.** Guess at a solution, $\mathbf{x}^0$, and set $s = 1$.

**Step 2.** Select the $\check{\mathbf{d}}^s$ that is expected to minimize $f(\hat{\mathbf{x}}^{s-1} + \check{\mathbf{d}}^s, \hat{\mathbf{p}})$ in the worst-case.

**Step 3.** Search for the $a$ that minimizes $f(\hat{\mathbf{x}}^{s-1} + a\check{\mathbf{d}}^s, \hat{\mathbf{p}})$ in the worst-case; set $\mathbf{d}^s = a\check{\mathbf{d}}^s$ and $\mathbf{x}^s = \mathbf{x}^{s-1} + \mathbf{d}^s$.

**Step 4.** If $\mathbf{d}^s < tolerance$, then return $\mathbf{x}^s$ as the solution and terminate. Else, set $s = s + 1$ and go back to Step 2.

### 5.2.1 Sampled worst-case approximation

#### Update direction selection

Shown schematically in Fig. 5-2, the sampling-based method for determining the $\check{\mathbf{d}}^s$ in Step 2 of the robust iterative procedure is as follows:

1. Sample $N$ sets of $\{\triangle\mathbf{x}, \triangle\mathbf{p}\}$ from $\triangle\mathbf{x} \in U^{\triangle\mathbf{x}}$ and $\triangle\mathbf{p} \in U^{\triangle\mathbf{p}}$.

2. Of the $N$ sets sampled, select as $\{\triangle\mathbf{x}^{worst}, \triangle\mathbf{p}^{worst}\}$ the set that maximizes $f(\mathbf{x}^{s-1} + \triangle\mathbf{x}, \mathbf{p} + \triangle\mathbf{p})$.

3. Select the $\check{\mathbf{d}}^s$ that is expected to minimize $f(\mathbf{x}^{s-1} + \check{\mathbf{d}}^s + \triangle\mathbf{x}^{worst}, \mathbf{p} + \triangle\mathbf{p}^{worst})$ using Newton's method.

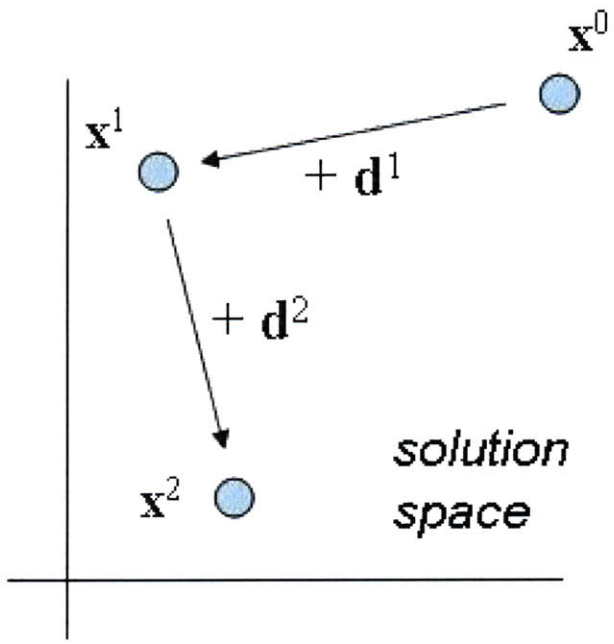


Figure 5-1: **Schematic representation of standard iterative procedure for finding solution x in solution space that minimizes objective function $\mathbf{f}(\mathbf{x}, \mathbf{p})$.**

**Update magnitude selection**

The sampling-based criterion for determining the $a$ in Step 3 of the robust iterative procedure is as follows:

1. Sample $N$ sets of $\{\triangle\mathbf{x}, \triangle\mathbf{p}\}$ from $\triangle\mathbf{x} \in U^{\triangle\mathbf{x}}$ and $\triangle\mathbf{p} \in U^{\triangle\mathbf{p}}$.

2. Of the $N$ sets sampled, designate $\{\triangle\mathbf{x}_a^{worst}, \triangle\mathbf{p}_a^{worst}\}$ for a given $a$ as the set that maximizes $f(\mathbf{x}^{s-1} + a\check{\mathbf{d}}^s + \triangle\mathbf{x}, \mathbf{p} + \triangle\mathbf{p})$.

3. Search for the $a$ that minimizes $f(\mathbf{x}^{s-1} + a\check{\mathbf{d}}^s + \triangle\mathbf{x}_a^{worst}, \mathbf{p} + \triangle\mathbf{p}_a^{worst})$.

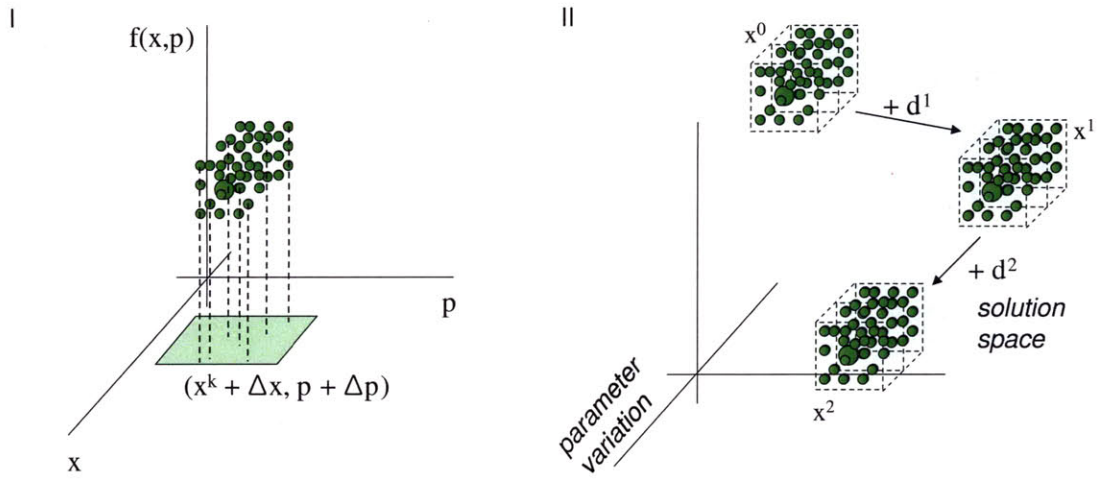


Figure 5-2: **Schematic representation of sampling-based robust iterative minimization.** (I) $N$ sets of $\{\mathbf{x}, \mathbf{p}\}$ are sampled from $\{\triangle\mathbf{x}, \triangle\mathbf{p}\}$-variation around $\{\mathbf{x}^k, \mathbf{p}\}$; maximum $f(\mathbf{x}, \mathbf{p})$ of these approximates worst-case. (II) For finding solution $\mathbf{x}$ in solution space that minimizes worst-case $f(\hat{\mathbf{x}}, \hat{\mathbf{p}})$, sampling takes place at each iteration to account for variations in both solution value and parameters.

### 5.2.2 Linearized worst-case approximation

#### Ellipsoidal uncertainty

Let $E$ denote an ellipsoid in $\mathbb{R}^n$ centered at $\mathbf{0}$, whose $j$th semi-axis has a length of $|\lambda_j|$, i.e.,

$$\{E = \mathbf{\Lambda u} \mid \|\mathbf{u}\|_2 \leq 1\} \ , \tag{5.1}$$

where

$$\lambda = (\lambda_1, ..., \lambda_n) \tag{5.2}$$

and

$$\mathbf{\Lambda} = diag(\lambda) \ . \tag{5.3}$$

Regarding uncertainty sets $U^{\triangle \mathbf{x}}$ and $U^{\triangle \mathbf{p}}$ as ellipsoid $E_{\mathbf{x}}$ around $\mathbf{x}$ and ellipsoid $E_{\mathbf{p}}$ around $\mathbf{p}$, respectively, finding the $\mathbf{x}$ that minimizes $f(\hat{\mathbf{x}}, \hat{\mathbf{p}})$ in the worst-case is to solve

$$\min_{\mathbf{x}} \max_{\triangle \mathbf{x} \in E_{\mathbf{x}}, \triangle \mathbf{p} \in E_{\mathbf{p}}} f(\mathbf{x} + \triangle \mathbf{x}, \mathbf{p} + \triangle \mathbf{p}) \ . \tag{5.4}$$

As one way of designating the lengths of the semi-axes for the uncertainty ellipsoids to be proportional to the uncertainty ranges in each dimension, consider an uncertainty set $U^{\triangle \mathbf{x}}$ in $\mathbb{R}^n$ that consists of all vectors $(\triangle x_1, ..., \triangle x_n)$, where $\triangle x_j \in [-c_j, c_j]$, $c_j \geq 0$, $j = \{1, ..., n\}$. Place the foci of the associated ellipsoid to be along its semimajor axis at $(0, ..., -c_i, ..., 0)$ and $(0, ..., c_i, ..., 0)$, where $c_i \geq c_j$, $\forall j$. Let

$$\sqrt{(2c_i)^2 + \sum_{j \neq i} c_j^2} + \sqrt{\sum_{j \neq i} c_j^2} = 2\lambda_i \ , \tag{5.5}$$

where $\lambda_i$ becomes the length of the ellipsoid's semimajor axis. Since the sum of the distances from the foci to any point on the surface of the ellipsoid is $2\lambda_i$,

$$\sqrt{\sum_{j \neq i} \lambda_j^2} = \sqrt{\lambda_i^2 - c_i^2} \ . \tag{5.6}$$

Maintaining the proportionality using $\frac{\lambda_j}{\lambda_k} = \frac{c_j}{c_k}$ leads to replacing $\lambda_j$, $j \neq \{i, k\}$, with $\frac{\lambda_k c_j}{c_k}$, which gives rise to

$$\lambda_k = \frac{\sqrt{\lambda_i^2 - c_i^2}}{\sqrt{1 + \frac{1}{c_k^2} \sum_{j \neq \{i,k\}} c_j^2}} \ , \tag{5.7}$$

where $\lambda_k$ then becomes the length of the ellipsoid's $k$th semi-axis. $\lambda_j$, $j \neq \{i, k\}$, which are the lengths of the ellipsoid's remaining semi-axes, can then be computed using $\lambda_j = \frac{\lambda_k c_j}{c_k}$ once again. A two-dimensional illustration of this ellipsoid designation process is shown in Fig. 5-3.

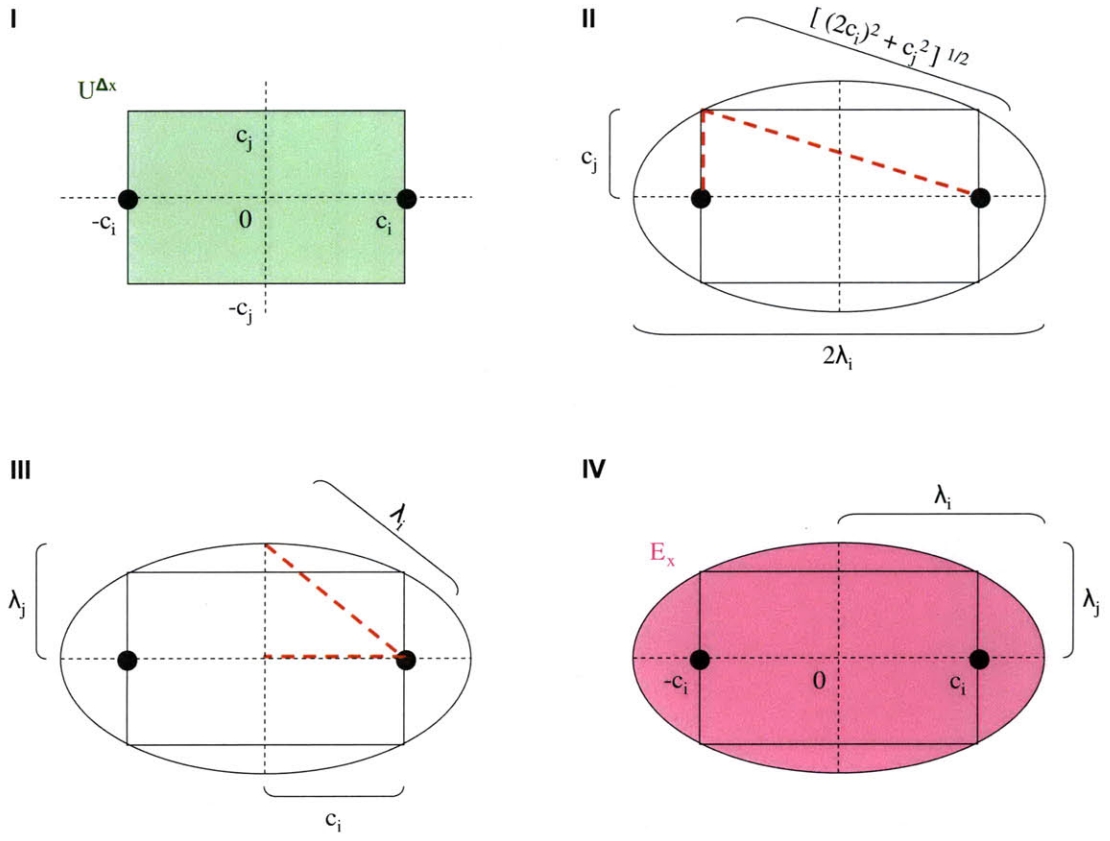


Figure 5-3: **Two-dimensional illustration of method used for specifying uncertainty ellipsoid $\mathbf{E_x}$ from uncertainty set $\mathbf{U^{\Delta x}}$.** (I) Place the foci of the eventual $E_\mathbf{x}$ to be along its semimajor axis, corresponding to the widest dimension of $U^{\Delta\mathbf{x}}$, at $(-c_i, 0)$ and $(c_i, 0)$. (II) Specify $\lambda_i$, the length of $E_\mathbf{x}$'s semimajor axis, by choosing to make the surface of $E_\mathbf{x}$ intersect with the corners of $U^{\Delta\mathbf{x}}$. (III) Specify $\lambda_j$, the length of $E_\mathbf{x}$'s semiminor axis, by using the fact that the sum of the distances from the foci to any point on the surface of $E_\mathbf{x}$ is $2\lambda_i$. (IV) The resulting $E_\mathbf{x}$ has semiaxis lengths of $\lambda_i$ and $\lambda_j$, with foci at $(-c_i, 0)$ and $(c_i, 0)$.

**Update direction selection**

Shown schematically in Fig. 5-4, the linearization-based method for selecting the $\check{\mathbf{d}}^s$ in Step 2 of the robust iterative procedure outlined above is as follows:

1. Assemble the following entities:

(a) $\mathbf{J}_{\mathbf{x}}^{s-1}$, the matrix of partial derivatives of $f(\mathbf{x}^{s-1}, \mathbf{p})$ with respect to each element of $\mathbf{x}^{s-1}$

(b) $\mathbf{J}_{\mathbf{x},\mathbf{p}}^{s-1}$, the matrix of partial derivatives of each element of $\mathbf{J}_{\mathbf{x}}^{s-1}$ with respect to each element of $\mathbf{p}$

(c) $\mathbf{J}_{\mathbf{p}}^{s-1}$, the matrix of partial derivatives of $f(\mathbf{x}^{s-1}, \mathbf{p})$ with respect to each element of $\mathbf{p}$

(d) $\mathbf{J}_{\mathbf{p},\mathbf{x}}^{s-1}$, the matrix of partial derivatives of each element of $\mathbf{J}_{\mathbf{p}}^{s-1}$ with respect to each element of $\mathbf{x}^{s-1}$

2. Approximate $f(\mathbf{x}^{s-1} + \check{\mathbf{d}}^s + \triangle\mathbf{x}, \mathbf{p} + \triangle\mathbf{p})$ as

$$\begin{aligned} & f(\mathbf{x}^{s-1}, \mathbf{p}) \\ & + \mathbf{J}_{\mathbf{x}}^{s-1}(\check{\mathbf{d}}^s + \triangle\mathbf{x}) \\ & + \tfrac{1}{2}\triangle\mathbf{p}^T \mathbf{J}_{\mathbf{x},\mathbf{p}}^{s-1}(\check{\mathbf{d}}^s + \triangle\mathbf{x}) \\ & + \mathbf{J}_{\mathbf{p}}^{s-1}\triangle\mathbf{p} \\ & + \tfrac{1}{2}(\check{\mathbf{d}}^s + \triangle\mathbf{x})^T \mathbf{J}_{\mathbf{p},\mathbf{x}}^{s-1}\triangle\mathbf{p} \ . \end{aligned} \tag{5.8}$$

Distributing out the terms in Eqn. (5.8) gives

$$\begin{aligned} & f(\mathbf{x}^{s-1}, \mathbf{p}) \\ & + \mathbf{J}_{\mathbf{x}}^{s-1}\check{\mathbf{d}}^s + \mathbf{J}_{\mathbf{x}}^{s-1}\triangle\mathbf{x} \\ & + \tfrac{1}{2}\triangle\mathbf{p}^T \mathbf{J}_{\mathbf{x},\mathbf{p}}^{s-1}\check{\mathbf{d}}^s + \tfrac{1}{2}\triangle\mathbf{p}^T \mathbf{J}_{\mathbf{x},\mathbf{p}}^{s-1}\triangle\mathbf{x} \\ & + \mathbf{J}_{\mathbf{p}}^{s-1}\triangle\mathbf{p} \\ & + \tfrac{1}{2}(\check{\mathbf{d}}^s)^T \mathbf{J}_{\mathbf{p},\mathbf{x}}^{s-1}\triangle\mathbf{p} + \tfrac{1}{2}\triangle\mathbf{x}^T \mathbf{J}_{\mathbf{p},\mathbf{x}}^{s-1}\triangle\mathbf{p} \ , \end{aligned} \tag{5.9}$$

which can be rearranged to be

$$
\begin{aligned}
& f(\mathbf{x}^{s-1}, \mathbf{p}) \\
& + \mathbf{J}_{\mathbf{x}}^{s-1} \check{\mathbf{d}}^s + \mathbf{J}_{\mathbf{x}}^{s-1} \triangle \mathbf{x} + \mathbf{J}_{\mathbf{p}}^{s-1} \triangle \mathbf{p} \\
& + \tfrac{1}{2} \triangle \mathbf{p}^T [\mathbf{J}_{\mathbf{x},\mathbf{p}}^{s-1} + (\mathbf{J}_{\mathbf{p},\mathbf{x}}^{s-1})^T] \triangle \mathbf{x} \\
& + \tfrac{1}{2} \triangle \mathbf{p}^T [\mathbf{J}_{\mathbf{x},\mathbf{p}}^{s-1} + (\mathbf{J}_{\mathbf{p},\mathbf{x}}^{s-1})^T] \check{\mathbf{d}}^s \ .
\end{aligned}
\tag{5.10}
$$

3. Including bounds on $\check{\mathbf{d}}^s$ as constraints (e.g., $\mathbf{x}^{s-1} + \check{\mathbf{d}}^s \geq 0$), solve

$$
\begin{aligned}
\min_{\check{\mathbf{d}}^s} \max_{\triangle \mathbf{x} \in E_{\mathbf{x}^s}, \triangle \mathbf{p} \in E_{\mathbf{p}}} \quad & \mathbf{J}_{\mathbf{x}}^{s-1} \check{\mathbf{d}}^s + \mathbf{J}_{\mathbf{x}}^{s-1} \triangle \mathbf{x} + \mathbf{J}_{\mathbf{p}}^{s-1} \triangle \mathbf{p} \\
& + \tfrac{1}{2} \triangle \mathbf{p}^T [\mathbf{J}_{\mathbf{x},\mathbf{p}}^{s-1} + (\mathbf{J}_{\mathbf{p},\mathbf{x}}^{s-1})^T] \triangle \mathbf{x} \\
& + \tfrac{1}{2} \triangle \mathbf{p}^T [\mathbf{J}_{\mathbf{x},\mathbf{p}}^{s-1} + (\mathbf{J}_{\mathbf{p},\mathbf{x}}^{s-1})^T] \check{\mathbf{d}}^s \ ,
\end{aligned}
\tag{5.11}
$$

where

$$
\{ E_{\mathbf{x}^s} = \mathbf{\Lambda}_{\mathbf{x}^s} \mathbf{u}_{\mathbf{x}^s} \ \mid \ \| \mathbf{u}_{\mathbf{x}^s} \|_2 \leq 1 \} \ , \tag{5.12}
$$

and

$$
\{ E_{\mathbf{p}} = \mathbf{\Lambda}_{\mathbf{p}} \mathbf{u}_{\mathbf{p}} \ \mid \ \| \mathbf{u}_{\mathbf{p}} \|_2 \leq 1 \} \ , \tag{5.13}
$$

for $\mathbf{x}^s$ in $\mathbb{R}^n$ and $\mathbf{p}$ in $\mathbb{R}^m$. $\lambda_{\mathbf{x}^s j}$ and $\lambda_{\mathbf{p}_i}$ represent the amounts of uncertainty around $\mathbf{x}^s$ and $\mathbf{p}$ in dimension $j$ and dimension $i$, respectively.

### Min-max formulation

Using Eqns. (5.12) and (5.13), the inner maximization problem of Eqn. (5.11) can be written as

$$
\begin{aligned}
\max_{j,i,w \in \{-1,1\}, v \in \{-1,1\}} \quad & \mathbf{J}_{\mathbf{x}}^{s-1} \check{\mathbf{d}}^s + w J_{\mathbf{x}}^{s-1}{}_j \lambda_{\mathbf{x}^s j} + v J_{\mathbf{p}_i} \lambda_{\mathbf{p}_i} \\
& + \tfrac{1}{2} w v \lambda_{\mathbf{x}^s j} \lambda_{\mathbf{p}_i} (\mathbf{J}_{\mathbf{x},\mathbf{p}}^{s-1}{}_{i,j} + \mathbf{J}_{\mathbf{p},\mathbf{x}}^{s-1}{}_{j,i}) \\
& + \tfrac{1}{2} \| \mathbf{\Lambda}_{\mathbf{p}} [\mathbf{J}_{\mathbf{x},\mathbf{p}}^{s-1} + (\mathbf{J}_{\mathbf{p},\mathbf{x}}^{s-1})^T] \check{\mathbf{d}}^s \|_2 \ .
\end{aligned}
\tag{5.14}
$$

Substituting the inner maximization problem of Eqn. (5.11) with Eqn. (5.14) gives

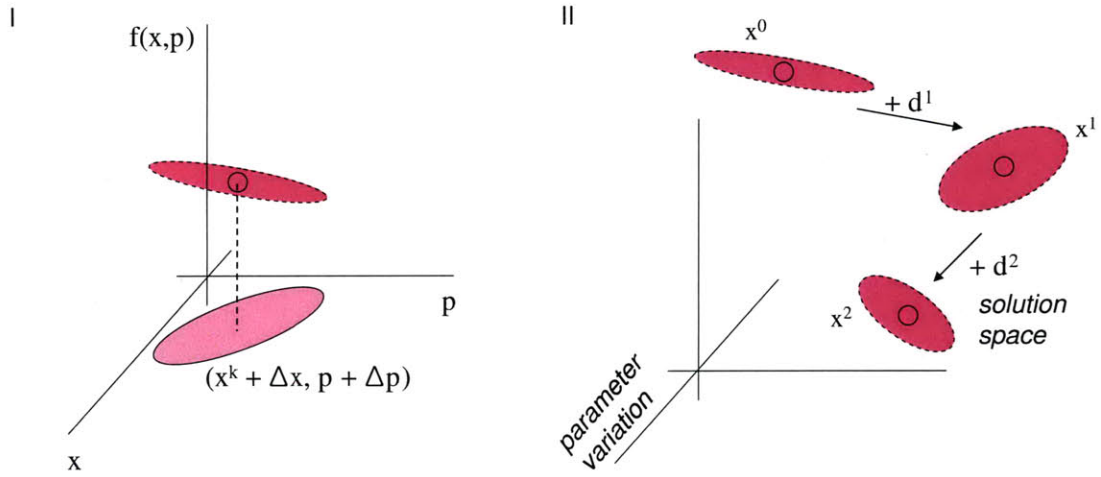


Figure 5-4: **Schematic representation of linearization-based robust iterative minimization.** (I) $f(\mathbf{x}, \mathbf{p})$ is linearized across ellipsoidal $\{\triangle\mathbf{x}, \triangle\mathbf{p}\}$-variation around $\{\mathbf{x}^k, \mathbf{p}\}$; maximum of this linearized $f(\mathbf{x}, \mathbf{p})$ approximates worst-case. (II) For finding solution $\mathbf{x}$ in solution space that minimizes worst-case $f(\hat{\mathbf{x}}, \hat{\mathbf{p}})$, linearization takes place at each iteration to account for variations in both solution value and parameters.

$$\begin{aligned} \min_{\check{\mathbf{d}}^s} \max_{j,i,w\in\{-1,1\},v\in\{-1,1\}} \quad & \mathbf{J}_{\mathbf{x}}^{s-1}\check{\mathbf{d}}^s + wJ_{\mathbf{x}}^{s-1}{}_j\lambda_{\mathbf{x}^s j} + vJ_{\mathbf{p}_i}\lambda_{\mathbf{p}_i} \\ & + \tfrac{1}{2}wv\lambda_{\mathbf{x}^s j}\lambda_{\mathbf{p}_i}(\mathbf{J}_{\mathbf{x},\mathbf{p}}^{s-1}{}_{i,j} + \mathbf{J}_{\mathbf{p},\mathbf{x}}^{s-1}{}_{j,i}) \\ & + \tfrac{1}{2}\|\mathbf{\Lambda}_{\mathbf{p}}[\mathbf{J}_{\mathbf{x},\mathbf{p}}^{s-1} + (\mathbf{J}_{\mathbf{p},\mathbf{x}}^{s-1})^T]\check{\mathbf{d}}^s\|_2 \ , \end{aligned} \tag{5.15}$$

which is equivalent to solving

$$
\begin{array}{lll}
\min_{\check{\mathbf{d}}^s, z} & z & \\
s.t. & \mathbf{J}_{\mathbf{x}}^{s-1}\check{\mathbf{d}}^s + wJ_{\mathbf{x}}^{s-1}{}_j\lambda_{\mathbf{x}^s j} + vJ_{\mathbf{p}_i}\lambda_{\mathbf{p}_i} \leq z, & \forall\{j,i,w,v\}, \\
& +\frac{1}{2}wv\lambda_{\mathbf{x}^s j}\lambda_{\mathbf{p}_i}(\mathbf{J}_{\mathbf{x},\mathbf{p}}^{s-1}{}_{i,j} + \mathbf{J}_{\mathbf{p},\mathbf{x}}^{s-1}{}_{j,i}) & j \in \{1,...,n\},\ i \in \{1,...,m\}, \\
& +\frac{1}{2}\|\mathbf{\Lambda}_{\mathbf{p}}[\mathbf{J}_{\mathbf{x},\mathbf{p}}^{s-1} + (\mathbf{J}_{\mathbf{p},\mathbf{x}}^{s-1})^T]\check{\mathbf{d}}^s\|_2 & w \in \{-1,1\},\ v \in \{-1,1\}\ ,
\end{array}
\tag{5.16}
$$

where each of the $2^2nm$ constraints is a second-order cone in $\check{\mathbf{d}}^s$ and $z$. Rearranging the terms gives

$$
\begin{array}{lll}
\min_{\check{\mathbf{d}}^s, z} & z & \\
s.t. & \frac{1}{2}\|\mathbf{\Lambda}_{\mathbf{p}}[\mathbf{J}_{\mathbf{x},\mathbf{p}}^{s-1} + (\mathbf{J}_{\mathbf{p},\mathbf{x}}^{s-1})^T]\check{\mathbf{d}}^s\|_2 \leq & -\mathbf{J}_{\mathbf{x}}^{s-1}\check{\mathbf{d}}^s + z \\
& & -wJ_{\mathbf{x}}^{s-1}{}_j\lambda_{\mathbf{x}^s j} - vJ_{\mathbf{p}_i}\lambda_{\mathbf{p}_i} \\
& & -\frac{1}{2}wv\lambda_{\mathbf{x}^s j}\lambda_{\mathbf{p}_i}(\mathbf{J}_{\mathbf{x},\mathbf{p}}^{s-1}{}_{i,j} + \mathbf{J}_{\mathbf{p},\mathbf{x}}^{s-1}{}_{j,i}), \\
& \forall\{j,i,w,v\}, & \\
& j \in \{1,...,n\},\ i \in \{1,...,m\}, & \\
& w \in \{-1,1\},\ v \in \{-1,1\}\ , &
\end{array}
\tag{5.17}
$$

and if the additional constraints expressing the bounds on $\check{\mathbf{d}}^s$ are also second-order cones or are linear in $\check{\mathbf{d}}^s$ and $z$ (e.g., $\mathbf{x}^{s-1} + \check{\mathbf{d}}^s \geq 0$), Eqn. (5.17) can be solved as a second-order cone program.

### Update magnitude selection

The linearization-based criterion for determining the $a$ in Step 3 of the robust iterative procedure is as follows:

1. Designate the following entities for a given $a$:

(a) $\check{\mathbf{J}}_{\mathbf{x},a}^{s-1}$, the matrix of partial derivatives of $f(\mathbf{x}^{s-1} + a\check{\mathbf{d}}^s, \mathbf{p})$ with respect to each element of $\mathbf{x}^{s-1} + a\check{\mathbf{d}}^s$

(b) $\check{\mathbf{J}}_{\mathbf{x},\mathbf{p},a}^{s-1}$, the matrix of partial derivatives of each element of $\check{\mathbf{J}}_{\mathbf{x},a}^{s-1}$ with respect to each element of $\mathbf{p}$

(c) $\check{\mathbf{J}}^{s-1}_{\mathbf{p},a}$, the matrix of partial derivatives of $f(\mathbf{x}^{s-1} + a\check{\mathbf{d}}^s, \mathbf{p})$ with respect to each element of $\mathbf{p}$

(e) $\check{\mathbf{J}}^{s-1}_{\mathbf{p},\mathbf{x},a}$, the matrix of partial derivatives of each element of $\check{\mathbf{J}}^{s-1}_{\mathbf{p},a}$ with respect to each element of $\mathbf{x}^{s-1} + a\check{\mathbf{d}}^s$

2. Approximate $f(\mathbf{x}^{s-1} + a\check{\mathbf{d}}^s + \triangle\mathbf{x}, \mathbf{p} + \triangle\mathbf{p})$ as

$$\begin{aligned} & f(\mathbf{x}^{s-1} + a\check{\mathbf{d}}^s, \mathbf{p}) \\ & + \check{\mathbf{J}}^{s-1}_{\mathbf{x},a}\triangle\mathbf{x} + \check{\mathbf{J}}^{s-1}_{\mathbf{p},a}\triangle\mathbf{p} \\ & + \tfrac{1}{2}\triangle\mathbf{p}^T\check{\mathbf{J}}^{s-1}_{\mathbf{x},\mathbf{p},a}\triangle\mathbf{x} + \tfrac{1}{2}\triangle\mathbf{x}^T\check{\mathbf{J}}^{s-1}_{\mathbf{p},\mathbf{x},a}\triangle\mathbf{p} \ , \end{aligned} \tag{5.18}$$

and in turn the maximum of $f(\mathbf{x}^{s-1} + a\check{\mathbf{d}}^s + \triangle\mathbf{x}, \mathbf{p} + \triangle\mathbf{p})$ as

$$\begin{aligned} & f(\mathbf{x}^{s-1} + a\check{\mathbf{d}}^s, \mathbf{p}) \\ & + \max_{j,i,w\in\{-1,1\},v\in\{-1,1\}} \quad w(\check{J}^{s-1}_{\mathbf{x},a})_j\lambda_{\mathbf{x}^s j} + v(\check{J}^{s-1}_{\mathbf{p},a})_i\lambda_{\mathbf{p}_i} \\ & \qquad\qquad + \tfrac{1}{2}wv\lambda_{\mathbf{x}^s j}\lambda_{\mathbf{p}_i}[(\check{\mathbf{J}}^{s-1}_{\mathbf{x},\mathbf{p},a})_{i,j} + (\check{\mathbf{J}}^{s-1}_{\mathbf{p},\mathbf{x},a})_{j,i}] \ . \end{aligned} \tag{5.19}$$

3. Search for the $a$ that minimizes Eqn. (5.19).

## 5.3 Application to BCG immunotherapy

### 5.3.1 Methods

The linearized worst-case approximation procedure is applied to designing robust protocols for continuous-dose therapy of superficial bladder cancer using BCG, as specified in Sec. 4.2.1. The types of uncertainty considered here are as follows:

**Type A.** BCG is administered at some rate $\hat{b} = b + z_1(0.5)$, where $-1 \leq z_1 \leq 1$, instead of at $b$.

**Type B.** At $t = 0$, the initial concentrations of the species are $\hat{B}_0 = B_0 + z_2 B_0$, $\hat{E}_0 = E_0 + z_3 E_0$, $\hat{T}_{i0} = T_{i0} + z_4 T_{i0}$, $\hat{T}_{u0} = T_{u0} + z_5 T_{u0}$, where $-1 \leq z_k \leq 1$, $k = \{2, ..., 5\}$, instead of $B_0$, $E_0$, $T_{i0}$, $T_{u0}$, respectively.

**Type C.** $\beta = z_6$ and $r = z_7$, where $0.013 \leq z_6 \leq 0.022$ and $0.1 \leq z_7 \leq 0.45$ [34], instead of $\beta = 0.0155$ and $r = 0.12$.

**Type D.** $\{\mu, p_1, p_2, p_3, p_4, p_5, \alpha\} = \{(\mu + z_8\mu), (p_1 + z_9 p_1), (p_2 + z_{10} p_2), (p_3 + z_{11} p_3), (p_4 + z_{12} p_4), (p_5 + z_{13} p_5), (\alpha + z_{14}\alpha)\}$, where $-1 \leq z_Q \leq 1$, $Q = \{8, ..., 14\}$, instead of $\{\mu, p_1, p_2, p_3, p_4, p_5, \alpha\} = \{0.41, 1.25, 0.285, 1.1, 0.12, 0.003, 0.52\}$.

### Handling uncertainty types A, B, and C

Define $U(b)$ as the neighborhood of uncertainty that consists of all vectors $\mathbf{z} = (z_1, ..., z_7)$, such that $-M_1 \leq z_1 \leq M_1$, where $0 \leq M_1 \leq 1$, $-M_k \leq z_k \leq M_k$ for $k = \{2, ..., 5\}$, where $0 \leq M_k \leq 1$, $M_{l6} \leq z_6 \leq M_{u6}$, where $0 \leq M_{l6} \leq 0.0155$ and $M_{u6} \geq 0.0155$, and $M_{l7} \leq z_7 \leq M_{u7}$, where $0 \leq M_{l7} \leq 0.12$ and $M_{u7} \geq 0.12$. Let $Z(b)$ be a subset of $U(b)$, made up of $\mathbf{z} = (0, 0, 0, 0, 0, 0.0155, 0.12)$ and additional vectors sampled from $U(b)$. Unless otherwise stated, this work specifies this uncertainty hypercube $U(b)$ with $M_1 = 1$, $M_k = 0.25$ for $k = \{2, ..., 5\}$, $M_{l6} = 0.013$, $M_{u6} = 0.022$, $M_{l7} = 0.1$, and $M_{u7} = 0.45$.

When the performance of a protocol $b$ against uncertainty scenarios sampled from within the hypercube is evaluated, $F(b)$ is computed under every member of $Z(b)$ drawn from $U(b)$. In addition to $\mathbf{z} = (0, 0, 0, 0, 0, 0.0155, 0.12)$, members of $Z(b)$ for this evaluation are chosen to be $\mathbf{z}$ made up of every combination of $z_1 = \{-p, p\}$, $z_k = \{-q, q\}$ for $k = \{2, ..., 5\}$, $z_6 = \{M_{l6}, M_{u6}\}$, and $z_7 = \{M_{l7}, M_{u7}\}$, for every 0.2 increment of $p$ between 0 and 1 and every 0.05 increment of $q$ between 0 and 0.25. The worst uncertainty scenario $\mathbf{z} \in Z(b)$ that maximizes $F(b)$ is designated as $\mathbf{z}_{ABC}^{worst}$.

### Handling uncertainty types A, B, C, and D

Define $U(b)$ as the neighborhood of uncertainty that consists of all vectors $\mathbf{z} = (z_1, ..., z_{14})$, such that $-M_1 \leq z_1 \leq M_1$, where $0 \leq M_1 \leq 1$, $-M_k \leq z_k \leq M_k$ for $k = \{2, ..., 5\}$, where $0 \leq M_k \leq 1$, $M_{l6} \leq z_6 \leq M_{u6}$, where $0 \leq M_{l6} \leq 0.0155$ and $M_{u6} \geq 0.0155$, $M_{l7} \leq z_7 \leq M_{u7}$, where $0 \leq M_{l7} \leq 0.12$ and $M_{u7} \geq 0.12$, and $-M_Q \leq z_Q \leq M_Q$ for $Q = \{8, ..., 14\}$, where $0 \leq M_Q \leq 1$. Let $Z(b)$ be a subset of $U(b)$, made up of $\mathbf{z} = (0, 0, 0, 0, 0, 0.0155, 0.12, 0.41, 1.25, 0.285, 1.1, 0.12, 0.003, 0.52)$

and additional vectors sampled from $U(b)$. Unless otherwise stated, this work specifies this uncertainty hypercube $U(b)$ with $M_1 = 1$, $M_k = 0.25$ for $k = \{2, ..., 5\}$, $M_{l6} = 0.013$, $M_{u6} = 0.022$, $M_{l7} = 0.1$, $M_{u7} = 0.45$, and $M_Q = 0.25$ for $Q = \{8, ..., 14\}$.

When the performance of a protocol $b$ against uncertainty scenarios sampled from within the hypercube is evaluated, $F(b)$ is computed under every member of $Z(b)$ drawn from $U(b)$. In addition to $\mathbf{z} = (0, 0, 0, 0, 0, 0.0155, 0.12, 0.41, 1.25, 0.285, 1.1, 0.12, 0.003, 0.52)$, members of $Z(b)$ for this evaluation are chosen to be $\mathbf{z}$ made up of every combination of $z_1 = \{-p, p\}$, $z_k = \{-q, q\}$ for $k = \{2, ..., 5\}$, $z_6 = \{M_{l6}, M_{u6}\}$, $z_7 = \{M_{l7}, M_{u7}\}$, and $z_Q = \{-q, q\}$ for $Q = \{8, ..., 14\}$, for every 0.2 increment of $p$ between 0 and 1 and every 0.05 increment of $q$ between 0 and 0.25. The worst uncertainty scenario $\mathbf{z} \in Z(b)$ that maximizes $F(b)$ is designated as $\mathbf{z}^{worst}_{ABCD}$.

### 5.3.2 Results

The protocol designed using the standard approach, denoted $b^{stn}$, was $b^{stn} = 2.8375$ reduced units (equal to 283750 $cells\ days^{-1}$), associated with an objective function value of $F(b^{stn}) = 2.4659$. A trajectory of the total number of tumor cells as a function of time $[T(t) = T_i(t) + T_u(t)]$ under this protocol $b^{stn}$ is shown in Fig. 5-5 (solid blue line).

We first enumerated variation in the applied therapeutic dose, the initial conditions of the model, and the parameters $\beta$ and $r$ (see Sec. 5.3.1). The least favorable objective function value was observed for one corner of the uncertainty hypercube at $\mathbf{z}^{stn,worst}_{ABC} = (-1, -0.25, 0.25, 0.25, 0.25, 0.013, 0.45)$ with objective function value $F(b^{stn}) = 2051.8$, and the resulting trajectory is shown (dashed blue line) alongside the perfect trajectory (solid blue line) in Fig. 5-5.

A new treatment was designed using the sampling-based robust approach, designating a range of uncertainty corresponding to that used to test the standard optimized therapy above. The resulting optimized treatment was computed to be $b^{robsmp}_{ABC} = 4.4762$ reduced units (equal to 447620 $cells\ days^{-1}$), with objective function value $F(b^{robsmp}_{ABC}) = 2.6225$. A trajectory of tumor cell number versus time under this protocol is shown in Fig. 5-5 (solid green line). Evaluating the behavior of this

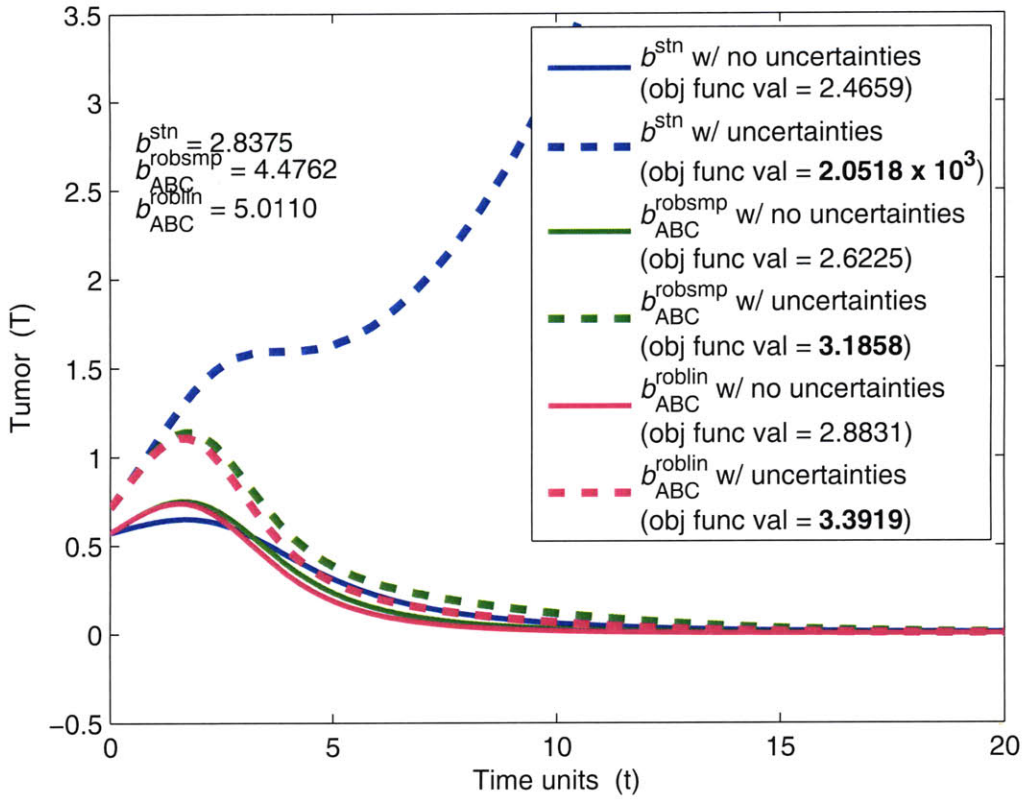


Figure 5-5: **Tumor response under designed BCG therapy when uncertainty types A, B, and C are present.** Total number of tumor cells $[T(t) = T_i(t) + T_u(t)]$ under standardly designed protocol $b^{stn}$ (solid blue) and with its worst-case uncertainty $\mathbf{z}^{stn,worst}_{ABC}$ (dashed blue); $T(t)$ under sampled-robust protocol $b^{robsmp}_{ABC}$ (solid green) and with its worst-case uncertainty $\mathbf{z}^{robsmp,worst}_{ABC}$ (dashed green); $T(t)$ under linearized-robust protocol $b^{roblin}_{ABC}$ (solid pink) and with its worst-case uncertainty $\mathbf{z}^{roblin,worst}_{ABC}$ (dashed pink).

sampled-robust protocol across the same uncertainties in model and treatment tested for the standard treatment optimum, its worst point within the uncertainty hypercube is at $\mathbf{z}^{robsmp,worst}_{ABC} = (1, -0.25, -0.25, 0.25, 0.25, 0.013, 0.45)$, and the resulting trajectory is shown in Fig. 5-5 (green dashed line) with associated objective value $F(b^{robsmp}_{ABC}) = 3.1858$.

A treatment was then designed using the linearization-based robust approach developed here. A detailed description is given in Sec. 5.2. Briefly stated, the worst objective function value across a range of uncertainties in the model and the delivery

of the intended therapy is approximated by a linearization of the objective funcation at each iteration of the minimization process. Once again using a range of uncertainty corresponding to that used to test the standard optimized therapy, this time by designating analogous ellipsoid-shaped uncertainty spaces (see Sec. 5.2), the resulting optimized treatment was $b^{roblin}_{ABC} = 5.0110$ reduced units (equal to 501100 $cells\ days^{-1}$), with objective function value $F(b^{roblin}_{ABC}) = 2.8831$. The tumor trajectory versus time under this linearized-robust protocol is shown in Fig. 5-5 (solid pink line). And subjecting it to the same uncertainties within the uncertainty hypercube as the other protocols, its worst point is at $\mathbf{z}^{roblin,worst}_{ABC} = (1, -0.25, -0.25, 0.25, 0.25, 0.013, 0.45)$, associated with an objective function value of $F(b^{roblin}_{ABC}) = 3.3919$, and its resulting tumor trajectory is shown in Fig. 5-5 (pink dashed line) as well.

We then allowed variation to also exist in model parameters other than $\beta$ and $r$ (see Sec. 5.3.1). Subject to this higher-dimensional uncertainty hypercube, the number of tumor cells rises uncontrollably through time under the standardly designed protocol's worst associated uncertainty $[\mathbf{z}^{stn,worst}_{ABCD} = (-1, -0.25, 0.25, 0.25, 0.25, 0.013, 0.45, -0.25, 0.25, -0.25, -0.25, 0.25, -0.25, 0.25)]$, as shown in Fig. 5-6 (blue dashed line). This worst objective function value is $F(b^{stn}) = 11845$. Also shown here, once again for comparison, is the number of tumor cells in the system with no model or therapeutic uncertainties (solid blue line), being treated with the same standard protocol.

A protocol was then designed using the linearization-based robust approach, denoted $b^{roblin}_{ABCD}$, accounting for the enlarged space of potential model and therapeutic uncertainties. Shown in Fig. 5-6 (solid pink line) is the number of tumor cells in the system with no model or therapeutic uncertainties, being treated with this lineared-robust protocol. The protocol administers BCG at a rate of $b^{roblin}_{ABCD} = 9.4893$ reduced units (equal to 948930 $cells\ days^{-1}$), with objective function value $F(b^{roblin}_{ABCD}) = 5.1678$. Its worst point is at $\mathbf{z}^{roblin,worst}_{ABCD} = (1, -0.25, 0.25, 0.25, 0.25, 0.013, 0.45, -0.25, 0.25, -0.25, -0.25, 0.25, -0.25, 0.25)$, associated with an objective function value of $F(b^{roblin}_{ABCD}) = 6.0944$, even under which the number of tumor cells remains under control, as shown in Fig. 5-6 (pink dashed line).

The results obtained illustrate the effectiveness of using the robust optimization

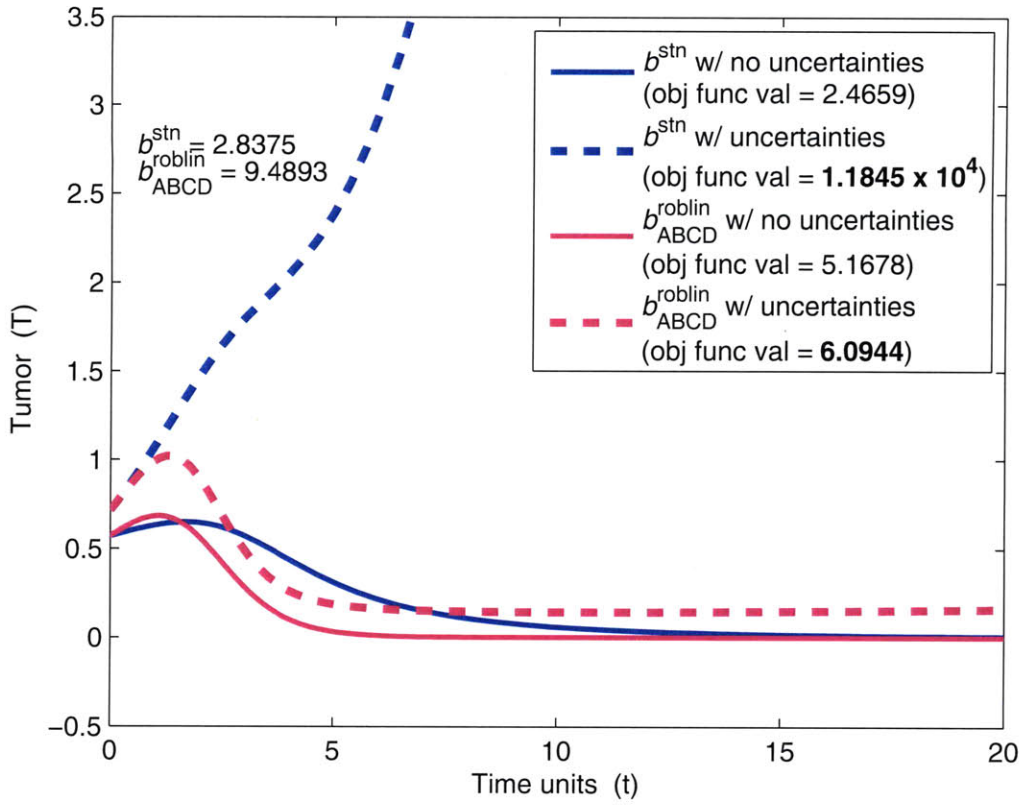


Figure 5-6: **Tumor response under designed BCG therapy when uncertainty types A, B, C, and D are present.** Total number of tumor cells $[T(t) = T_i(t) + T_u(t)]$ under standardly designed protocol $b^{stn}$ (solid blue) and with its worst-case uncertainty $\mathbf{z}^{stn,worst}_{ABCD}$ (dashed blue); $T(t)$ under linearized-robust protocol $b^{roblin}_{ABCD}$ (solid pink) and with its worst-case uncertainty $\mathbf{z}^{roblin,worst}_{ABCD}$ (dashed pink).

method based on linearized worst-case uncertainty approximation for designing cancer immunotherapeutic protocols in the presence of uncertainties. Fig. 5-5 shows that, for handling uncertainty types A, B, and C (see Sec. 5.3.1), the linearized-robust protocol $b^{roblin}_{ABC}$ maintains the objective function value relatively low even in its worst uncertainty scenario $\mathbf{z}^{roblin,worst}_{ABC}$, when compared to the standard protocol $b^{stn}$ in $\mathbf{z}^{stn,worst}_{ABC}$. The same holds true when comparing the linearized-robust protocol $b^{roblin}_{ABCD}$ in $\mathbf{z}^{roblin,worst}_{ABCD}$ against $b^{stn}$ in $\mathbf{z}^{stn,worst}_{ABCD}$, for handling uncertainty types A, B, C, and D, as shown in Fig. 5-6.

To select the update direction during every iteration of the minimization process,

the sampling-based robust method evaluates the objective function value at each of the $N$ samples taken from the uncertainty sets. For $n$ dimensions of uncertainty in the vector of decision variables and $m$ dimensions of uncertainty in other parameters upon which the objective function value depends, the number of samples expected to be necessary in making a valid approximation to the worst uncertainty scenario grows exponentially with $n + m$. Contrastingly, the number of constraints in (5.17), the optimization problem solved by the linearization-based robust method to select the update direction, grows linearly with $nm$. For handling uncertainty types A, B, and C, Fig. 5-5 shows the comparable performance of the linearized-robust protocol $b^{roblin}_{ABC}$ to that of the sampled-robust protocol $b^{robsmp}_{ABC}$.

## 5.4 Robustness-based experimental guidance

How sensitive the objective function value at a protocol $b$ is, to a parameter $p$ that it depends on, can be analyzed by assessing how much the value changes under a change in $p$. These changes at the standard protocol $b^{stn}$ (blue square) and at the linearized-robust protocol $b^{roblin}_{ABCD}$ (pink circle) under 1% increase in $p$, taking as $p$ every parameter in Table 4.1 and $b^{stn}$ and $b^{roblin}_{ABCD}$, respectively, are shown in Fig. 5-7I. Since $b^{roblin}_{ABCD}$ is explicitly designed to be robust to variability in the parameters, the changes are greater in magnitude at $b^{stn}$ than at $b^{roblin}_{ABCD}$ as expected.

One can also assess how much the worst-case objective function value under $b^{roblin}_{ABCD}$, denoted $F^{worst}(b^{roblin}_{ABCD})$, changes as the uncertainty range of a parameter $p$ decreases. Shown in Fig. 5-7II are these values for the uncertainty range of $p$ decreasing by 25% (pink triangle), once again taking as $p$ every parameter in Table 4.1 and $b^{roblin}_{ABCD}$. The values found here can help indicate having more certainty about which single parameter can improve the worst-case performance under protocol $b^{roblin}_{ABCD}$; out of these single-parameter uncertainty changes considered, having either $r$ or $p_2$, the tumor growth rate or the infection rate of uninfected tumor cells with BCG [34], respectively, be subject to less uncertainty seems to improve the worst-case performance of $b^{roblin}_{ABCD}$ the most. This type of assessment can certainly be further carried out for pairs and

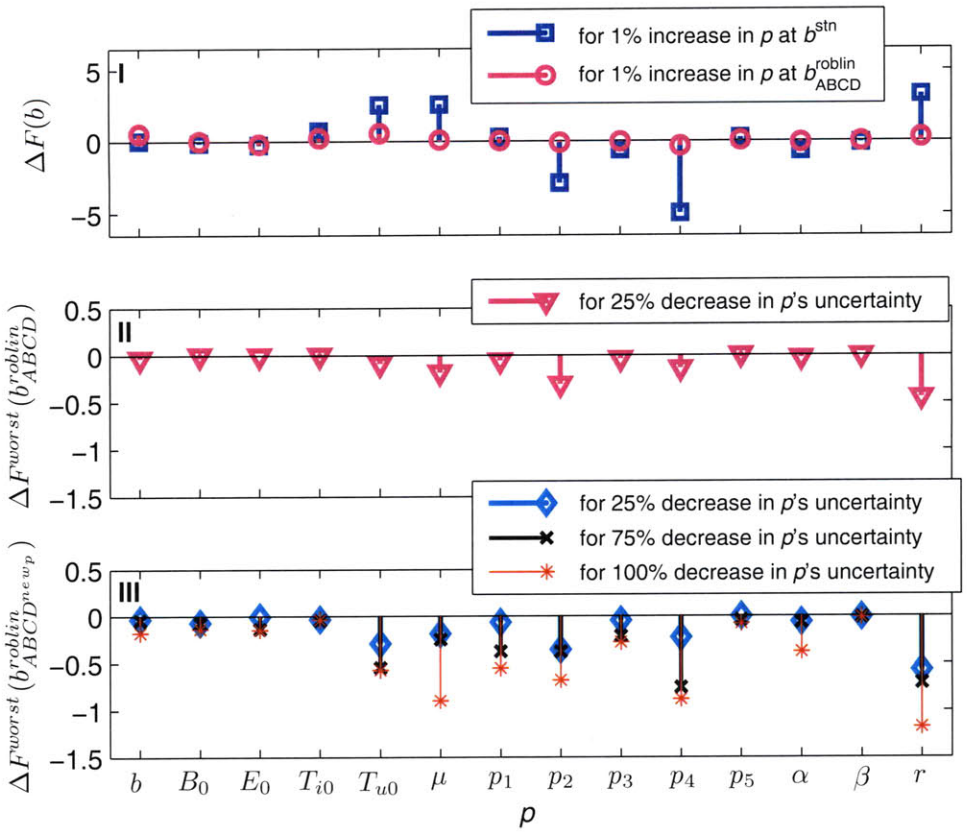


Figure 5-7: **Effect of parameter and parameter uncertainty changes on therapeutic performance.** (I) Change in the objective function value at the standard protocol $b^{stn}$ (blue square) and at the linearized-robust protocol $b^{roblin}_{ABCD}$ (pink circle) under 1% increase in $p$, where $p$ is every parameter in Table 4.1 and $b^{stn}$ and $b^{roblin}_{ABCD}$, respectively. (II) Change in the worst-case objective function value under $b^{roblin}_{ABCD}$ as the uncertainty range of $p$ is decreased by 25% (pink triangle). (III) Change in the worst-case objective function value under each respective newly determined linearized-robust protocol $b^{roblin}_{ABCD^{new_p}}$ as the uncertainty range of $p$ is decreased by 25% (light blue diamond), by 75% (black x), and by 100% (red star).

even higher-order combinations of parameter uncertainties decreasing simultaneously.

However, what is of greater interest is not the performance of $b^{roblin}_{ABCD}$ given a decreased uncertainty range for a parameter, but rather the performance of a robust protocol that has been newly optimized for handling the worst-case given the new decreased uncertainty range. Shown in Fig. 5-7III are these values for the uncertainty range of $p$ decreasing by 25% (light blue diamond), by 75% (black x), and by 100% (red star), once again taking as $p$ every parameter in Table 4.1 and the

respective new optimal robust protocol given the uncertainty decrease in $p$, denoted $b^{roblin}_{ABCD^{new_p}}$. Although a decrease in the uncertainty of $r$ still remains as the strongest single-parameter effect, notice that $p_4$, the rate of immune response activation by the encounter of effector cells with BCG [34], increases in significance as its uncertainty is decreased by 75%. Also, $\mu$, the ratio of effector cell and BCG mortality rates, increases in significance as its uncertainty is further decreased. The values found here indicate having how much more certainty about which single parameter can improve the best worst-case performance, and thus can more directly point to which parameters experiments should concentrate on precisely specifying for improved robust therapy.

Determining which experimental efforts to pursue through this type of approach requires a large number of worst-case optimization problems to be solved, particularly as one wishes to simulate higher-order combinations of changes in parameter uncertainties. Besides being capable of designing robust treatment protocols, the linearization-based robust method introduced in this work, by enabling multiple dimensions of uncertainties to be considered in a more computationally efficient manner, makes plausible such a novel approach to guiding experimental planning towards improving the worst-case performance of protocols designed for cancer immunotherapy.

## 5.5 Discussion

The robust optimization method introduced in this work that uses the linearized worst-case approximation, together with the robustness-based experimental guidance that it enables, is applicable to therapy beyond immunotherapy. Radiation oncology is a field that already actively applies robust optimization to handling the potentially hazardous radiation equipment. Among many sources of uncertainty in the radiation therapy procedure, Unkelbach et al. report their consideration of the possibility that the position of the patient's body and the ranges of the proton beams that are directed at the tumor from outside the body may deviate from the situation under which optimal therapy is designed [60]. Comparing the probabilistic approach that they take

to incorporate the uncertainties into the optimization with the linearization-based approach, the relationship between the specifications of the random distributions that they use and the lengths of the semi-axes of the uncertainty ellipsoids characterized during the linearization here can be studied.

Further improvement of analytically formulating the min-max problem for optimizing the worst-case is also conceivable. Such improvement may consist of considering whether including additional higher-order terms when linearizing the objective function is helpful for locating more favorable robust minima. If all second-order terms were to be included in the approximation, for instance, $f(\mathbf{x}^{s-1} + a\check{\mathbf{d}}^s + \triangle\mathbf{x}, \mathbf{p} + \triangle\mathbf{p})$ would be approximated as

$$\begin{aligned}
&f(\mathbf{x}^{s-1}, \mathbf{p}) \\
&+\mathbf{J}_{\mathbf{x}}^{s-1}(\check{\mathbf{d}}^s + \triangle\mathbf{x}) \\
&+\tfrac{1}{2}(\check{\mathbf{d}}^s + \triangle\mathbf{x})^T\mathbf{J}_{\mathbf{x},\mathbf{x}}^{s-1}(\check{\mathbf{d}}^s + \triangle\mathbf{x}) \\
&+\tfrac{1}{2}\triangle\mathbf{p}^T\mathbf{J}_{\mathbf{x},\mathbf{p}}^{s-1}(\check{\mathbf{d}}^s + \triangle\mathbf{x}) \\
&+\mathbf{J}_{\mathbf{p}}^{s-1}\triangle\mathbf{p} \\
&+\tfrac{1}{2}(\check{\mathbf{d}}^s + \triangle\mathbf{x})^T\mathbf{J}_{\mathbf{p},\mathbf{x}}^{s-1}\triangle\mathbf{p} \\
&+\tfrac{1}{2}\triangle\mathbf{p}^T\mathbf{J}_{\mathbf{p},\mathbf{p}}^{s-1}\triangle\mathbf{p} \ .
\end{aligned} \tag{5.20}$$

instead of as Eqn. (5.8), where $\mathbf{J}_{\mathbf{x},\mathbf{x}}^{s-1}$ is the matrix of partial derivatives of each element of $\mathbf{J}_{\mathbf{x}}^{s-1}$ with respect to each element of $\mathbf{x}^{s-1}$ and $\mathbf{J}_{\mathbf{p},\mathbf{p}}^{s-1}$ is the matrix of partial derivatives of each element of $\mathbf{J}_{\mathbf{p}}^{s-1}$ with respect to each element of $\mathbf{p}$. This version of the linear approximation would require a different set of subsequent equation manipulations to take part in a computationally reasonable formulation of the min-max optimization problem, such as the second-order programming formulation in Eqn. (5.17) used in this work. Having multiple versions of the linearization-based formulation at hand can then enable investigation into how different orders of linear approximation trade off against computational efficiency for running the optimizer on a variety of network models, which may in turn offer additional dimensions of analysis that shine light on inherent properties of the networks modeled.

Relating to Ch. 3 of this work, the linearization-based method can also be applied

to network calibration in systems biology. The methodology of robust optimization itself is yet to be extensively used for biological network calibration, with robust parameter estimation most often being aligned rather with the ability of an estimation method to consistently reach one parameter set more often than other sets in the midst of limited data quality and nonlinearity, as in ref. [57]. With one of the major next steps to take following the robust calibration efforts explored thus far being systematic characterization of robustness levels for analyzing networks, this worst-case approximation through linearization can potentially serve as the alternative efficient mathematical representation needed for such characterization, taking the place of the sampling process previously used.

# Chapter 6

# Contributions and Future Work

This dissertation began with trying to answer one question of whether or not using robust optimization can make a difference in estimating parameters of quantitative biological models from experimental data. Realizing that the answer to the question is not a simple yes or no was a critical step in adjusting the focus to look more carefully into the capabilities of robust optimization for systems biological research as a whole. Applying robust methods to design therapeutic protocols showed the difference that considering robustness can make in efforts involving model-based design that need to reliably handle expected uncertainties that exist in both model accuracy and the precision with which the design can be implemented. Formulating the computational methodology for solving worst-case optimization problems beyond extensive sampling of possible uncertainty scenarios, this work also made plausible a novel approach to carrying out experimental guidance that is aimed at lowering the cost of making robust decisions.

There are three directions towards which work from here onwards can move in. The first of the three is further development of the worst-case robust optimization method. This refinement includes experimenting with other mathematical methods of approximating the worst-case, particularly in terms of using any application-specific knowledge to decrease the computational burden while increasing the accuracy with which robust optima can be found. The second direction is branching out with the robust tools developed here, such as the optimization methods and the approach

to experimental guidance, and applying them to where robust determination would be critical. One interesting field would be quantitative epidemiology, which uses mathematical models of infectious diseases in planning the intervention needed to track and prevent outbreaks at the population level. The third direction is concerned with using the robust tools for system identification beyond parameter estimation. For example, combining robust calibration with experimental model discrimination can help classify models or individual components of models into being robust or not and to what degree, contributing to enhancing the understanding of why nature has designed biological systems to behave the way they do.

Optimization is one of many mathematical ideas being actively applied to the field of systems biology. Whether or not such an idea can directly solve an existing problem may actually be just the beginning of the application. More often than not, that beginning can serve as the entrance into new dimensions of analysis that can be made using the idea in ways that have not been explored previously. Such interaction that leads to synergistic development in the areas involved is where the strength of interdisciplinary research lies, as is shown by this work and others that are in the midst of active progress towards advancing the study of biological systems from a mathematical perspective.

# Bibliography


[1] J.F. Apgar, J.E. Toettcher, D. Endy, F.M. White, and B. Tidor: Stimulus design for model selection and validation in cell signaling. PLoS Comput. Biol., **4** (2008) e30.

[2] T. Maiwald and J. Timmer: Dynamical modeling and multi-experiment fitting with PottersWheel. Bioinformatics, **24** (2008) 2037–2043.

[3] T. Hirmajer, E. Balsa-Canto, and J.R. Banga: DOTcvpSB, a software toolbox for dynamic optimization in systems biology. BMC Bioinformatics, **10** (2009) 199.

[4] R. Dilão and D. Muraro: A software tool to model genetic regulatory networks. Applications to the modeling of threshold phenomena and of spatial patterning in Drosophila. PLoS One, **5** (2010) e10743.

[5] F. Jacob and J. Monod: Genetic regulatory mechanisms in the synthesis of proteins. J. Mol. Biol., **3** (1961) 318–356.

[6] R.N. Gutenkunst, J.J. Waterfall, F.P. Casey, K.S. Brown, C.R. Myers, and J.P. Sethna: Universally sloppy parameter sensitivities in systems biology models. PLoS Comput. Biol., **3** (2007) 1871–1878.

[7] P.M. Coelho, A. Salvador, and M.A. Savageau: Quantifying global tolerance of biochemical systems: design implications for moiety-transfer cycles. PLoS Comput. Biol., **5** (2009) e1000319.

[8] M. Vilela, S. Vinga, M.A. Maia, E.O. Voit, and J.S. Almeida: Identification of neutral biochemical network models from time series data. BMC Syst. Biol., **3** (2009) 47.

[9] H. Braat, P. Rottiers, D.W. Hommes, N. Huyghebaert, E. Remaut, J.P. Remon, S.J. van Deventer, S. Neirynck, M.P. Peppelenbosch, and L. Steidler: A phase I trial with transgenic bacteria expressing interleukin-10 in Crohn's disease. Clin. Gastroenterol. Hepatol., **4** (2006) 754–759.

[10] M. Ashyraliyev, J. Jaeger, and J.G. Blom: Parameter estimation and determinability analysis applied to Drosophila gap gene circuits. BMC Syst. Biol., **2** (2008) 83.

[11] J.F. Apgar, D.K. Witmer, F.M. White, and B. Tidor: Sloppy models, parameter uncertainty, and the role of experimental design. Mol. Biosyst., [Epub ahead of print] (2010).

[12] S. Bandara, J.P. Schlöder, R. Eils, H.G. Bock, and T. Meyer: Optimal experimental design for parameter estimation of a cell signaling model. PLoS Comput. Biol., **5** (2009) e1000558.

[13] B. Mélykúti, E. August, A. Papachristodoulou, and H. El-Samad: Discriminating between rival biochemical network models: three approaches to optimal experiment design. BMC Syst. Biol., **4** (2010) 38.

[14] B.M. Donckels, D.J. De Pauw, P.A. Vanrolleghem, and B. De Baets: A kernel-based method to determine optimal sampling times for the simultaneous estimation of the parameters of rival mathematical models. J. Comput. Chem., **30** (2009) 2064–2077.

[15] R. Tasseff, S. Nayak, S. Salim, P. Kaushik, N. Rizvi, and J.D. Varner: Analysis of the molecular networks in androgen dependent and independent prostate cancer revealed fragile and robust subsystems. PLoS One, **5** (2010) e8864.

[16] N.A. van Riel: Dynamic modelling and analysis of biochemical networks: mechanism-based models and model-based experiments. Brief. Bioinform., **7** (2006) 364–374.

[17] K.G. Gadkar, R. Gunawan, and F.J. Doyle, III: Iterative approach to model identification of biological networks. BMC Bioinform., **6** (2005) 155.

[18] J.C. Locke, A.J. Millar, and M.S. Turner: Modelling genetic networks with noisy and varied experimental data: the circadian clock in Arabidopsis thaliana. J. Theor. Biol., **234** (2005) 383–393.

[19] M. Bentele, I. Lavrik, M. Ulrich, S. Stösser, D.W. Heermann, H. Kalthoff, P.H. Krammer, and R. Eils: Mathematical modeling reveals threshold mechanism in CD95-induced apoptosis. J. Cell Biol., **166** (2004) 839–851.

[20] H. Kitano: Towards a theory of biological robustness. Mol. Syst. Biol., **3** (2007) 137.

[21] H. Kitano: Biological robustness. Nat. Rev. Genet., **5** (2004) 826–837.

[22] N. Barkai and S. Leibler: Robustness in simple biochemical networks. Nature, **387** (1997) 913–917.

[23] M. Morohashi, A.E. Winn, M.T. Borisuk, H. Bolouri, J. Doyle, and H. Kitano: Robustness as a measure of plausibility in models of biochemical networks. J. Theor. Biol., **216** (2002) 19–30.

[24] V.A. Kuznetsov, I.A. Makalkin, M.A. Taylor, and A.S. Perelson: Nonlinear dynamics of immunogenic tumors: parameter estimation and global bifurcation analysis. Bull. Math. Biol., **56** (1994) 295–321.

[25] H. Zhu, R.J. Melder, L.T. Baxter, and R.K. Jain: Physiologically based kinetic model of effector cell biodistribution in mammals: implications for adoptive immunotherapy. Cancer Res., **56** (1996) 3771–3781.

[26] S.W. Friedrich, S.C. Lin, B.R. Stoll, L.T. Baxter, L.L. Munn, and R.K. Jain: Antibody-directed effector cell therapy of tumors: analysis and optimization using a physiologically based pharmacokinetic model. Neoplasia, **4** (2002) 449–463.

[27] P. Bühler, P. Wolf, D. Gierschner, I. Schaber, A. Katzenwadel, W. Schultze-Seemann, U. Wetterauer, M. Tacke, M. Swamy, W.W. Schamel, and U. Elsässer-Beile: A bispecific diabody directed against prostate-specific membrane antigen and CD3 induces T-cell mediated lysis of prostate cancer cells. Cancer Immunol. Immunother., **57** (2008) 43–52.

[28] U. Reusch, M. Sundaram, P.A. Davol, S.D. Olson, J.B. Davis, K. Demel, J. Nissim, R. Rathore, P.Y. Liu, and L.G. Lum: Anti-CD3 x anti-epidermal growth factor receptor (EGFR) bispecific antibody redirects T-cell cytolytic activity to EGFR-positive cancers in vitro and in an animal model. Clin. Cancer Res., **12** (2006) 183–190.

[29] D. Kirschner and J.C. Panetta: Modeling immunotherapy of tumor-immune interaction. J. Math. Biol., **37** (1998) 235–252.

[30] N. Halama, I. Zoernig, and D. Jaeger: Advanced malignant melanoma: immunologic and multimodal therapeutic strategies. J. Oncol., **2010** (2010) 689893.

[31] R.L. Schilsky: Personalized medicine in oncology: the future is now. Nat. Rev. Drug Discov., **9** (2010) 363–366.

[32] Y. Lu, D. Bellgrau, L.D. Dwyer-Nield, A.M. Malkinson, R.C. Duke, T.C. Rodell, and A. Franzusoff: Mutation-selective tumor remission with Ras-targeted, whole yeast-based immunotherapy. Cancer Res., **64** (2004) 5084–5088.

[33] E.K. Wansley, M. Chakraborty, K.W. Hance, M.B. Bernstein, A.L. Boehm, Z. Guo, D. Quick, A. Franzusoff, J.W. Greiner, J. Schlom, and J.W. Hodge: Vaccination with a recombinant Saccharomyces cerevisiae expressing a tumor antigen breaks immune tolerance and elicits therapeutic antitumor responses. Clin. Cancer Res., **14** (2008) 4316–4325.

[34] S. Bunimovich-Mendrazitsky, E. Shochat, and L. Stone: Mathematical model of BCG immunotherapy in superficial bladder cancer. Bull. Math. Biol., **69** (2007) 1847–1870.

[35] S.M. Mangsbo, C. Ninalga, M. Essand, A. Loskog, and T.H. Tötterman: CpG therapy is superior to BCG in an orthotopic bladder cancer model and generates CD4+ T-cell immunity. J. Immunother., **31** (2008) 34–42.

[36] T.P. Kresowik and T.S. Griffith: Bacillus Calmette-Guerin immunotherapy for urothelial carcinoma of the bladder. Immunotherapy, **1** (2009) 281–288.

[37] H.M. Rosevear, A.J. Lightfoot, M.A. O'Donnell, and T.S. Griffith: The role of neutrophils and TNF-related apoptosis-inducing ligand (TRAIL) in bacillus Calmette-Gurin (BCG) immunotherapy for urothelial carcinoma of the bladder. Cancer Metastasis Rev., **28** (2009) 345–353.

[38] J.H. Stegehuis, L.H. de Wilt, E.G. de Vries, H.J. Groen, S. de Jong, and F.A. Kruyt: TRAIL receptor targeting therapies for non-small cell lung cancer: current status and perspectives. Drug Resist. Updat., **13** (2010) 2–15.

[39] D.C. Chade, R.C. Borra, I.P. Nascimento, F.E. Villanova, L.C. Leite, E. Andrade, M. Srougi, K.L. Ramos, and P.M. Andrade: Immunomodulatory effects of recombinant BCG expressing pertussis toxin on TNF-alpha and IL-10 in a bladder cancer model. J. Exp. Clin. Cancer Res., **27** (2008) 78.

[40] J. Arnold, E.C. de Boer, M.A. O'Donnell, A. Böhle, and S. Brandau: Immunotherapy of experimental bladder cancer with recombinant BCG expressing interferon-gamma. J. Immunother., **27** (2004) 116–123.

[41] A. Cappuccio, F. Castiglione, and B. Piccoli: Determination of the optimal therapeutic protocols in cancer immunotherapy. Math. Biosci., **209** (2007) 1–13.

[42] A. Cappuccio, M. Elishmereni, and Z. Agur: Optimization of interleukin-21 immunotherapeutic strategies. J. Theor. Biol., **248** (2007) 259–266.

[43] B. Ludewig, P. Krebs, T. Junt, H. Metters, N.J. Ford, R.M. Anderson, and G. Bocharov: Determining control parameters for dendritic cell-cytotoxic T lymphocyte interaction. Eur. J. Immunol., **34** (2004) 2407–2418.

[44] M.Y. Park, C.H. Kim, H.J. Sohn, S.T. Oh, S.G. Kim, and T.G. Kim: The optimal interval for dendritic cell vaccination following adoptive T cell transfer is important for boosting potent anti-tumor immunity. Vaccine, **25** (2007) 7322–7330.

[45] S. Teitz-Tennenbaum, Q. Li, M.A. Davis, K. Wilder-Romans, J. Hoff, M. Li, and A.E. Chang: Radiotherapy combined with intratumoral dendritic cell vaccination enhances the therapeutic efficacy of adoptive T-cell transfer. J. Immunother., **32** (2009) 602–612.

[46] L.G. de Pillis, W. Gu, and A.E. Radunskaya: Mixed immunotherapy and chemotherapy of tumors: modeling, applications and biological interpretations. J. Theor. Biol., **238** (2006) 841–862.

[47] C.J. Wheeler, A. Das, G. Liu, J.S. Yu, and K.L. Black: Clinical responsiveness of glioblastoma multiforme to chemotherapy after vaccination. Clin. Cancer Res., **10** (2004) 5316–5326.

[48] S. Chareyron and M. Alamir: Mixed immunotherapy and chemotherapy of tumors: feedback design and model updating schemes. J. Theor. Biol., **258** (2009) 444–454.

[49] G.P. Karev, A.S. Novozhilov, and E.V. Koonin: Mathematical modeling of tumor therapy with oncolytic viruses: effects of parametric heterogeneity on cell dynamics. Biol. Direct, **1** (2006) 30.

[50] B.W. Bridle, K.B. Stephenson, J.E. Boudreau, S. Koshy, N. Kazdhan, E. Pullenayegum, J. Brunellière, J.L. Bramson, B.D. Lichty, and Y. Wan: Potentiating Cancer Immunotherapy Using an Oncolytic Virus. Mol. Ther., [Epub ahead of print] (2010).

[51] A. Ben-Tal and A. Nemirovski: Robust optimization – methodology and applications. Math. Program., **92** (2002) 453–480.

[52] Z. Luo: Applications of convex optimization in signal processing and digital communication. Math. Program., **97** (2003) 177–207.

[53] A. Atamtürk and M. Zhang: Two-stage robust network flow and design under demand uncertainty. Operat. Res., **55** (2007) 662–673.

[54] Y. Zhang: General robust-optimization formulation for nonlinear programming. J. Optim. Theor. Applicat., **132** (2007) 111–124.

[55] D. Bertsimas, O. Nohadani, and K.M. Teo: Robust optimization in electromagnetic scattering problems. J. Appl. Phys., **101** (2007) 74507–74507-7.

[56] M. Apri, J. Molenaar, M. de Gee, and G. van Voorn: Efficient estimation of the robustness region of biological models with oscillatory behavior. PLoS One, **5** (2010) e9865.

[57] M. Rodriguez-Fernandez, P. Mendes, and J.R. Banga: A hybrid approach for efficient and robust parameter estimation in biochemical pathways. BioSyst., **83** (2006) 248–265.

[58] J.M. Balter, K.K. Brock, K.L. Lam, D. Tatro, L.A. Dawson, D.L. McShan, and R.K. Ten Haken: Evaluating the influence of setup uncertainties on treatment planning for focal liver tumors. Int. J. Radiat. Oncol. Biol. Phys., **63** (2005) 610–614.

[59] S.Y. Zhu, T. Mizowaki, Y. Norihisa, K. Takayama, Y. Nagata, and M. Hiraoka: Comparisons of the impact of systematic uncertainties in patient setup and prostate motion on doses to the target among different plans for definitive external-beam radiotherapy for prostate cancer. Int. J. Clin. Oncol., **13** (2008) 54–61.

[60] J. Unkelbach, T. Bortfeld, B.C. Martin, and M. Soukup: Reducing the sensitivity of IMPT treatment plans to setup errors and range uncertainties via probabilistic treatment planning. Med. Phys., **36** (2009) 149–163.

[61] J. Unkelbach, T.C. Chan, and T. Bortfeld: Accounting for range uncertainties in the optimization of intensity modulated proton therapy. Phys. Med. Biol., **52** (2007) 2755–2773.

[62] D. Pflugfelder, J.J. Wilkens, and U. Oelfke: Worst-case optimization: a method to account for uncertainties in the optimization of intensity modulated proton therapy. Phys. Med. Biol., **53** (2008) 1689–1700.

[63] M.R. Mahfouz, W.A. Hoff, R.D. Komisek, and D.A. Dennis: A robust method for registration of three-dimensional knee implant models to two-dimensional fluoroscopy images. IEEE Trans. Med. Imag., **22** (2003) 1561–1574.

[64] F. Hua, M.G. Cornejo, M.H. Cardone, C.L. Stokes, and D.A. Lauffenburger: Effects of Bcl-2 levels on Fas signaling-induced caspase-3 activation: molecular genetic tests of computational model predictions. J. Immunol., **175** (2005) 985–995.

[65] B.S. Adiwijaya, P.I. Barton, and B. Tidor: Biological network design strategies: discovery through dynamic optimization. Mol. BioSyst., **2** (2006) 650–659.

[66] J.B. Johnston, S. Navaratnam, M.W. Pitz, J.M. Maniate, E. Wiechec, H. Baust, J. Gingerich, G.P. Skliris, L.C. Murphy, and M. Los: Targeting the EGFR pathway for cancer therapy. Curr. Med. Chem., **13** (2006) 3483–3492.

[67] C.F. Huang and J.E. Ferrell, Jr.: Ultrasensitivity in the mitogen-activated protein kinase cascade. Proc. Natl. Acad. Sci. USA, **93** (1996) 10078–10083.

[68] L.F. Shampine and M.W. Reichelt: The MATLAB ODE suite. SIAM J. Sci. Comput., **18** (1997) 1–22.

[69] F. Mc. Johnston, M.C.B. Tan, B.R. Tan, Jr., M.R. Porembka, E.M. Brunt, D.C. Linehan, P.O. Simon, Jr., S. Plambeck-Suess, T.J. Eberlein, K.E. Hellstrom, I. Hellstrom, W.G. Hawkins, and P. Goedegebuure: Circulating mesothelin protein and cellular antimesothelin immunity in patients with pancreatic cancer. Clin. Cancer Res., **15** (2009) 6511–6518.

[70] D.A. Oble, R. Loewe, P. Yu, and M.C. Mihm, Jr.: Focus on TILs: prognostic significance of tumor infiltrating lymphocytes in human melanoma. Cancer Immun., **9** (2009) 3.

[71] N. Kronik, Y. Kogan, V. Vainstein, and Z. Agur: Improving alloreactive CTL immunotherapy for malignant gliomas using a simulation model of their interactive dynamics. Cancer Immunol. Immunother., **57** (2008) 425–439.

[72] H. Bönig, H.J. Laws, A. Wundes, J. Verheyen, M. Hannen, Y.M. Kim, U. Banning, W. Nürnberger, and D. Körholz: In vivo cytokine responses to interleukin-2 immunotherapy after autologous stem cell transplantation in children with solid tumors. Bone Marrow Transpl., **26** (2000) 91–96.

[73] B.J. Kennedy: Cyclic leukocyte oscillations in chronic myelogenous leukemia during hydroxyurea therapy. Blood, **35** (1970) 751–760.

[74] R.A. Gatti, W.A. Robinson, A.S. Deinard, M. Nesbit, J.J. McCullough, M. Ballow, and R.A. Good: Cyclic leukocytosis in chronic myelogenous leukemia: new perspectives on pathogenesis and therapy. Blood, **41** (1973) 771–782.

[75] N. Blumberg, C. Chuang-Stein, and J.M. Heal: The relationship of blood transfusion, tumor staging, and cancer recurrence. Transfusion, **30** (1990) 291–294.

[76] Y. Hirao, E. Okajima, S. Ozono, S. Samma, K. Sasaki, T. Hiramatsu, K. Babaya, S. Watanabe, and Y. Maruyama: A prospective randomized study of prophylaxis of tumor recurrence following transurethral resection of superficial bladder cancer–intravesical thio-TEPA versus oral UFT. Cancer Chemother. Pharmacol., **30** (1992) S26–S30.

[77] J.M. Weiss, T.C. Back, A.J. Scarzello, J.J. Subleski, V.L. Hall, J.K. Stauffer, X. Chen, D. Micic, K. Alderson, W.J. Murphy, and R.H. Wiltrout: Successful immunotherapy with IL-2/anti-CD40 induces the chemokine-mediated mitigation of an immunosuppressive tumor microenvironment. Proc. Natl. Acad. Sci. U.S.A., **106** (2009) 19455–19460.

[78] R. Tomova, K. Antonov, A. Ivanova, J.J. Jacobs, J.W. Koten, W. Den Otter, and Z. Krastev: Low-dose IL-2 therapy reduces HCV RNA and HBV DNA: case report. Anticancer Res., **29** (2009) 5241–5244.

[79] J.A. Westwood, P.K. Darcy, P.M. Guru, J. Sharkey, H.J. Pegram, S.M. Amos, M.J. Smyth, and M.H. Kershaw: Three agonist antibodies in combination with high-dose IL-2 eradicate orthotopic kidney cancer in mice. J. Transl. Med., **8** (2010) 42.

[80] K. Liu, S.A. Caldwell, K.M. Greeneltch, D. Yang, and S.I. Abrams: CTL adoptive immunotherapy concurrently mediates tumor regression and tumor escape. J. Immunol., **176** (2006) 3374–3382.

[81] J. Clarke, N. Butowski, and S. Chang: Recent advances in therapy for glioblastoma. Arch. Neurol., **67** (2010) 279–283.

[82] E. Mehrara, E. Forssell-Aronsson, H. Ahlman, and P. Bernhardt: Quantitative analysis of tumor growth rate and changes in tumor marker level: specific growth rate versus doubling time. Acta Oncologica, **48** (2009) 591–597.

[83] R. Rockne, J.K. Rockhill, M. Mrugala, A.M. Spence, I. Kalet, K. Hendrickson, A. Lai, T. Cloughesy, E.C. Alvord, Jr., and K.R. Swanson: Predicting the efficacy of radiotherapy in individual glioblastoma patients in vivo: a mathematical modeling approach. Phys. Med. Biol., **55** (2010) 3271–3285.

[84] M.J. van Vliet, H.J. Harmsen, E.S. de Bont, and W.J. Tissing: The role of intestinal microbiota in the development and severity of chemotherapy-induced mucositis. PLoS Pathog., **6** (2010) e1000879.

[85] L. Zappa, R. Savady, and P.H. Sugarbaker: Gastric perforation following cytoreductive surgery with perioperative intraperitoneal chemotherapy. J. Surg. Oncol., **101** (2010) 634–636.

[86] P. Seminara, T. Losanno, A. Emiliani, and G. Manna: Cancer chemotherapy and cardiovascular risks: is capecitabine-induced hypertriglyceridemia a rare adverse effect? Cardiology, **116** (2010) 42–44.

[87] R. Ramakrishnan, D. Assudani, S. Nagaraj, T. Hunter, H.I. Cho, S. Antonia, S. Altiok, E. Celis, and D.I. Gabrilovich: Chemotherapy enhances tumor cell susceptibility to CTL-mediated killing during cancer immunotherapy in mice. J. Clin. Invest., **120** (2010) 1111–1124.

[88] A.K. Nowak, R.A. Lake, and B.W. Robinson: Combined chemoimmunotherapy of solid tumours: improving vaccines? Adv. Drug Deliv. Rev., **58** (2006) 975–990.

[89] C.N. Baxevanis, S.A. Perez, and M. Papamichail: Combinatorial treatments including vaccines, chemotherapy and monoclonal antibodies for cancer therapy. Cancer Immunol. Immunother., **58** (2009) 317–324.

[90] M.R. Owen, H.M. Byrne, and C.E. Lewis: Mathematical modelling of the use of macrophages as vehicles for drug delivery to hypoxic tumour sites. J. Theor. Biol., **226** (2004) 377–391.

[91] A. Safwat, S.M. Bentzen, I. Turesson, and J.H. Hendry: Deterministic rather than stochastic factors explain most of the variation in the expression of skin telangiectasia after radiotherapy. Int. J. Radiat. Oncol. Biol. Phys., **52** (2002) 198–204.

[92] C.N. Andreassen, J. Alsner, and J. Overgaard: Does variability in normal tissue reactions after radiotherapy have a genetic basis–where and how to look for it? Radiother. Oncol., **64** (2002) 131–140.

[93] I. Solassol, F. Bressolle, L. Caumette, F. Garcia, S. Poujol, S. Culine, and F. Pinguet: Inter- and intraindividual variabilities in pharmacokinetics of fentanyl after repeated 72-hour transdermal applications in cancer pain patients. Ther. Drug Monit., **27** (2005) 491–498.

[94] T. Giese, C. Sommerer, M. Zeier, and S. Meuer: Monitoring immunosuppression with measures of NFAT decreases cancer incidence. Clin. Immunol., **132** (2009) 305–311.

[95] D. Dias-Santagata, S. Akhavanfard, S.S. David, K. Vernovsky, G. Kuhlmann, S.L. Boisvert, H. Stubbs, U. McDermott, J. Settleman, E.L. Kwak, J.W. Clark, S.J. Isakoff, L.V. Sequist, J.A. Engleman, T.J. Lynch, D.A. Haber, D.N. Louis, L.W. Ellisen, D.R. Borger, and A.J. Iafrate: Rapid targeted mutational analysis of human tumours: a clinical platform to guide personalized cancer medicine. EMBO Mol. Med., **2** (2010) 146–158.

[96] T.W. Flaig and L.M. Glodé: Management of the side effects of androgen deprivation therapy in men with prostate cancer. Expert Opin. Pharmacother., **9** (2008) 2829–2841.

[97] P.E. Kintzel, S.L. Chase, L.M. Schultz, and T.J. O'Rourke: Increased risk of metabolic syndrome, diabetes mellitus, and cardiovascular disease in men receiving androgen deprivation therapy for prostate cancer. Pharmacotherapy, **28** (2008) 1511–1522.

[98] R.S. Israeli, C.W. Ryan, and L.L. Jung: Managing bone loss in men with locally advanced prostate cancer receiving androgen deprivation therapy. J. Urol., **179** (2008) 414–423.

[99] P.G. Komarov, E.A. Komarova, R.V. Kondratov, K. Christov-Tselkov, J.S. Coon, M.V. Chernov, and A.V. Gudkov: A chemical inhibitor of p53 that protects mice from the side effects of cancer therapy. Science, **285** (1999) 1733–1737.

[100] J.A. Files, M.G. Ko, and S. Pruthi: Managing aromatase inhibitors in breast cancer survivors: not just for oncologists. Mayo Clin. Proc., **85** (2010) 560–566.